

Towards Enhanced Safety and Enriched Infotainment for Connected Vehicles: Modeling, Design and Implementation

Xi Chen

School of Computer Science,
McGill University, Montreal, Canada



A thesis submitted to McGill University
in partial fulfillment of the requirements of the degree of

DOCTOR of PHILOSOPHY

July 2017

Abstract

Automobile manufacturers are actively delivering a new generation of connected vehicles. These vehicles are driving a far-reaching revolution in the modern society. They will not only save a huge amount of lives and property from traffic accidents, but also fundamentally change the way we travel. As an essential building block of connected vehicles, Vehicle-to-Vehicle (V2V) communication technologies have become a major research and development priority of both governments and car manufacturers.

Driving safety and In-Vehicle Infotainment (IVI) services are two primary categories of services enabled by V2V communications. They are not only complementary to, but also mutually beneficial to, each other. On one hand, enhancing driving safety is the most critical issue in current traffic systems. A study [1] led by the U.S. Department of Transportation (U.S. DOT) estimated that V2V technologies can avoid 74 percent of car accidents, potentially saving thousands of lives and billions of dollars each year. Infotainment, on the other hand, not only provides extra encouragement to consumers in purchasing V2V devices, but also brings large economic incentives to manufactures in increasing the market penetration of V2V devices. As a result of this increased penetration, each vehicle can gather more information from other surrounding vehicles, leading to a large improvement in the safety of the whole traffic system. In return, enhanced safety allows everyone to better enjoy infotainment services during reassuring journeys. In this sense, safety and infotainment services are mutualistic in the vehicular ecosystem.

In this thesis, we focus on two promising V2V technologies, i.e., the Dedicated Short-Range Communication (DSRC) technology for driving safety and the in-cabin Wi-Fi technology for vehicular infotainment. While DSRC has been recognized by U.S. DOT as the enabling technology of the Intelligent Transportation System (ITS), the in-cabin Wi-Fi technology is recently deployed by many car manufacturers, such as General Motors, Ford, BMW, and Mercedes, to enhance travelling experience for both drivers and passengers. We first characterize these new technologies and their unique features with analytical models, and validate these models with extensive simulations. We then manage to improve the performance of these technologies with several novel solutions. In this way, we not only enhance the driving safety, but also provide better Quality of Service (QoS) for IVI. We implement these technologies in evaluation platforms, and conduct both analytical and simulation analyses to evaluate their communication reliability, efficiency and fairness. We

further implement and test them on real test-beds to demonstrate their large improvements over the state of the art.

Résumé

Les constructeurs automobiles livrent activement une nouvelle génération de véhicules connectés. Ces véhicules sont à l'origine d'une profonde révolution dans la société moderne. Ils ne nous permettent pas seulement de grandement diminuer le nombre de vies et de biens perdus au accident de la route, mais changerons aussi fondamentalement la façon dont nous voyageons. En tant que composante essentielle des véhicules connectés, les technologies de communications de véhicule à véhicule (V2V) sont devenues une priorité majeure en recherche et développement pour les gouvernements et les fabricants de voiture.

La sécurité au volant et les services d'infodivertissement embarqué sont deux principales catégories de services rendus possible par les communications V2V. Elles sont non seulement complémentaires, mais aussi mutuellement bénéfique. D'une part, l'amélioration de la sécurité au volant est le problème le plus critique dans les systèmes de circulations actuelles. Une étude [1] menée par le ministère des Transports des États-Unis a estimé que les technologies V2V pouvaient éviter 74 pour cent des accidents de voiture, ce qui pourrait sauver des milliers de vies et des milliards de dollars chaque année. L'infodivertissement, d'autre part, ne fournit pas seulement un encouragement supplémentaire pour les consommateurs dans l'achat d'appareils V2V, mais apporte aussi de grandes motivations économiques aux fabricants pour qu'ils augmentent la pénétration des appareils V2V sur le marché. À la suite de cette augmentation de la pénétration, chaque véhicule peut recueillir plus d'informations des autres véhicules environnants, menant à une grande amélioration de la sécurité de l'ensemble du système de circulation. En retour, la sécurité renforcée permet à chacun de mieux profiter des services d'infodivertissement durant des voyages rassurants. En ce sens, les services de sécurité et d'infodivertissement forment une association mutualiste dans l'écosystème véhiculaire.

Dans cette thèse, nous nous concentrons sur deux technologies de V2V prometteuses, à savoir, les technologies de communications dédiées à courte portée (DSRC) pour la sécurité au volant et la technologie de Wi-Fi dans l'habitacle pour l'infodivertissement automobile. Alors que le DSRC a été reconnu par le ministère des Transports des États-Unis comme la technologie habilitante du système de transport intelligent, la technologie de Wi-Fi dans l'habitacle a été récemment déployée par de nombreux constructeurs automobiles tels que General Motors, Ford, BMW et Mercedes, afin d'améliorer l'expérience de voyage pour les conducteurs et les passagers. Nous caractérisons d'abord ces nouvelles technologies et leurs

éléments uniques avec des modèles analytiques, et validons ces modèles avec des simulations poussées. Nous réussissons ensuite à améliorer les performances de ces technologies à l'aide de plusieurs solutions novatrices. De cette façon, non n'améliorons pas seulement la sécurité au volant, mais fournissons aussi une meilleure qualité de service (QoS) pour IVI. Nous mettons en œuvre ces technologies dans des plateformes d'évaluation, et nous effectuons à la fois des analyses analytique et en simulation pour évaluer leur fiabilité de communication, leur efficacité et leur équité. De plus, nous les mettons en œuvre et les testons sur de véritables bancs d'essai pour démontrer leurs grandes améliorations par rapport aux technologies de pointe.

Acknowledgements

This thesis represents not only my work in front of the screen, it is also a milestone in almost five years of my study, research and life at McGill University and especially the Cyber-Physical System Laboratory. The path to my doctoral degree was rugged, along with many intellectual challenges and psychological frustrations. I could never overcome them without the valuable help, support, advice and suggestions from many good and honest, brilliant and professional people. Their love and kindness have changed my toughest years into an enjoyable and rewarding experience.

First and foremost, I would like to thank my advisor, Professor Xue Liu, for being supportive since day one. This thesis could never be accomplished without his valuable guidance and continuous encouragement. He has been always patient with me, and thoroughly taught me how to become a good researcher and scientist. He has given me unique opportunities to participate in cutting-edge research topics, which I have taken great advantage of. His assistance, comments, and suggestions on my study, research, and career are my life's treasures. I feel very fortunate to have this five-year relationship with him.

My thesis committee guided me through all these years. My great appreciation goes (alphabetically) to Professor Xiao-Wen Chang, Professor Wenbo He, and Professor Muthucumar Maheswaran for being on my committee, and led me through the challenges. I would also like to thank (alphabetically) Professor Jackie Cheung, Professor Luc Devroye, Professor Prakash Panangaden, Professor Doina Precup, and Professor Micheal Rabbat for their insightful comments and suggestions to my research and study during my defense, my proposal, the classes and many other occasions.

I have also received valuable help and support from my collaborators. Together we have delivered impactful research results, interesting demos, practical test-beds, and profitable commercial products. Especially, I would like to express my appreciation to (alphabetically) Dr. Michel Allegue, Dr. Fan Bai, Dr. Negar Ghourchian, Dr. Hongxing Li, Professor Hang Luo, Dr. Lei Rao, and Professor Xinbing Wang.

I am also grateful for the chance to study, research and live with my labmates and friends in McGill. We have always supported each other, and worked through a great number of problems and challenges. I will always remember the time we spent together in writing and polishing papers, discussing research ideas, brainstorming during coffee breaks, playing basketball and working out, and dreaming about our bright future. I would like to

thank (alphabetically) Jing Chen, Yixin Chen, Dr. Xi Chen (Ms), Dr. Hanqiang Cheng, Shuonan Dong, Dr. Yi Gao, Landu Jiang, Dr. Fanxin Kong, Dr. Linghe Kong, Xinye Lin, Chen Ma, Zhonghao Sun, Qinglong Wang, Dr. Wen Wang, Dr. Qiao Xiang, Kai Xiong, Xuepeng Xu, Shen Yan, Dr. Yuan Yao, Jianan Yue, Jing Zhang, and Dr. Nan Zhu.

Furthermore, I would like to express my greatest gratitude to my family. My beloved wife, Lu Fang, is the one who always stands by my side, sharing my happiness and successes, facing my frustrations and failures together, taking care of our health, making a great deal of sacrifice for me, and giving birth to our son. Her love and care is the biggest reason to support me through all the difficulties. My son, Fangze Chen, is the most lovely surprise ever happened to me. His birth not only brings pride and joy to my life, but also drives me to fulfill my duties as a father. My sincere appreciation also goes to my parents, Dr. Zili Chen and Mrs. Long Guo, who raised me up and taught me how to be a responsible and humble person.

I have also received valuable help and support from many other wonderful people during my PhD journey. It is a pity that I cannot list all their names in a limited space. I would like to thank them for being in my life and sharing their precious time with me. I wish everyone a happy, healthy and prosperous life.

Contents

1	Introduction	1
1.1	Dedicated Short-Range Communications for Driving Safety	2
1.2	In-Cabin Wi-Fi for In-Vehicle Infotainment	4
1.3	Research Objectives and Contributions	5
1.3.1	Research objectives	5
1.3.2	Contributions	6
1.4	Road Map	8
2	Related Work	10
2.1	The Deployment of Communication Devices on Wheels	10
2.2	Modeling and Measurement of Vehicular Communications and Networks .	12
2.2.1	Capacity of Mobile ad hoc Networks	12
2.2.2	Measuring IEEE 802.11 based Communications	12
2.2.3	Modeling IEEE 802.11 based Communications	13
2.3	Adaptive Techniques to Improve the Performance of Vehicular Communica- tions	14
2.3.1	The adaptations of communication variables	14
2.3.2	Adaptive Protocols	18
3	Enhancing the Safety of Connected Vehicles	22
3.1	Overview	22
3.2	Performance Metrics	24
3.3	Online Synchronous Control Approach of Multiple Communication Variables	25
3.3.1	Observations and Challenges	26
3.3.2	Overview of OnCAR	29

3.3.3	Design of MIMO Model Based Predictor	31
3.3.4	Design of Adaptive Controller	32
3.3.5	Measuring System Outputs and Environment Parameters	36
3.4	Evaluating OnCAR with Simulations	37
3.4.1	Evaluation Setup	38
3.4.2	Approaches Studied	40
3.4.3	DSRC Reliability in Real-life Scenarios	41
3.4.4	DSRC Efficiency in Real-life Scenarios	42
3.4.5	DSRC Fairness in Real-life Scenarios	43
3.4.6	Convergence Speed in Real-life Scenarios	45
3.4.7	Evaluation in Synthetic Scenarios	45
3.5	Evaluating OnCAR on a Testbed	46
3.5.1	Testbed Setup	46
3.5.2	Experiment Results	49
3.6	Strictly Distributed Coordination	53
3.6.1	Problem Statement and Challenges	54
3.6.2	DisCo with Fixed Coordination Targets	54
3.6.3	Discretization of the Controller	59
3.6.4	DisCo with Adaptive Coordination Targets	60
3.6.5	Estimation of Neighbor Number	64
3.6.6	Estimation of ePDR	64
3.7	Evaluation of DisCo	64
3.7.1	Evaluation Setup	64
3.7.2	Schemes Studied	66
3.7.3	DSRC Reliability	66
3.7.4	DSRC Fairness	68
3.7.5	Convergence	71
3.8	Concluding Remarks	73
4	Providing Infotainment Services to Connected Vehicles	74
4.1	Overview	74
4.1.1	In-cabin Wi-Fi Services	75
4.1.2	Differences from Other Communication Techniques	76

4.1.3	Unique Features and Their Impacts	77
4.2	Metrics	79
4.2.1	The average queueing delay and delay jitter	79
4.2.2	The deadline missing ratio	80
4.2.3	The average and regional throughput	80
4.2.4	The average and regional goodput	81
4.3	Modelling the In-Cabin Wi-Fi Communications	81
4.3.1	MAC Layer Modelling	81
4.3.2	PHY Layer Modelling	84
4.3.3	Calculation of Throughput and PLR	85
4.3.4	Model Validation	87
4.3.5	System Analysis based on Extensive Simulations	90
4.4	In-cabin Wi-Fi Video Streaming and its Challenges	99
4.4.1	Challenges	100
4.5	Design of the DRIVING Framework	101
4.5.1	Overall Design	101
4.5.2	Solving the Challenges with DRIVING	101
4.6	Analytical Modeling of DRIVING	103
4.6.1	Analytical Models in Two Levels	103
4.6.2	The Packet Level Model	103
4.6.3	The Queue Level Models	105
4.6.4	Average Queueing Delay	106
4.6.5	Model Validation	113
4.7	Tuning DRIVING with the Models	115
4.8	Evaluation of DRIVING	115
4.8.1	Evaluation Setup	116
4.8.2	The Queueing Delay and Jitter Performance	119
4.8.3	The Deadline Missing Ratio Performance	122
4.8.4	The Goodput Performance	122
4.9	Concluding Remarks	125
5	Conclusion and Future Work	128
5.1	Conclusion	128

5.2	Future Work	129
5.2.1	Interaction between Cellular and Wi-Fi Links	129
5.2.2	Enabling 3D GPS with FM signals	130
A	Acronyms, Abbreviations and Samples	131
A.1	Acronyms and Abbreviations	131
A.2	Mathematical Samples	134
B	Publications	138
	Bibliography	141

List of Figures

1.1	The mutually beneficial DSRC and in-cabin Wi-Fi.	3
1.2	The road map of this thesis.	9
2.1	The flow of the related work section.	11
3.1	Traffic accident rate across different time of day.	26
3.2	The simulated highway scenario.	27
3.3	Illustration of performance degradations due to negligence of the power-rate coupling.	28
3.4	Architecture of OnCAR.	29
3.5	Architecture of the MIMO model based predictor.	30
3.6	Architecture of the adaptive controller.	33
3.7	Real-life traffic density traces.	38
3.8	CDFs of ePDRs in real-life scenarios at rush hours.	41
3.9	CDFs of eTPUT in real-life scenarios at rush hours.	42
3.10	CV of ePDR in real-life scenarios.	44
3.11	Convergence in San Diego Scenario.	44
3.12	A testbed to evaluate OnCAR.	47
3.13	The components of a DSRC-enabled vehicle and their connections.	48
3.14	Average ePDRs of DSRC-enabled vehicles in the existence of hidden terminals.	50
3.15	CDFs of eTPUTs of DSRC-enabled vehicles.	51
3.16	Convergence of power and rate adaptations when there are 10 hidden terminals.	52
3.17	The architecture of DisCo-FT.	55
3.18	The architecture of DisCo-AT.	61
3.19	The architecture of the adaptive target controller.	62

3.20	The average ePDRs of different schemes.	67
3.21	The ePDR improvements of all schemes over the Max-Power scheme.	67
3.22	CDF of ePDRs under different traffic densities.	68
3.23	CoV of ePDRs under different traffic densities.	69
3.24	Occurrence rates of transmission power when density is 0.2 vehicles per meter.	70
3.25	Convergence of CV.	71
3.26	Convergence of ePDRs.	72
4.1	An example of the in-cabin Wi-Fi system.	75
4.2	An example for in-cabin Wi-Fi hidden terminals	78
4.3	2D Markov chain for in-cabin backoff process	82
4.4	Empirical SINR-PLR curves	85
4.5	Model evaluation via average and regional goodputs. The simulated goodputs are denoted as "Sim" and marked by dots. The modeled goodputs of our model are denoted as "Anal" and marked by solid lines. The modeled goodputs of Yao's model are denoted as "Yao" and marked by dash lines.	90
4.6	Average goodput when transmission power is 20dBm and data rate is 48Mbps	92
4.7	Regional goodput when transmission power is 20dBm and data rate is 48Mbps	92
4.8	Average goodputs of different transmission powers.	93
4.9	Regional goodputs of different transmission powers.	94
4.10	Average goodputs of different transmission data rates.	96
4.11	Regional goodputs of different transmission data rates.	98
4.12	Differences between a traditional scenario and the in-cabin Wi-Fi scenario.	100
4.13	The block diagram of DRIVING.	102
4.14	The two-level models.	104
4.15	The DTMC for the queueing process of each node in priority level k when $\lambda_k < \mu_k$	105
4.16	The DTMC for the queueing process of each node in priority level k when $\lambda_k \geq \mu_k$	107
4.17	The model validation results.	114
4.18	The queueing delays under different settings of DRIVING.	116
4.19	The average queueing delays.	119
4.20	The delay jitters.	121

4.21	The average deadline missing ratios.	123
4.22	The average goodputs of four different data rates.	124
4.23	The CDFs of goodputs with 80 vehicles.	126

List of Tables

3.1	Settings of the bi-directional highway.	39
3.2	Empirical values of parameters in DSRC propagation model [2].	40
3.3	Statistics of ePDRs at rush hours of Berkeley.	41
3.4	Statistics of ePDRs at rush hours of San Diego.	42
3.5	Statistics of eTPUT at rush hours of Berkeley.	43
3.6	Statistics of eTPUT at rush hours of San Diego.	43
3.7	OnCAR's improvements in fairness over others.	44
3.8	Traffic densities of ten synthetic scenarios.	45
3.9	OnCAR's improvements over others in the synthetic scenarios.	46
4.1	Settings for the highway scenario	88
4.2	Settings for in-cabin Wi-Fi device	88
4.3	Data rates in this thesis	89
4.4	Parameters for the propagation model	89
4.5	Candidate delay sets for DRIVING.	115
4.6	Settings for the highway scenario.	116
4.7	Settings for in-cabin Wi-Fi device.	117
4.8	Settings for the propagation model.	118
A.1	Acronyms and Abbreviations.	131
A.2	Mathematical Samples.	134

Chapter 1

Introduction

The automobile industry is undergoing a profound revolution, which is going to change the way people travel and live. During the past few years, customer preferences and expectations in safety, technology, and, connectivity, have changed significantly, as pointed out by General Motors President Dan Ammann. He believes that the automaker's future relies heavily on a plan to engage customers beyond vehicles to mobile devices and connectivity.

Connected vehicles are the pioneers in this revolution, significantly enhancing the traffic safety and fundamentally redefining the personal mobility. On one hand, they have been considered as a remedy for modern traffic issues, potentially saving hundreds of thousands of lives and billions of dollars every year worldwide. On the other hand, they provide an always-connected Internet experience for drivers and passengers, and make the driving experience easier to everyone with services such as instant streaming of music and movies.

To realize this bright future, wireless connections are required to connect a vehicle to other vehicles, as well as the roadside infrastructure. In order to enhance the driving safety and improve the quality of vehicular services, it is of vital importance to establish and maintain Vehicle-to-Vehicle (V2V) and Vehicle-to-Infrastructure (V2I) communications in a stable and high-speed manner. Two promising technologies, i.e., the Dedicated Short-Range Communications (DSRC) technology and the in-cabin Wi-Fi technology, are envisioned as the enablers of the next generation vehicular networks.

While the DSRC technology is mainly developed for enhancing driving safety, the in-cabin Wi-Fi technology aims to provide better In-Vehicle Infotainment (IVI) services. These two technologies are complementary and *mutually beneficial* to each other. On one hand,

when the driving safety is greatly enhanced with the deployment of the DSRC technology, drivers and passengers feel secure and relaxed during the smoother trips. With such an emotionally secure state, they are willing to enjoy more IVI services. In short, the DSRC technology creates more demands on the in-cabin Wi-Fi services, by making people feel more secure. On the other hand, IVI services provided by the in-cabin Wi-Fi technology already opens up a large multimedia market, which is expected to grow to the level of hundreds of billions dollars. This tremendous economic incentive will certainly drive manufacturers to deploy more and more vehicular communication devices. (Adding a DSRC or Wi-Fi chip on an in-vehicle wireless radio will only raise the cost by several dozens of dollars.) Therefore, with an increasing penetration of V2V and V2I devices, the DSRC technology can be embedded on more vehicles, allowing it to have a more comprehensive understanding of the current traffic situation. In this way, the driving safety is further enhanced.

More importantly, the above mentioned procedures form a closed loop, which keeps boosting the benefits to both ends with positive feedbacks. The enhanced safety improves emotional security of passengers, and thus creates more infotainment service demands and larger economic benefits to the car manufacturers and IVI services providers. This enlarged economic incentive drives the related companies to deploy more vehicular communication devices, allowing all traffic participants to better coordinate with each other for an enhanced safety. Such a positive feedback loop is illustrated in Figure 1.1.

1.1 Dedicated Short-Range Communications for Driving Safety

As an essential building block of the connected vehicles, the DSRC technology has become a major research priority of both governments and automobile manufactures. In the year of 2014, the U.S. Department of Transportation (U.S. DOT) announced its commitment to DSRC for driving safety [3]. In North America, 75 MHz of spectrum in the 5.9 GHz frequency band has been allocated to DSRC exclusively. This spectrum is divided into several channels, among which the DSRC Channel 172 is a specific channel that is designated for safety. The DSRC technology enables a variety of safety-critical applications, such as adaptive cruise control, lane change assist, and forward collision warning.

The performance of DSRC plays a fundamental role in supporting these safety-critical applications. These applications require vehicles to exchange their dynamics including lo-

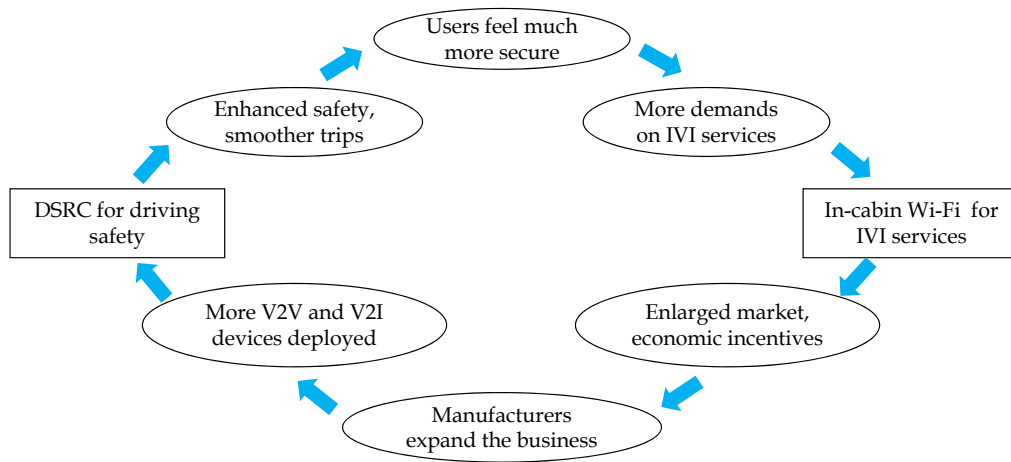


Figure 1.1 The mutually beneficial DSRC and in-cabin Wi-Fi.

cations, directions, route plans, velocities, accelerations, steering, and other information. Upon receiving DSRC messages encapsulating these dynamics, the safety-critical applications can make decisions and recommendations to avoid collisions, assist lane changing, coordinate intersection crossing, etc. However, these safety-related functionalities cannot be fulfilled, if DSRC messages are delayed or lost. For example, to avoid a collision between two vehicles, DSRC messages have to be delivered successfully to both vehicles before the collision. This implies at least three conditions. 1) The messages need to be delivered successfully (i.e., reliability). 2) The delivery of messages must be done before the collision (i.e., efficiency). Otherwise, the messages are useless for collision avoidance or other applications. 3) The delivery should be guaranteed for both vehicles (i.e., fairness). Otherwise, the collision may still happen, since one of the vehicles is still unaware of the incoming danger. Therefore, the performance of DSRC is of critical importance to the driving safety.

To ensure the performance of DSRC in the dynamic vehicular environment, communication variables must be adjusted appropriately in an online manner. We first attack this problem from the level of an individual vehicle. Existing communication variable adaptation approaches in this vehicle level only achieve a suboptimal performance, mainly due to 1) the overlook of the strong coupling between variables and 2) the use of heuristic algorithms. Previous approaches either focus on the adaptation of one single variable, or adjust them one by one. These sequential approaches result in unavoidable performance degradation, due to the error propagation in the multi-stage variable adjustment. In ad-

dition, heuristic algorithms may fail to provide consistent performance in highly dynamic environments. To address these issues, in this thesis, we propose an adaptive approach to simultaneously adjust multiple variables based on systematic control theories, and thus largely improve the performance of DSRC.

We then go from the vehicle level to the network level, and consider the communication coordination between vehicles. As more and more DSRC-enabled vehicles are to be deployed in the near future, the DSRC safety channel will become more and more congested. Individual adaptations of communication variables may not achieve the optimal global performance. The lack of coordination between vehicles is going to cause severe interference and collisions in wireless channels, greatly compromising the performance of DSRC. Moreover, it is also very likely that some vehicles obtain much less traffic information than others. These vehicles could make poor judgements that completely contradict with the majority, leading to grave consequences. To avoid these disasters, vehicles have to coordinate their transmissions to eliminate interference, collisions and misunderstandings. Coordinating the adaptations between DSRC devices allow us to further approach the optimal result. However, existing coordination solutions adopt either feedback, handshaking or probing mechanisms, and thus introduce large coordination overhead that increases explosively with traffic density. Allowing individual vehicles to coordinate their communications in a completely decentralized manner without any information exchange is desirable yet very challenging. To accomplish this difficult mission, in this thesis, we develop a series of strictly distributed coordination schemes, which enhances the global performance with purely local power adjustments.

1.2 In-Cabin Wi-Fi for In-Vehicle Infotainment

Car manufactures, such as General Motors [4], Ford [5], BMW [6], and Mercedes [7], are actively deploying the in-cabin Wi-Fi technology to make the travelling easier for everyone onboard. In this newly deployed in-cabin Wi-Fi system, a built-in Wi-Fi hotspot powers all the Wi-Fi devices inside the vehicle, bridging the communication gap between these devices and cellular networks. This system enables a wide range of in-vehicle communications and infotainment services.

Wireless communication performance has been widely studied through analytical models as well as simulation and experimental evaluations in existing literatures [8, 9]. However,

the existing work mainly considers Wi-Fi hotspots located in static structures, but does not take the features of in-cabin Wi-Fi communications into consideration. Due to the mobility of vehicles, the density of Wi-Fi hotspots can vary frequently, and can become very large during rush hours. A fundamental question remains to be explored: as every running vehicle is equipped with an in-cabin Wi-Fi, how will be the communication performance affected by the varied number of surrounding vehicles, the transmission power and the data rate? In order to answer this question, in this thesis, we establish new analytical models that embody the novel features of in-cabin Wi-Fi systems.

We then go further to explore how to improve the performance of the in-cabin Wi-Fi system, as well as the Quality of Service (QoS) it provides. Among all infotainment services enabled by this system, mobile video streaming is expected to be the dominating one, accounting for over 69 percent of data traffic by 2018 [10]. Video streaming in the in-cabin Wi-Fi system has two distinct features. First of all, the in-cabin Wi-Fi Access Points (APs) belong to different individuals, who are unlikely to collaborate with each other in streaming videos of their own interests. Second, the video streaming service requires low delays and jitters in providing smooth viewing experience. The coexistence of these two features pose new requirements in scheduling the transmissions of individual in-cabin Wi-Fi APs. A proper scheduling algorithm should be both completely decentralized and delay sensitive. To this end, in this thesis, we propose to schedule the in-cabin Wi-Fi video streaming with our new framework, which exhibits both the fully distributed and delay-aware features.

1.3 Research Objectives and Contributions

In this section, we present the research objectives of this thesis, along with the achievements.

1.3.1 Research objectives

Addressing the strong coupling between communication variables

Existing adaptation approaches overlook the strong coupling between communication variables, and adjust them one by one. Consequently, they introduce error propagations in their sequential variable adjustments. Therefore, the **research objective 1** is *to develop an adaptation approach that addresses the strong coupling between communication variables*

and adjusts all of them at the same time.

Coordinating vehicles in a fully distributed manner

Existing coordination approaches mainly depend on extra message exchanges to coordinate distributed DSRC units. However, the overhead of these messages could be tremendous in large-scale vehicular networks, and is expected to grow explosively during rush hours. Furthermore, because of the high mobility of vehicles, coordination decisions will be quickly outdated, making the message exchanges meaningless in high speed scenarios. Hence, it is desired to achieve the **research objective 2**, i.e., *developing a strictly distributed scheme to coordinate transmission power of DSRC units with zero coordination overhead.*

Modeling this newly deployed system

Although the communication distance of an in-cabin Wi-Fi system can be much smaller than those of conventional Wi-Fi hotspots, it still remains an open problem how the in-cabin Wi-Fi communication performance looks like in a dynamic vehicular environment. Therefore, the **research objective 3** is *to develop analytical models that capture the unique features of in-cabin Wi-Fi systems under different traffic conditions.*

Distributed scheduling for in-cabin Wi-Fi video streaming

We then procedure one step forward and try to improve the QoS of in-cabin Wi-Fi services, and focus on the most dominating service - the video streaming. The QoS of in-cabin Wi-Fi video streaming would be significantly compromised by poorly scheduled transmissions. To schedule the video streaming effectively, we need to jointly consider the completely decentralized feature of in-cabin Wi-Fi APs and the delay-sensitive feature of video services. Therefore, our **research objective 4** is *to develop a scheduling framework, which is both fully distributed and delay-sensitive.*

1.3.2 Contributions

In the processes of achieving the aforementioned research objectives, several important contributions have been made.

Contribution 1 We propose an online multi-variable synchronous control approach based on systematic control theories. To better illustrate the design concept, we take the transmission power and data rate as example variables, and present an **Online Control Approach of power and Rates (OnCAR)**. To produce a synchronous combination of communication variables, OnCAR adopts a Multiple-Input Multiple-Output (MIMO) model based controller. This MIMO model characterizes the variable-performance mapping, which implicitly captures the coupling between variables as well as its impact on DSRC performance. Leveraging this online updated model, OnCAR determines all communication variables synchronously to optimize DSRC performance. It significantly improves the reliability, efficiency and fairness of DSRC by up to 23.7%, 30.1% and 40.1%, respectively. With this contribution, we achieve research objective 1.

Contribution 2 We develop a series of strictly **Distributed Coordination** schemes, namely DisCo. DisCo first enables the strictly distributed coordination with an efficient distributed control technique, assuming that all units have the same performance targets. By applying an online control loop, DisCo releases the assumption of identical targets by adaptively estimating the optimal targets, and thus further enhances DSRC performance. Extensive simulations demonstrate that DisCo increases DSRC reliability significantly over the state-of-the-art (by up to 85.8%), and at the same time largely improves the fairness across all DSRC units (by up to 83.7%). In this way, we achieve research objective 2.

Contribution 3 We develop novel cross-layer models that consider the unique features of in-cabin Wi-Fi, including the unique space layout of in-cabin Wi-Fi APs and clients, the unique power loss feature due to vehicle cabins, and the fast mobility of APs. We further establish a new evaluation platform for in-cabin Wi-Fi communications to validate these analytical models, and illustrate that the proposed models are much more accurate than the existing ones. Therefore, we achieve research objective 3.

Contribution 4, we design the **Delay-awaRe DIstributed Video schedulING (DRIVING)** framework for in-cabin Wi-Fi systems. It retrofits existing Carrier Sense Multiple Access (CSMA) schemes by prioritizing packets with large queueing delays. In this way, DRIVING schedules the transmissions in a fully distributed and delay-aware manner. In addition, DRIVING is lightweight, and only requires a software upgrade to deploy on commodity Wi-Fi APs. With the help of DRIVING, we achieve research objective 4.

The publications related to these contributions are listed in Appendix B.

1.4 Road Map

The road map of this thesis is presented in Figure 1.2. In Chapter 3, we study and apply adaptive DSRC to enhance driving safety of connected vehicles. In this chapter, we start from the vehicle-level adaptation, and investigate an important yet unsolved issue - the coupling between multiple DSRC variables. To tackle this issue, we propose an online control approach to embrace the coupling in the synchronous adjustment of variables. We then proceed to the network-level coordination, and study the major issue of coordination overhead, which increases exponentially with traffic density. To eliminate this overhead and further enhance the coordination, we develop a series of strictly distributed coordination schemes with zero message exchange.

In Chapter 4, we focus on another equivalently important subtopic, i.e., applying in-cabin Wi-Fi for enriched IVI services. We first establish cross-layer models to characterize the newly deployed in-cabin Wi-Fi systems, and demonstrate the modelling accuracy with extensive simulations. Based on the models, we have a better understanding on the challenges of the in-cabin Wi-Fi systems, especially when these systems are used to deliver the most popular and bandwidth consuming service - the video streaming service. To improve the QoS of in-cabin Wi-Fi video streaming, we design a distributed scheduling framework to ensure the delay awareness and fulfill distributed requirement of this service.

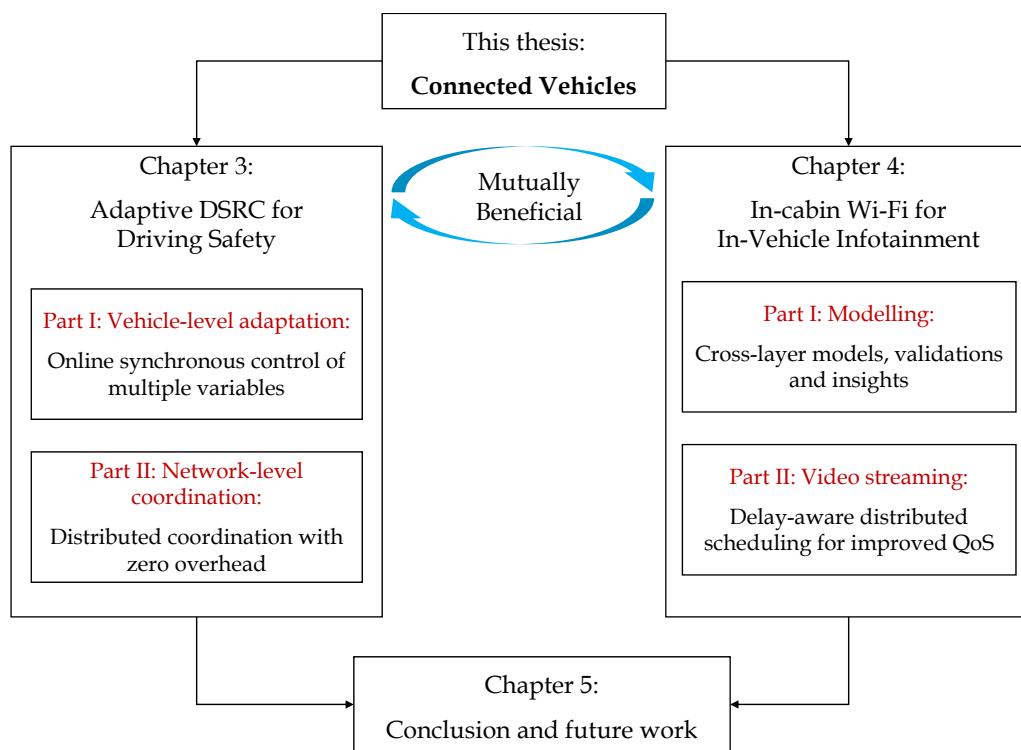


Figure 1.2 The road map of this thesis.

Chapter 2

Related Work

In this chapter, we review the related work, and discuss how this thesis advances the state of the art. The whole flow of this chapter is illustrated in Figure 2.1. We first present the current deployment efforts made by the governments and the automobile industry, so as to demonstrate that the research on connected vehicles is critical and necessary. We then discuss the first stage of the related research - the understanding and modeling the connected vehicles and their networks. With a comprehensive understanding, we then proceed to the next stage and try to improve the performance of connected vehicle technologies. Alongside the discussions of related papers and articles, we present the drawbacks of the existing studies and demonstrate the necessity and novelty of the algorithms, approaches, frameworks and theories proposed in this thesis.

2.1 The Deployment of Communication Devices on Wheels

In the year of 2014, the U.S. DOT announced its commitment to DSRC [3] for driving safety. Regulations of DSRC are expected to be finalized around 2017-2018 in North America, and initial mandated deployment will be around 2019-2020 [11]. Before that, the deployment of DSRC devices is and will be mostly on test vehicles. In August of 2012, the U.S. DOT launched the Connected Vehicle Safety Pilot Model Deployment in University of Michigan. This program involves 3,000 private vehicles, which are equipped with DSRC devices to allow wireless communications with each other and with devices in roadside infrastructure. The industry obviously wants more than test vehicles. General Motors, for example, plans to launch voluntary deployment in its Cadillac 2017 models. Chip manufactures, such

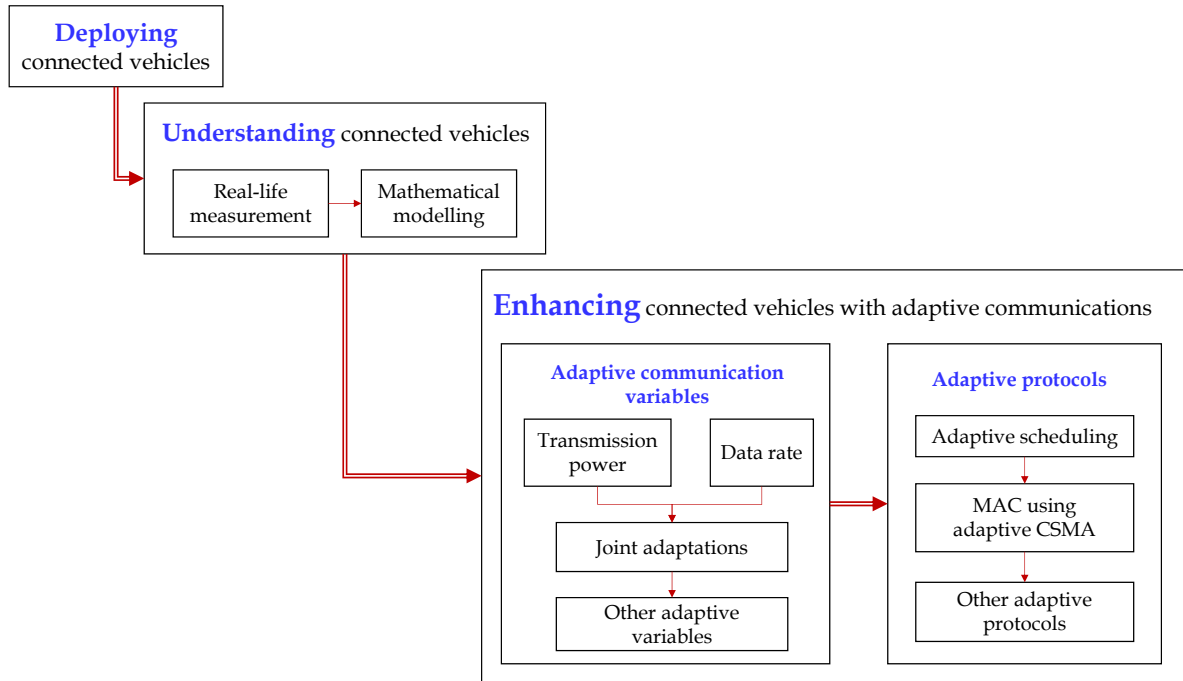


Figure 2.1 The flow of the related work section.

as Qualcomm [12], have already started providing DSRC solutions for both vehicles and smartphones.

The deployment of in-vehicle Wi-Fi hotspots is faster than that of DSRC devices. Starting from the year of 2014, General Motors partners with AT&T to offer embedded 4G broadband on most of its vehicles [13]. This built-in broadband connection not only powers passengers' cellphones and laptops through high-speed Wi-Fi interface, but also provides the potential to improve driving safety. General Motors is not the only manufacturer providing this technology. Ford [5], BMW [6], and Audi [14] are actively deploying similar in-cabin Wi-Fi devices in their vehicles. Meanwhile, standalone mobile Wi-Fi hotspots are designed by telecommunication companies like Huawei [15]. To offer an attractive in-cabin Wi-Fi service to the customers, it is of critical importance to analyze the performance and develop a comprehensive model of in-cabin Wi-Fi communications.

2.2 Modeling and Measurement of Vehicular Communications and Networks

In order to improve the safety and performance of vehicles that are connected via vehicular communications, it is of significant importance to first characterize the communications and networks. Modeling and measurement results provide critical guidelines to enhance the efficient, reliability, robustness and fairness of vehicular communications.

2.2.1 Capacity of Mobile ad hoc Networks

Connected vehicles are a concrete example of mobile ad hoc networks (MANETs). Previous work (e.g., Zhang et al. in [16], Wang et al. in [17], Han et al. in [18]) extensively studied the capacity and delay of MANETs. For enhanced reliability and efficiency, connected vehicles also communicate with infrastructure units. Together they form a hybrid ad hoc network, of which the throughput and latency has been widely discussed (e.g., Li et al. in [19], Chen et al. in [20], and the references therein). Lu et al. in [21] gave a comprehensive survey of capacity and delay in MANETs. However, existing work in this thread has not considered some important mechanisms in DSRC and Wi-Fi standards, such as the random backoff, the Distributed Coordination Function (DCF), Ready-to-send/clear-to-send (RTS/CTS) mechanism and the Enhanced Distributed Channel Access (EDCA). To better understand DSRC and in-cabin Wi-Fi, we need approaches that are more specified for IEEE 802.11 based communications.

2.2.2 Measuring IEEE 802.11 based Communications

Measurement study is of critical importance for us to understand IEEE 802.11 based communications. A comprehensive overview of existing measurement tools, as well as their effectiveness in estimating wireless parameters, was presented by Dujovne et al. in [22]. Non-intrusive methods, such as Jigsaw (proposed by Cheng et al. in [23]), Wit (proposed by Mahajan et al. in [24]) and Pie (proposed by Shrivastava et al. in [25]), were designed to monitor enterprise Wireless Local Area Networks (WLANs) with little system downtime. Measurement study of vehicular networks has also been conducted by, for example, Cheng et al. in [2], Sukuvaara et al. in [26] and Martelli et al. in [27].

Nevertheless, measurement study has its inherent limitations. For instance, only to

2.2 Modeling and Measurement of Vehicular Communications and Networks

investigate the impact of the transmission power, it is necessary to conduct multiple tests under the same traffic condition. Yet, it would be hard to maintain the same traffic condition for multiple tests. Theoretical analysis and mathematical models are required to provide guidelines for real system designs, while measurement study should be utilized as an important complement to validate the theories, models and designs.

2.2.3 Modeling IEEE 802.11 based Communications

Analytical models of IEEE 802.11 based communications have been extensively studied. Qiu et al. in [8] developed a general interference model for wireless communication, based on a Markov chain and a log-normal assumption of interference. However, this method and its extensions are not suitable for large scale in-cabin Wi-Fi networks, due to the fact that the sizes of their Markov chains increase quadratically with the number of vehicles. Therefore, we employ a scalable framework, which models the 802.11 DCF and the EDCA mechanism. In the seminal work, Bianchi developed in [9] a two-dimension (2D) Markov chain to analyze 802.11 saturated unicast throughput with unlimited retransmissions. Subsequent papers extended the study to understand the unsaturated throughput with limited retransmissions (e.g., Malone et al. in [28], Daneshgaran et al. in [29] and Nguyen et al. in [30]). Meanwhile, IEEE 802.11p based communications in Vehicular Ad hoc Networks (VANETs) have been discussed in the literature (e.g., Ma et al. in [31], Misic et al. in [32], Campolo et al. in [33], and Yao et al. in [34]). While the above approaches were based on per-slot statistics, Tinnirello et al. in [35] utilized channel access cycles and design an enhanced non-slot method, which further increases the modeling accuracy.

However, the existing literature is still in lack of an cross-layer study/modelling, which combines the unique features of in-cabin Wi-Fi physical (PHY) layer with its Media Access Control (MAC) layer. In addition, existing models still exhibit some errors in high-density scenarios, mainly due to their imprecise estimations of time slot length. In this thesis, we improve the modeling accuracy with a precise estimation of time slot length, and utilize it in the development of cross-layer models to better characterize the in-cabin Wi-Fi systems.

2.3 Adaptive Techniques to Improve the Performance of Vehicular Communications

Considering the unpredictable dynamics in the driving environments, vehicular communications must be adaptive to guarantee a reliable and efficient performance. Various adaptive communication techniques have been developed for this purpose. They can be divided into two general types: the adaptations of communication variables and the adaptive protocols. Techniques of the first type conduct their adaptations within some established and fixed protocols, while techniques of the second type adjust the settings of protocols to satisfy the communication requirements.

2.3.1 The adaptations of communication variables

We next discuss the related work on the adaptations of communication variables. The transmission power and the data rate are two major dominating factors of communication performance. The adaptations of these two factors have been proven as effective and were utilized widely in industrial practice. Therefore, we mainly focus our discussions on these two factors. We also present several other variables being jointly used with the transmission power or the data rate.

Transmission Power Adaptation

Transmission power is a dominating factor determining the reliability of wireless communications. Power adaptation approaches have been studied in different systems including cellular networks, WLANs, and VANETs. Critical power in ad hoc networks has been extensively studied after the seminal work conducted by Gupta et al. in [36]. However, work in this line of research assumes that the total number of nodes in a network is known, which is not the case in many realistic scenarios. In addition, the theoretical mobility models (e.g., i.i.d. model and random walk models) may not be suitable for VANETs.

Another line of research focuses on adapting transmission power based on available context information, which is measured by and exchanged between communication units. There exist a large number of approaches based on centralized controller, such as those proposed by Zhang et al. in [37], by Tan in [38], by Helmy et al. in [39] and etc. However, they cannot be directly applied in MANETs and VANETs, due to the distributed nature

of such networks.

To align with the decentralized characteristic, approaches have been proposed to adapt transmission power in a (partially) distributed manner. Feedback mechanisms have been adopted. For example, Guan et al. in [40] effectively controlled the target transmission range by selecting a power setting no greater than necessary. The selection of transmission power relies on feedback beacons. Xu et al. in [41] utilized feedback information from the receiver and designed a joint frequency hopping and power adaptation approach for anti-jamming communication. Chen et al. in [42] established a power allocation game cognitive wireless mesh networks, and adopted feedback beacons to efficiently allocate transmission power of users. Mayers et al. in [43] adopted feedback based power control to achieve high energy efficiency and maintain quality of service simultaneously.

Handshaking mechanisms such as RTS/CTS have been also leveraged. For instance, Li et al. in [44] designed a power controlled MAC protocol based on RTS/CTS message exchanges to enable spatial reuse. Luo et al. in [45] developed a joint power and rate control method also utilizing RTS/CTS and channel reciprocity. Unfortunately, RTS/CTS packets are not applied by DSRC active safety applications.

There also exist approaches based on probing messages or extra message exchanges. Ramachandran et al. in [46] developed a systematic two-phase power and rate control approach. The proposed power control is based on a heuristic method, which transmits a series of probing packets to find minimum power for transmission. Being developed for general 802.11 WLANs, this heuristic method is not suitable for vehicular networks, where the probing results can be easily outdated due to dynamic movements of vehicles. In addition, the probing procedure introduces unavoidable overhead. Torrent-Moreno et al. in [47] developed a efficient transmission power control scheme to enhance fairness in V2V communications. The proposed scheme disseminates power settings to all neighboring vehicles via extra messages. Lu et al. in [48] proposed to piggyback the power setting in safety messages to reduce overhead. But the power adaptation would degenerate greatly if the delivery of safe messages is already unreliable.

In general, the overhead introduced by all aforementioned methods could be very large. To guarantee the timeliness of the shared information, feedback, handshaking or probing messages need to be exchanged frequently, consuming a great amount of the precious channel resource. In addition, as the traffic density increases, this overhead may raise exponentially.

More recently, several heuristic approaches have been proposed to avoid message exchange overhead in VANETs. Huang et al. in [49] developed a distributed method based a local metric named average channel occupancy. Based on this metric, each vehicle adapts its transmission power according to an empirical linear relation. Rawat et al. in [50] leveraged traffic flow theory in designing a joint power and contention window size adaptation method, which adjusts power based on traffic density. The traffic density is estimated locally using the 12-bit sequence number of the IEEE 802.11 MAC header. However, all these methods adopt an identical power level for vehicles in proximity, which is merely a suboptimal coordination policy. Moreover, these methods rely on empirical relations between transmission power and certain context parameters. Such relations require a great amount of work in measurement, yet may easily change in different scenarios, making huge efforts in vain.

To avoid these drawbacks, in this thesis, we develop a fully distributed power coordination method named DisCo. It adaptively coordinates the transmission power of each vehicle with purely local information, yet still achieves a significant improvement in the global communication performance.

Data Rate Adaptation

Classic data rate adaptation methods have been widely developed for stationary wireless networks. For example, Kamerman et al. in [51] developed a rate adaptation method ARF, which adjusts the data rate according to the number of successive packet losses. Wong et al. in [52] proposed to adapt data rates according to packet loss ratios, so as to guarantee the robustness of static IEEE 802.11 based networks. Bicket in [53] designed SampleRate, which takes the average of per-packet transmission delay as the rate adaptation criterion. However, these methods neglect the mobility of nodes, and usually require a relatively long measurement period to sample the information. Therefore, they cannot adapt to the dynamic vehicular environment. In addition, they never consider the coupling between transmission power and data rate. They may result in suboptimal performance of DSRC, and even fail to converge.

On the contrary, in MANETs or VANETs, the impact of mobility has been explicitly considered. Holland et al. in [54] developed RBAR, which adapts the data rate based on a receiver-based SNR measurement approach. This approach allows RBAR to operate

distributively. Chen et al. in [55] extended the design of the receiver-based approach, and proposed a rate adaptation method named RAM to handle the channel asymmetry. Vutukuru et al. in [56] designed a rate adaptation method SoftRate, which adjusts the data rate according to the channel bit error rate. Shankar et al. in [57] proposed to leverage context information such as velocity and distance in rate adaptation. They developed CARS, which is a customized rate selection method for VANETs. Lee et al. in [58] gathered empirical data from a vehicular testbed to objectively compare different rate adaptation schemes in VANETs.

However, adapting either data rate or transmission power (or any other individual communication variable) is not adequate to achieve the optimal communication performance. To this end, we should simultaneously optimize and adjust several variables.

Joint Adaptation and Other Adaptive Variables

There exist a number of joint transmission power and data rate adaptation methods in VANETs. We next discuss several cutting-edge ones. Li et al. in [44] proposed MRPC, which controls the multi-rate power leveraging RTS-CTS messages. Nevertheless, methods based on handshaking or feedback messages are not suitable for DSRC safety communications. This is because DSRC safety communications are based on broadcast and provide no handshaking nor feedback messages. Ramachandran et al. in [46] developed Symphony, which is a fully distributed synchronous two-phase power and rate adaptation strategy. The first step of Symphony is to estimate the best performance and selects the corresponding data rate. The second step is to tune transmission power to approach estimated performance with the selected data rate. However, tuning the power setting in the second step costs a lot of time, and thus significantly reduces Symphony's efficiency in the highly dynamic vehicular environment.

Besides transmission power and data rate, other variables have also been utilized in the designs of joint adaptation approaches. For instance, Huang et al. in [49] proposed a joint transmission probability and power adaptation method to enhance the safety of driving. Rawat et al. in [50] proposed to jointly select transmission power and contention window size control, so as to improve the performance of data dissemination. Zhang et al. in [37] improved QoS of VANETs with a joint adaptation of power and sub-carrier allocation. Tielert et al. in [59] designed a joint approach that adjusts transmission power and beacon

generation frequency to reduce congestion and collisions in the wireless channels.

Nevertheless, most existing joint control methods are sequential connections of individual adaptation methods. Hence, they only provide suboptimal adaptation results and may not adapt quickly enough to the vehicular environment. Furthermore, the coupling among communication variables (e.g., transmission power, data rate, contention window size, and etc.) have not been fully explored. Neglecting this critical coupling would lead to unexpected performance degradation when we are trying to adapt several variables simultaneously.

To address these drawbacks, in this thesis, we propose an online control approach named OnCAR, which is able to capture the coupling between multiple communication variables and synchronously adjust them to the changing environment.

2.3.2 Adaptive Protocols

Beside the adaptations of communication variables, we can also adjust the settings of protocols to improve communication performance. We mainly discuss the existing adaptive scheduling protocols and adaptive MAC protocols with CSMA. The reason why we focus on these two types of adaptive protocols is that they have been extensively adopted in existing Wi-Fi and cellular networks. We further present several other adaptive protocols including adaptive Time Division Multiple Access (TDMA). For techniques in each sub-category, we point out their drawbacks in the vehicular environments, and discuss how our proposed schemes and frameworks address these drawbacks.

Adaptive Scheduling

A wealth of work exists on the scheduling of multimedia streaming over wireless networks. For example, Pahalawatta et al. [60] proposed to adjust the scheduling decisions based on channel quality. Dua et al. [61] jointly considered the impacts of channel, deadline and distortion in the design. Li et al. [62] combine the scheduling with the OFDMA subcarrier assignment to improve end-to-end video quality. However, the above algorithms are designed for a centralized network. Hence, they are not suitable to schedule the fully distributed in-cabin Wi-Fi APs.

A number of distributed video scheduling algorithms have been proposed. For instance, Chuah et al. [63] designed an energy-efficient scheduling and resource allocation scheme

for video streaming in wireless mesh networks (WMNs). However, the assumption that no packet is lost due to delay is invalid in a vehicular scenario. Zhang et al. [64] develop a packet-level transmission distortion model, where content priority, delay and channel condition are jointly considered. This algorithm would consume a large amount of time to estimate the dynamic parameters of a changing AP topology. In general, we are still in need of a fully distributed scheduling algorithm that is robust in a varying environment.

To support delay sensitive applications, such as video streaming in VANETs, a delay/deadline-aware scheduling algorithm is a must. A number of generalized delay/deadline-aware scheduling algorithms have been proposed in the literature. Centralized algorithms, such as those proposed by Hou et al. in [65] and by Wu et al. in [66], are not suitable for a fully distributed vehicular network. Besides centralized approaches, distributed delay/deadline-aware scheduling algorithms have been proposed. Caccamo et al. [67] proposed a distributed approach named implicit Earliest Deadline First (EDF) scheduling, which establish the scheduling pattern with a relative long initiation stage. Kanodia et al. in [68] designed a distributed algorithm, which exchanges the EDF priorities among nodes. Bai et al. [69] designed a joint rate adaption and scheduling scheme for wireless networked control systems. Given the knowledge of the network structure, this scheme is robust to environmental disturbances. However, all these scheduling schemes require either an initiation stage, message exchanges or prior knowledge of topology, and thus are impractical in highly dynamic scenarios such as the in-cabin Wi-Fi scenarios.

Instead, in this thesis, we proposed DRIVING, which exhibits both the fully distributed and delay-aware features required by the in-cabin Wi-Fi systems. DRIVING eliminates the uses of message exchanges and initiation stage, and explicitly considers the delay of video packets in the scheduling decisions. As a result, it achieves much better QoS than that of existing scheduling algorithms in the context of video streaming.

MAC with Adaptive CSMA

In order to improve the communication performance in a dynamic scenario, a variety of adaptive CSMA algorithms have been proposed. The basic idea of adaptive CSMA algorithms is to adjust the channel access probabilities of wireless nodes according to local and/or neighbouring information. A number of these algorithms are based on message exchanges. For example, Gupta et al. in [70] designed Q-SCHED, which relies on queue

length information exchanges during the control slots. Qian et al. in [71] encapsulated the interference tolerance in the exchange messages to minimize interference. Zhou et al. in [72] proposed a distributed scheduling and routing scheme, where congestion messages are exchanged among neighbors. AkulaAneesh et al. in [73] analyzed the impact of delayed information exchanges, and quantified the throughput loss due to the delay. In [74], Si et al. proposed a selection mechanism for multimedia P2P networks. To maximize throughput and energy efficiency, receivers are required to send multicast messages to potential senders in each transmitting time slot. However, message exchanges introduce a large communication overhead in a dense VANET. Meanwhile, protocols based on message exchanges are hardly supported by commodity Wi-Fi APs.

Another line of research develops adaptive CSMA without message exchanges. Jiang et al. [75] proposed a transmission length control algorithm, which adjusts CSMA parameters according to historical AP service rates locally. Rad et al. [76] considered discrete time collisions and unsaturated transmissions in their adaptive CSMA design, and developed a Network Utility Maximization (NUM) based algorithm. They also discuss the tradeoff between long-term efficiency and short-term fairness. Ni et al. [77] proposed the Hybrid Q-CSMA algorithm, which assigns small backoff counters to nodes with long queues. However, the delay and deadline of video packets have not been considered. In addition, the above algorithms assume a random packet arrival process, which is different from the periodic video streaming traffics [78]. Scheduling multimedia streaming with these algorithms may lead to frequently lagging and buffering behaviors in video playback.

In this thesis, we retrofit the design of the distributed CSMA/CA scheme to embrace the delay-aware feature, and apply this upgraded scheme in the design of DRIVING. This allows DRIVING to have both delay-aware and distributed features.

Other Adaptive Communication Protocols

Adaptive routing in VANETs has been extensively studied. According to Dua et al. in [79], routing schemes in VANETs can be categorized into topology based routing (e.g., Toutouh et al. in [80] and Liu et al. in [81]), clustering based routing (e.g., Pan et al. in [82] and Wang et al. in [83]), geography based routing (e.g., Kim et al. in [84] and Lee et al. in [85]), data fusion based routing (e.g., Wagh et al. in [86] and Zhang et al. in [87]) and hybrid routing (e.g., Al-Rabayah et al. in [88] and Minh et al. in [89]).

Adaptive Time Division Multiple Access (TDMA) approaches have also been developed for VANETs. In [90], Rhee et al. proposed DRAND, which establishes a collision free TDMA-based scheduling with an initiation stage. In [91], Bilstrup et al. divided time into frames, each of which is a repeated sequence of a fixed number of slots. Each node listens to the channel before transmission, and selects an empty slot for transmission in the next frame. Omar et al. in [92] proposed VeMAC that reduces collisions by allocating disjoint sets of time slots to vehicles moving in opposite directions. To better support video streaming in 802.11p based VANETs, Han et al. in [93] integrated the EDCA scheme in their algorithm. Each Access Category (AC) obtains a certain share of time slots, and messages in one AC only access the Control Channel (CCH) during the corresponding share. As a result, collisions in the wireless channel is further decreased. Yet, TDMA based distributed scheduling algorithms usually waste a considerable portion of time resource when the vehicle density is low. To tackle this, Soldo et al. in [94] proposed to combine distributed TDMA and CSMA to reclaim part of the wasted time resource.

However, the above TDMA algorithms are still incompatible with most of today's Wi-Fi or DSRC devices.

Chapter 3

Enhancing the Safety of Connected Vehicles

3.1 Overview

A recent study by the U.S. DOT estimated that V2V communication systems can deal with 74 percent of crashes [1], potentially saving thousands of lives and billions of dollars every year. To boost the development of V2V communication systems, U.S. DOT announced to start working on regulations that require DSRC devices being installed on new light-duty vehicles. The DSRC technology enables a variety of safety-related vehicular applications including lane changing assistance, forward collision warning, blind spot warning, etc [11].

In North America, the most widely accepted DSRC standard employs IEEE 802.11p Wireless Access for Vehicular Environments (WAVE) at PHY and MAC layers. The 802.11p based DSRC is fundamentally different from other communication technologies such as Wi-Fi, Bluetooth, and Zigbee.

- DSRC functions in highly dynamic vehicular environments, where unpredictable disturbances may largely undermine communication performance.
- The licensed 5.9 GHz spectrum is exclusively allocated to DSRC. Thus, DSRC transmissions are free of interference from transmissions of other technologies. DSRC designates one specific channel for safety related messages. Hence, transmissions of safety messages are not affected by transmissions of non-safety messages.

- To meet the stringent delay requirements and benefit all surrounding vehicles, DSRC safety messages are transmitted in a broadcasting manner. Hence, it is highly possible that the channel becomes saturated in a dense traffic condition.

In DSRC, there are two types of safety-related messages: routine safety messages and emergency safety messages. Routine safety messages contain the kinematic information (e.g., GPS position, velocity and acceleration) and sensory information (e.g., braking and collision.) of vehicles. Each vehicle periodically broadcasts its routine safety messages with a frequency of 10-20 messages per second. Emergency safety messages are sent out if dangerous or abnormal events are detected. They have higher transmission priorities and higher reliability requirements than routine safety messages. Neighboring vehicles utilize both routine and emergency messages to infer the situation of the surrounding. Based on this knowledge, each vehicle quickly reacts to the traffic conditions, avoids potential collisions, and optimizes its future movements. In industrial practice, the size of safety messages is 300-500 bytes.

To enhance the driving safety of connected vehicles, it is of significant importance to improve the performance of DSRC. The reasons are as follows. The DSRC technology is the foundation of many safety-related applications. They rely on DSRC messages to exchange vehicle dynamics, which are utilized to make decisions for collision avoidance, lane changing, traffic scheduling, etc. In order to make effective and timely decisions, the DSRC messages must 1) be successfully transmitted; 2) be delivered as fast as possible; and 3) arrive as many traffic participants as possible. Otherwise, some vehicles may either fail to react to a danger, or react too late to avoid the emergency. The functionalities of vehicular applications are significantly degraded, failing to improve the driving safety. Therefore, to improve DSRC performance is essential in enhancing the driving safety of connected vehicles.

In order to guarantee its performance, DSRC has to adapt to highly dynamic, fully distributed and unpredictable vehicular environments. This mission is challenging, mainly due to the following two issues.

- 1) At the vehicle level, adapting multiple communication variables is difficult, because these variables are strongly coupled with each other. Such couplings, as well as their impacts on DSRC performance, are implicit and hard to be captured in advance. Neglecting these couplings results in poorly performed DSRC systems, especially in highly volatile

vehicular environments. Error propagation in multi-stage variable adjustment processes must be eliminated as well.

- 2) At the network level, due to the lack of coordination between vehicles, the global performance of DSRC could be significantly degraded by egocentric variable adaptations. The state-of-the-art approaches coordinate individual DSRC units with extra coordination messages. The corresponding overhead is expected to grow explosively during rush hours. To make things worse, the coordination messages will be outdated quickly in the dynamic vehicular environments.

To tackle these issues, we develop **advanced control approaches** in this chapter.

- 1) To address the strong coupling between communication variables in volatile environments, we develop a novel online synchronous control approach. We use transmission power and data rates as an example, and design the Online Control Approach of power and Rate (OnCAR) based on systematic control theories. OnCAR embraces the strong couplings between communication variables with a MIMO control model, and adjusts these variables in a joint and synchronous manner.
- 2) To coordinate DSRC units with zero coordination overhead, we propose a series of strictly distributed coordination schemes, namely DisCo. DisCo estimates the performance targets of neighbors, infers the potential interferences from and to the others, and coordinates its own communication variables based on these purely local estimations. In this way, it avoids the communication overhead while still coordinating the individuals effectively.

3.2 Performance Metrics

Before going into the design details, we first present the metrics used to evaluate the performance of DSRC. In this chapter, we consider three types of DSRC performance, the reliability, the efficiency and the fairness. Concretely, the DSRC reliability is captured by the effective Packet Delivery Ratio (ePDR), the DSRC efficiency is described by the effective throughput (eTPUT), and the DSRC fairness is represented by the Coefficient of Variation (CV) of ePDR. The term “effective” indicates that each vehicle is only interested in the information within an effective range d_{eff} (e.g., with a radius of 300m or 1000m from the

vehicle). The information from vehicles outside this range is irrelevant to the current safety. Packets from vehicles outside the effective range may be successfully received by PHY and MAC layers. But they will be discarded by upper layers, and will not be considered by the control approach.

The ePDR of a vehicle i is defined as

$$\text{ePDR}_i = \frac{\sum_{j \in \Omega_{eff}^{(i)}} N_r(i, j)}{\sum_{j \in \Omega_{eff}^{(i)}} N_t(j)}, \quad (3.1)$$

where i and j are vehicle IDs, $N_t(j)$ denotes the number of packets transmitted by j , $N_r(i, j)$ represents the number of packets transmitted by j while successfully received by i , and $\Omega_{eff}^{(i)}$ represents the set of neighbors within the effective range of i . $\Omega_{eff}^{(i)}$ is expressed as

$$\Omega_{eff}^{(i)} = \{j | j \neq i \text{ and } d(i, j) \leq d_{eff}\}, \quad (3.2)$$

where $d(i, j)$ is the distance between i and j .

The CV of ePDR across all vehicles is then adopted as the metric of fairness.

The eTPUT of a vehicle i is defined as

$$\text{eTPUT}_i = \sum_{j \in \Omega_{eff}^{(i)}} N_r(i, j) \times \Gamma, \quad (3.3)$$

where Γ is the packet length of safety messages.

Given the above definitions, we can now discuss how to improve the performance metrics of DSRC with our proposed approaches.

3.3 Online Synchronous Control Approach of Multiple Communication Variables

In this section, we aim to improve the DSRC performance by adapting communication variables at the vehicle level. We first illustrate the challenges of this mission, and then address these challenges with the online synchronous control approach of multiple communication variables. For the sake of clarity, we adopt the combination of two dominating variables, i.e., transmission power and data rates, as an example. The corresponding approach is

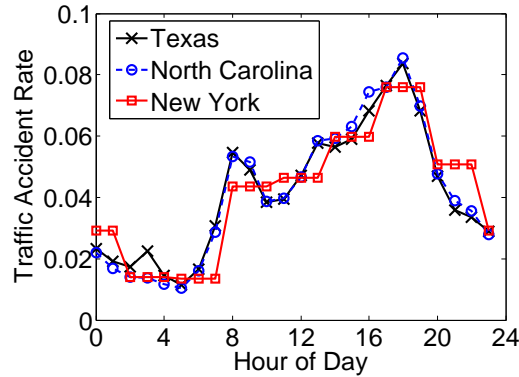


Figure 3.1 Traffic accident rate across different time of day.

called OnCAR - Online Control Approach of power and Rate.

3.3.1 Observations and Challenges

We next present several important observations to illustrate the challenges in improving DSRC performance at the vehicle level. These challenges are the major motivations for us to develop a new adaptation approach of communication variables.

The first observation is summarized as follows.

Observation 1. *The number of traffic accidents arrives its peak during **rush hours** (i.e., 16:00 to 20:00) .*

Observation 1 is supported by government sources such as Texas Motor Vehicle Crash Statistics [95], North Carolina Crash Data [96] and New York State Department of Motor Vehicles [97]. To demonstrate and validate this observation, we use the crash data of year 2014 from Texas, and that of year 2013 from North Carolina and New York (the latest available data). Figure 3.1 presents the traffic accident rate, i.e., the percentage of traffic accidents, across different time of day. Figure 3.1 confirms Observation 1, as the peaks of traffic accident rates appear during rush hours for all three states. In addition, the shapes of accident rates are very similar in different states, indicating a strong correlation between traffic accident rate and time. Therefore, in this thesis, we consider rush hours to be far more critical than other time periods.

To improve DSRC performance during both rush and regular hours, the **coupling** between transmission power and data rates must be carefully considered. This is motivated

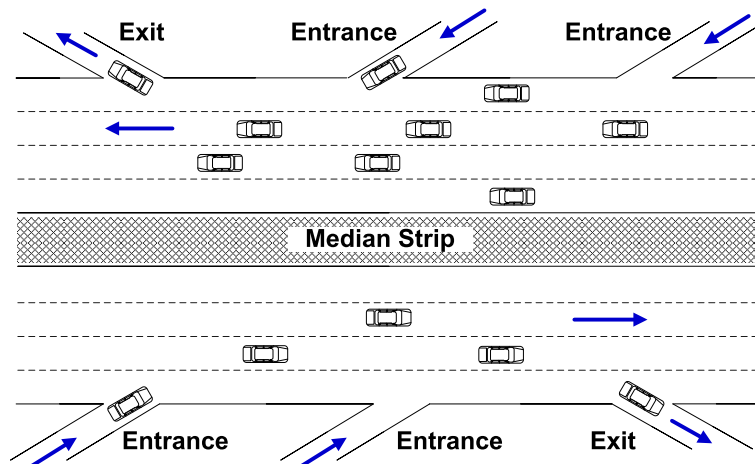


Figure 3.2 The simulated highway scenario.

by the second observation as follows.

Observation 2. *The coupling between transmission power and data rates is implicit and complicated, and may lead to largely degraded performance of DSRC.*

For example, higher transmission power could support higher data rates for potentially higher DSRC throughput. Yet, it also intensifies the interference, to which higher data rates are vulnerable. Lower power could alleviate interference for potentially better DSRC reliability. However, it supports only lower data rates, which deliver less information for safety. In addition, packets with lower data rates may be more vulnerable to hidden terminals due to the longer propagation delays. Such a complicated correlation can hardly be captured by existing heuristics, resulting in degraded performance of DSRC.

We further demonstrate Observation 2 with trace-driven ns-2 simulations in a bi-directional highway scenario as illustrated in Figure 3.2. This highway is of 2000 meters long and 30 meters wide with four lanes in each direction. There are two entrances and one exit along each direction.

We first implement a Transmission Power Adaptation (TPA) approach [37, 40] and a Data Rate Adaptation (DRA) approach [55, 57] (Both of them are state-of-the-art approaches on individual power or rate adaptation). TPA fixes the data rate as $3Mbps$ (the default data rate of DSRC) and adaptively adjusts transmission power. DRA fixes transmission power as $20dBm$ (the default power setting) and adaptively changes data rates. We then combine them sequentially to build a Joint Power and Rate Adaptation (JPRA)

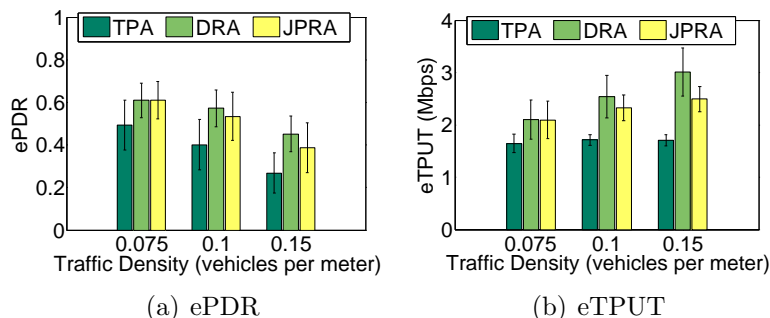


Figure 3.3 Illustration of performance degradations due to negligence of the power-rate coupling.

approach, which is extended from the one proposed in [46]). JPRA first selects power based on TPA, and then chooses a data rate based on DRA.

Figure 3.3 compares ePDR and eTPUT of the three approaches under different traffic density conditions. We observe that the joint approach JPRA performs much worse than the individual approach DRA in terms of both ePDR and eTPUT. This result suggests that the data rates selected by JPRA are not well supported by the chosen transmission power. Adjusting these two variables one by one (which is common practice in existing solutions) can lead to a mismatched pair of power and rate settings.

This observation indicates that a good approach must calculate and conduct the adjustments of power and rates at the same time (i.e., *synchronously*), instead of changing them sequentially. To design such a joint and synchronous control approach for DSRC, we have to tackle several challenges.

Challenge 1. *The coupling of variables, as well as their impacts on DSRC performance, is implicit and hard to be captured in advance. A mismatched combination of variables may be selected due to either the negligence of their coupling or an asynchronous adjustment procedure.*

Challenge 2. *The vehicular environment is extremely volatile, introducing a variety of unpredictable disturbances to the control and adaptations of variables.*

Challenge 3. *Due to the high density during rush hours and the lack of coordination between vehicles, the overall fairness of DSRC could be significantly degraded by egocentric power/rate adaptations. DSRC safety-related applications mainly adopt broadcast, which involves no feedback information.*

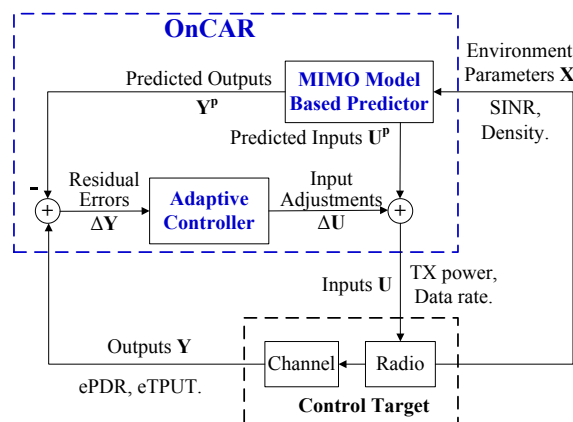


Figure 3.4 Architecture of OnCAR.

3.3.2 Overview of OnCAR

To address the aforementioned challenges, we propose OnCAR - the online control approach of power and rates. We first introduce the fundamental components of OnCAR, and discuss conceptually how the challenges are tackled.

Figure 3.4 presents the architecture of OnCAR. It is a controller that runs on each in-vehicle DSRC radio in a distributed manner. The objective of OnCAR is to optimize the system outputs (i.e., ePDR and eTPUT) of the target system by adjusting the system inputs (i.e., transmission power and data rates). Meanwhile, it has to take the fairness into consideration. OnCAR is composed of a feed forward control loop and an adaptive feedback control loop. The feed forward loop provides a baseline initiation to the feedback loop, so as to increase the convergence speed of OnCAR. Moreover, the feedback loop improves the baseline initiation and further increases the performance of OnCAR.

To address Challenge 1, the feed forward loop utilizes a MIMO model based predictor. This predictor takes measurements of environment parameters (i.e., a vector \mathbf{X} consists of the Signal-to-Interference-plus-Noise Ratio (SINR) value and the neighbor density) to select a pair of transmission power and data rate to optimize ePDR and eTPUT. The selected pair is used as the predicted inputs (denoted as \mathbf{U}^p) to the target system. The parameters of this MIMO model are updated periodically. They describe the input-output mapping, and capture the coupling between two system inputs (i.e., transmission power and data rates) as well.

However, the MIMO model used in the predictor can only serve as an approximation

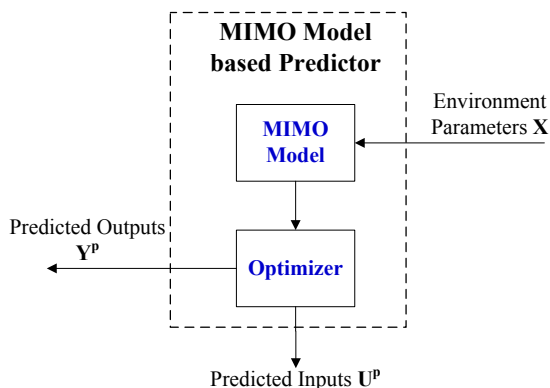


Figure 3.5 Architecture of the MIMO model based predictor.

of the dynamic target system. The predicted ePDR and eTPUT (denoted as predicted outputs \mathbf{Y}^p) may be off from the measured ePDR and eTPUT (denoted as system outputs \mathbf{Y}), resulting in “residual” control errors. Meanwhile, the unpredictable disturbances in the vehicular environments enlarge these errors.

To correct residual errors and **address Challenge 2**, we further develop an adaptive feedback control loop in OnCAR. This loop first compares the system outputs \mathbf{Y} with the predicted outputs \mathbf{Y}^p to calculate the residual errors (denoted as $\Delta\mathbf{Y}$). Then an online adaptive controller estimates a regression model of residual errors using these measurements. With this online trained regression model, the adaptive controller produces input adjustments (denoted as $\Delta\mathbf{U}$) to minimize the residual errors. The adaptive nature of this controller helps us cope with dynamic disturbances in the vehicular environment. The input adjustments are called control inputs, while the corresponding residual errors are control outputs. The adaptive nature of this controller helps us cope with dynamic disturbances in the vehicular environment and errors due to model inaccuracies.

To address Challenge 3, OnCAR utilizes receiver-side measurements of system outputs and environment parameters to feed the aforementioned control loops. Adopting such measurements makes each vehicle to consider the performance of its neighbors, and thus improves the overall fairness. It also enables OnCAR to operate on each vehicle in a fully distributed manner.

3.3.3 Design of MIMO Model Based Predictor

The core module of the feed forward control loop in OnCAR is the MIMO model based predictor, whose architecture is shown in Figure 3.5. For every pair of power and rate in DSRC, the predictor first uses a MIMO model to predict its corresponding output of ePDR and eTPUT. Based on these outputs, an optimizer selects the best pair to maximize ePDR and eTPUT. This selected pair is then provided to the target system as the predicted inputs \mathbf{U}^p , while the corresponding ePDR and eTPUT pair is provided to the feedback loop as the predicted outputs \mathbf{Y}^p . Note that measurements of environment parameters (i.e., SINR and neighbour density) are needed as the inputs of the MIMO model. We leave the detailed measurement process till Section 3.3.5.

The MIMO Model

The mathematical expression of the MIMO model is a function F mapping the environment parameter vector \mathbf{X} and input vector \mathbf{U} to output vector \mathbf{Y} :

$$\mathbf{Y} = F(\mathbf{X}, \mathbf{U}). \tag{3.4}$$

Note that this MIMO model F is a general model that can generalize most existing algorithms. There are a number of approaches in designing this MIMO model (i.e., the function F).

One candidate design of the MIMO model is to incorporate existing individual power control and rate adaptation algorithms. For example, to control the transmission power, the MIMO model could leverage the mapping from neighbour density to transmission power employed by Guan et al. in [40]. At the same time, the MIMO model could adapt the mapping from link quality to data rate used by Shankar et al. in CARS [57], so as to select the best data rate according to the environment parameters. In this way, the MIMO model based predictor can perform as well as the state-of-the-art schemes on individual rate adaptation or power control.

In this thesis, we adopt an approach that is more consistent with industry practice. Considering the potentially large measurement results of DSRC from current and future industry simulations and tests, we propose to train the MIMO model with them. This approach can be easily applied by automobile industry in deployments with their test data.

In this thesis, the MIMO model is trained with fine grained ns-2 simulation traces. We collected training data of 244 pairs of inputs (i.e., power and rate settings \mathbf{U}) in 3660 traffic conditions. We also recorded SINR values, and collected another group of training data for environment parameters \mathbf{X} . The total size of training data is over $1TB$ in binary format. Applying the least squares model fitting technique [98] on the training data, we obtained our MIMO model F .

The Optimizer

Based on the MIMO model F and measurements of the environment parameters \mathbf{X} , the optimizer produces the predicted inputs and outputs. Denote the predicted inputs as $\mathbf{U}^p = [u_1^p, u_2^p]$, where u_1^p denotes the predicted selection of transmission power and u_2^p represents the predicted selection of data rate. Denote the predicted outputs as $\mathbf{Y}^p = [y_1^p, y_2^p]$, where y_1^p is the predicted ePDR and y_2^p is the predicted eTPUT. The optimizer is designed to maximize a weighted sum of y_1^p and y_2^p as follows.

$$\begin{aligned} & \underset{\mathbf{U}^p}{\text{Maximize}} && y_1^p + \sigma y_2^p, \\ & \text{Subject to} && \mathbf{Y}^p = F(\mathbf{X}, \mathbf{U}^p), \\ & && u_1^p \in U_1, u_2^p \in U_2, \end{aligned}$$

where σ is a parameter that scales ePDR to the level of eTPUT, U_1 is a finite set of available power levels, and U_2 is a finite set of available data rates.

3.3.4 Design of Adaptive Controller

As mentioned in Section 3.3.2, the predicted outputs \mathbf{Y}^p of the MIMO model predictor may be off from the measured system outputs \mathbf{Y} . This leads to “residual” errors. In addition, these errors can be enlarged by the unpredictable disturbances in vehicular environments. To eliminate these errors and adapt to the dynamic environment, we further introduce an adaptive feedback control loop.

The key component of this adaptive feedback control loop is an adaptive controller, which is illustrated in Figure 3.6. This controller is composed of an online parameter estimator and an online parameter estimator with a control law. The online estimator provides estimates of time-varying parameters at each control instant. Based on these

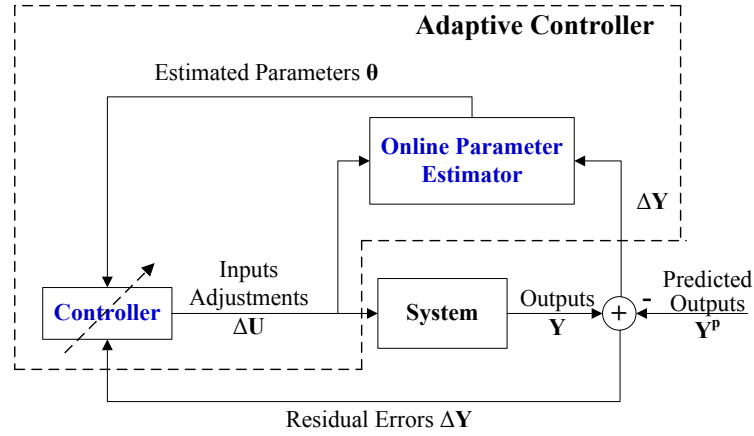


Figure 3.6 Architecture of the adaptive controller.

estimates, the control law calculates control inputs to achieve the control objective. Here the control objective is to minimize the residual errors. The calculated control inputs are then used to adjust the predicted inputs given by the MIMO model based predictor. We adopt a direct adaptive control scheme [99] for this adaptive controller.

In the design of the online parameter estimator, we apply a linear regression model to capture the relation between control inputs $\mathbf{S}(k)$ and control outputs $\mathbf{R}(k)$. Here $\mathbf{S}(k)$ represents the input adjustments $\Delta\mathbf{U}$ at time interval k , while $\mathbf{R}(k)$ corresponds to the residual errors $\Delta\mathbf{Y}$ at time interval k . Note that this regression model (which maps $\Delta\mathbf{U}$ to $\Delta\mathbf{Y}$) is different from the MIMO model F (which maps \mathbf{U} and \mathbf{X} to \mathbf{Y}). The adaptive feedback control scheme is described by a difference equation model as

$$A(q^{-1})\mathbf{R}(k) = B(q^{-1})\mathbf{S}(k) + e(k), \quad (3.5)$$

where

$$A(q^{-1}) = 1 - a_1q^{-1} - \dots - a_nq^{-n}, \quad (3.6)$$

$$B(q^{-1}) = b_0q^{-1} + \dots + b_{n-1}q^{-n}, \quad (3.7)$$

q^{-1} is the back shift operator (which operates on an element of a time series to produce the previous element), n is the order of the regression model (which is to be chosen in the evaluation part). Note that the digital implementation of the controller introduces a

one-step delay between the current control inputs and the corresponding control outputs. In this case, the control inputs at time interval $k - 1$ (i.e., $\mathbf{S}(k - 1)$) will affect the control outputs at time interval k (i.e., $\mathbf{R}(k)$).

In order to cope with the disturbances in the vehicular environments, the model parameters are updated periodically. At each time interval, control outputs are measured and fed into the online parameter estimator. The estimator combines these outputs with the corresponding past control inputs to estimate the model parameters $a_i (i = 1, \dots, n)$ and $b_j (j = 1, \dots, n)$. Based on these estimates, the controller calculates future control inputs to correct the residual errors. To this end, we apply a Recursive Least Square (RLS) scheme [100] for the online parameter estimator. Denote

$$\phi(k) = [\mathbf{R}(k - 1), \dots, \mathbf{R}(k - n), \mathbf{S}(k - 1), \dots, \mathbf{S}(k - n)]^T, \quad (3.8)$$

and

$$\theta(k) = [a_1(k), \dots, a_n(k), b_0(k), \dots, b_{n-1}(k)]^T. \quad (3.9)$$

We convert Eq. (3.5) to an RLS-friendly format as follows

$$\mathbf{R}(k) = \phi^T(k)\theta(k). \quad (3.10)$$

In Eq. (3.10), $\theta(k)$ denotes the true parameters to be estimated at time interval k . Applying the RLS algorithm, we can obtain the estimated parameters $\hat{\theta}(k)$ at time interval k . In detail, the RLS algorithm computes

$$\varepsilon(k) = \mathbf{R}(k) - \phi^T(k)\hat{\theta}(k - 1), \quad (3.11)$$

$$\begin{aligned} \mathbb{P}(k - 1) &= \mathbb{P}(k - 2) - [1 + \phi^T(k)\mathbb{P}(k - 2)\phi(k)]^{-1} \\ &\quad \cdot \mathbb{P}(k - 2)\phi(k)\phi^T(k)\mathbb{P}(k - 2), \end{aligned} \quad (3.12)$$

$$\hat{\theta}(k) = \hat{\theta}(k - 1) + \mathbb{P}(k - 1)\phi(k)\varepsilon(k), \quad (3.13)$$

where $\mathbb{P}(k)$ is an auxiliary matrix that is only used during the computation of the RLS algorithm. The estimated parameters $\hat{\theta}(k)$ contain the estimates of model parameters a_i and b_j . The RLS algorithm updates Eq. (3.12) and (3.13) in each sampling interval, and

thus the model parameters are estimated in an online manner. The initial condition of the above RLS algorithm is $\mathbb{P}(-1) = p_0 I$, where $p_0 > 0$ and I is an identity matrix.

Based on the estimated parameters $\hat{\theta}(k)$, the control law is calculated by solving the following equation

$$\phi^T(k)\hat{\theta}(k) = \mathbf{R}^*(k), \tag{3.14}$$

where $\mathbf{R}^*(k)$ is the control reference. As stated in the beginning of this subsection, the adaptive controller aims to minimize the residual errors. Hence, we set $\mathbf{R}^*(k) = 0$. As defined in Eq. (3.8), $\phi(k)$ encapsulates past control outputs $\mathbf{R}(k-1), \dots, \mathbf{R}(k-n)$, past control inputs $\mathbf{S}(k-2), \dots, \mathbf{S}(k-n)$, and current control inputs $\mathbf{S}(k-1)$. By solving Eq. (3.14), we achieve current control inputs $\mathbf{S}(k-1)$. Note that $\mathbf{S}(k-1)$ correspond to input adjustments $\Delta\mathbf{U}$. Here, the control law determines how the controller adjusts the control variables in each control interval.

However, directly applying the control law based on Eq. (3.14) may result in large variations in two consecutive control inputs, jeopardizing the stability and convergence of OnCAR. In addition, abrupt oscillations of transmission power and data rates would introduce undesirable disturbances to neighbor vehicles. To address this issue, we integrate a smooth control mechanism in the control law. The corresponding smooth control law aims to minimize the following cost function

$$\begin{aligned} \mathbb{J} = & E\{ \|\mathbb{W}(\mathbf{R}(k+1) - \mathbf{R}^*(k+1))\|^2 \\ & + \|\mathbb{Q}(\mathbf{S}(k) - \mathbf{S}(k-1))\|^2 \}, \end{aligned} \tag{3.15}$$

where $\|\cdot\|$ is the 2-norm operation, \mathbb{W} and \mathbb{Q} are weighting matrices. Their relative magnitude controls the tradeoff between performance and stability. In this thesis, \mathbb{W} and \mathbb{Q} are diagonal matrices, which are consistent with common practice. (Interested readers can refer to [99] for more details on settings of \mathbb{W} and \mathbb{Q} .) The goal of Eq. (3.15) can be interpreted as approaching the desired system outputs while controlling the changes of inputs.

Theorem 1. *The smooth control law is realized with the following control inputs*

$$\begin{aligned} \mathbf{S}(k) = & ((\mathbb{W}\hat{b}_0)^T \mathbb{W}\hat{b}_0 + \mathbb{Q}^T \mathbb{Q})^{-1} \cdot (\mathbb{Q}^T \mathbb{Q} \mathbf{S}(k-1) \\ & + (\mathbb{W}\hat{b}_0)^T \mathbb{W}(\mathbf{R}^*(k+1) - \hat{\theta}(k)\tilde{\phi}(k))). \end{aligned} \tag{3.16}$$

Proof. We first define

$$\tilde{\phi}(k) = [\mathbf{R}(k-1), \dots, \mathbf{R}(k-n), 0, \mathbf{S}(k-2), \dots, \mathbf{S}(k-n)]^T. \quad (3.17)$$

Substituting $\hat{\theta}(k)$ and Eq. (3.17) into Eq. (3.15), we have

$$\begin{aligned} \mathbb{J} &= E\{\|\mathbb{W}(\hat{\theta}(k)\tilde{\phi}(k) + \hat{b}_0\mathbf{S}(k) + \varepsilon(k+1)) \\ &\quad - \mathbf{R}^*(k+1)\|^2\} + \|\mathbb{Q}(\mathbf{S}(k) - \mathbf{S}(k-1))\|^2 \\ &= \|\mathbb{W}(\hat{\theta}(k)\tilde{\phi}(k) - \mathbf{R}^*(k+1))\|^2 + \|\mathbb{W}\hat{b}_0\mathbf{S}(k)\|^2 \\ &\quad + 2\mathbf{S}^T(k)\hat{b}_0^T\mathbb{W}^T\mathbb{W}(\hat{\theta}(k)\tilde{\phi}(k) - \mathbf{R}^*(k+1)) \\ &\quad + \|\mathbb{Q}\mathbf{S}(k)\|^2 + \|\mathbb{Q}\mathbf{S}(k-1)\|^2 \\ &\quad - 2\mathbf{S}^T(k-1)\mathbb{Q}^T\mathbb{Q}\mathbf{S}(k) + E\|\mathbb{W}\varepsilon(k+1)\|^2. \end{aligned} \quad (3.18)$$

The cost function \mathbb{J} is at its minimum where the following derivative is zero.

$$\begin{aligned} \frac{\partial \mathbb{J}}{\partial \mathbf{S}(k)} &= 2(\mathbb{W}\hat{b}_0)^T\mathbb{W}(\hat{\theta}(k)\tilde{\phi}(k) - \mathbf{R}^*(k+1)) \\ &\quad + 2(\mathbb{W}\hat{b}_0)^T\mathbb{W}\hat{b}_0\mathbf{S}(k) \\ &\quad + 2\mathbb{Q}^T\mathbb{Q}\mathbf{S}(k) - 2\mathbb{Q}^T\mathbb{Q}\mathbf{S}(k-1) = 0. \end{aligned} \quad (3.19)$$

Solving Eq. (3.19), we obtain the smooth control law

$$\begin{aligned} \mathbf{S}(k) &= ((\mathbb{W}\hat{b}_0)^T\mathbb{W}\hat{b}_0 + \mathbb{Q}^T\mathbb{Q})^{-1} \cdot (\mathbb{Q}^T\mathbb{Q}\mathbf{S}(k-1) \\ &\quad + (\mathbb{W}\hat{b}_0)^T\mathbb{W}(\mathbf{R}^*(k+1) - \hat{\theta}(k)\tilde{\phi}(k))). \end{aligned} \quad (3.20)$$

□

3.3.5 Measuring System Outputs and Environment Parameters

As we mentioned earlier, OnCAR needs the measurements of system outputs (i.e., ePDR and eTPUT) and environment parameters (i.e., SINR and neighbor density) to feed the MIMO model based predictor and the adaptive controller. In this thesis, we propose to measure these values at the receiver side. The reason of using receiver-side measurements

is two-fold. 1) Due to the channel reciprocity in DSRC¹, receiver-side measurements serve as a good estimation of a vehicle's own transmission performance. To enhance its own performance, a vehicle would improve receiver-side measurements. 2) Each vehicle would like to obtain more safety messages from its neighbor, so as to enhance its own driving safety with more information. Therefore, each vehicle is also self-motivated to improve the performance of its neighbors.

The measurements of system outputs are achieved as follows. At each time interval, each DSRC radio measures eTPUT by counting the number of received packets sent by neighbors within the effective range. To measure ePDR, each DSRC radio leverages the 12-bit sequence number in the sequence control field of an IEEE 802.11 MAC header. The expected number of transmitted packets is approximated by the difference between the maximum and minimum sequence numbers. Then ePDR is estimated as the ratio of the number of received packets to the expected number of transmitted packets.

To measure the density of neighbor, each DSRC radio extracts the sender's MAC address encapsulated in the MAC header, and counts the number of neighbors based on this distinct MAC address. To measure the SINR value, each DSRC radio first measures the SINR value of each packet sent by a neighbor within the effective range. Then an average value of SINR is calculated. Both parameters are then provided to OnCAR as the environment parameters.

3.4 Evaluating OnCAR with Simulations

In this section, we evaluate OnCAR with trace-driven ns-2 simulations. We demonstrate that OnCAR perform consistently well all the time including rush hours. Concretely, we first present the performance improvement of OnCAR during the most critical period (the rush hours), with real-life traces. We then adopt simulations with synthetic traces to demonstrate that OnCAR also bring large improvements in all time periods.

¹We are aware of the debate on the existence of channel reciprocity in general. In the context of DSRC, field tests [101] already confirmed the existence of channel reciprocity.

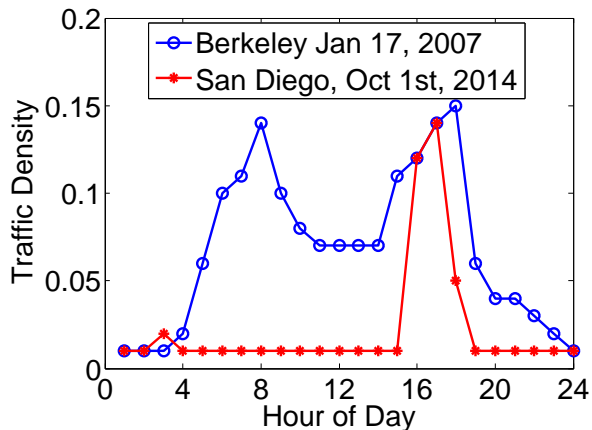


Figure 3.7 Real-life traffic density traces.

3.4.1 Evaluation Setup

Traffic Traces

We establish real-life traffic scenarios with two real-life traffic data sets. One data set [102] records the traffic density of Berkeley on Jan. 17, 2007. The other data set [103] traces the traffic density of San Diego on Oct. 1st, 2014. The traffic densities of Berkeley and San Diego data sets are presented in Figure 3.7. In both scenarios, traffic density achieves the maximum value during rush hours (i.e., 16:00 to 20:00 in this thesis).

Real-life traffic traces are mostly available in metropolis areas. There may be cases that are not covered by currently accessible traces. To cover as many those cases as possible, we also conduct simulations in ten synthetic scenarios representing a diverse group of traffic conditions.

Traffic data sets in the real-life and synthetic scenarios provide density information from the view of a highway. To generate microscopic vehicle dynamics, we combine the density information with a vehicle movement trace generator SUMO². In this way, we obtain a set of traces on vehicle dynamics, which describe the time-varying speeds, positions and destinations of all vehicles on a bi-directional highway.

This highway has a speed limit of 100 kilometers per hour. The layout of this highway has been illustrated in Figure 3.2. This highway is of 2000 meters long and 30 meters wide with four lanes in each direction. It has a median strip to separate two directions. Upon

²Simulation of Urban Mobility: <http://sumo-sim.org/>

Table 3.1 Settings of the bi-directional highway.

Description	Value
Total length	2000m
Total width	36m
Width of median strip	4m
Lanes in each direction	4
Speed limit	100km/h
Number of entrances	4
Number of exits	2

arriving at the end of one direction, vehicles re-enter the highway at the beginning of the other direction. There are two entrances and one exit along each direction., one locating at the beginning of that direction while the other locating at the 1-kilometer spot. In addition, there is an exit at the end of each direction. Upon arriving at the end of one direction, vehicles re-enter the highway at the beginning of the other direction. Meanwhile, vehicles that leave through the exits will re-enter the highway through the entrances. The above settings are summarized in Table 3.1.

DSRC Propagation Model

To capture the signal propagation in real DSRC scenarios, we adopt the field-test results reported by Cheng et al. in [2]. Concretely, the path loss function $L(d)$ of DSRC is modeled as a two-slope function, i.e.,

$$L(d) = \begin{cases} -10\tau_1 \log_{10}\left(\frac{d}{d_0}\right), & d_0 \leq d \leq d_c, \\ -10\tau_1 \log_{10}\left(\frac{d_c}{d_0}\right) - 10\tau_2 \log_{10}\left(\frac{d}{d_c}\right), & d \geq d_c, \end{cases} \quad (3.21)$$

where d denotes the distance between transmitter and receiver; d_0 is the reference distance; d_c is the equivalent transmission distance; τ_1 and τ_2 are both path loss factors. Empirical values of the parameters are summarized in Table 3.2.

Table 3.2 Empirical values of parameters in DSRC propagation model [2].

Description	Value
Reference distance d_0	1m
Equivalent transmission distance d_c	220m
path loss parameter τ_1	1.9
path loss parameter τ_2	4.0

DSRC Radio Settings

Each DSRC radio follows the DSRC standards and broadcasts safety messages periodically on DSRC Channel 172. The broadcasting period of messages is 0.05 seconds. The effective range of communication is 300 meters. The data encapsulated in each packet is of 500 bytes, while the packet headers are added based on IEEE 802.11p protocols. The options of data rates include $3Mbps$, $6Mbps$, $12Mbps$, and $24Mbps$. The available transmission power ranges from $10dBm$ to $30dBm$, with a $2dBm$ step. In addition, each vehicle is equipped with one DSRC radio.

3.4.2 Approaches Studied

We implement and evaluate the following four power/rate adaptation approaches in the simulations.

- OnCAR is our proposed approach. It combines a MIMO model based predictor with an online adaptive controller. OnCAR runs on each vehicle distributively.
- Transmission Power Adaptation (TPA) is an individual transmission power adaptation approach. It is developed based on state-of-the-art individual power adaptation approaches proposed in [37, 40]. TPA uses a fixed data rate of $3Mbps$.
- Data Rate Adaptation (DRA) is an individual rate adaptation approach. It is implemented based on state-of-the-art individual data rate adaptation approaches proposed in [55, 57]. DRA fixes transmission power as $20dBm$ and adapts data rates based on its measured environment parameters (i.e., channel SINR and neighbor density).
- Joint Power and Rate Adaptation (JPRA) is a joint and heuristic adaptation approach. We leverage state-of-the-art designs of joint approaches proposed in [46, 50, 59]

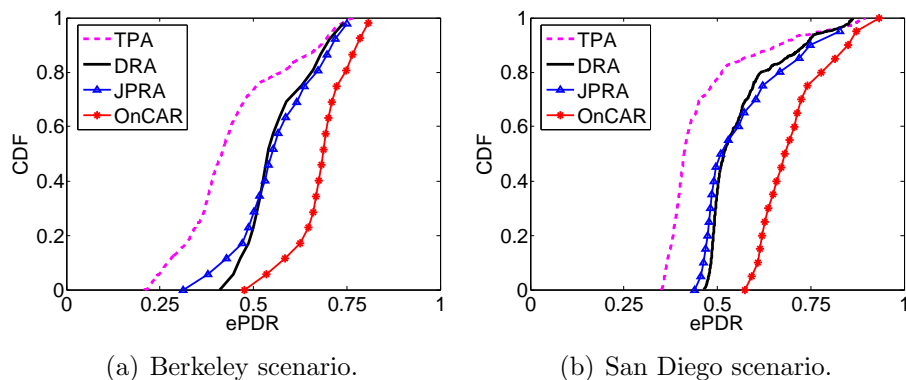


Figure 3.8 CDFs of ePDRs in real-life scenarios at rush hours.

Table 3.3 Statistics of ePDRs at rush hours of Berkeley.

Approach	mean	Improvement by OnCAR	max	min
TPA	0.4431	53.9%	0.7691	0.2084
DRA	0.5624	21.2%	0.8038	0.4091
JPRA	0.5593	21.9%	0.7686	0.3126
OnCAR	0.6818	—	0.8469	0.4768

to develop JPRA. It combines TPA and DRA sequentially: it first determines the transmission power, and then selects a data rate.

In the simulations, sampling and control intervals of all approaches are 1 second.

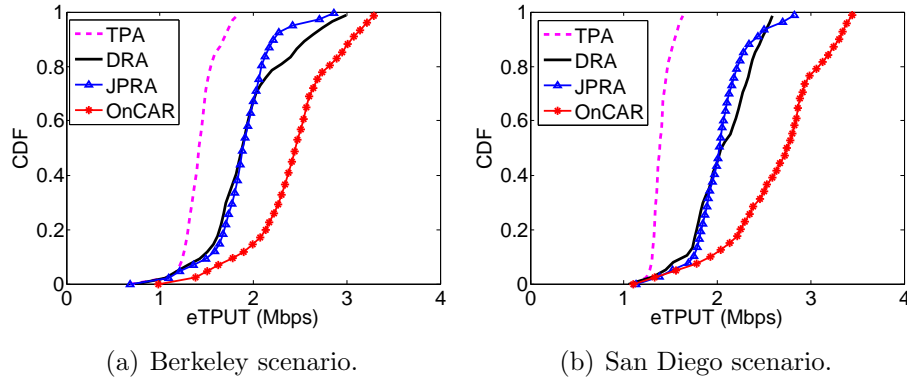
3.4.3 DSRC Reliability in Real-life Scenarios

We first evaluate the reliability in terms of ePDR. We focus on the rush hours, i.e., 16 : 00 to 20 : 00. The Cumulative Distribution Functions (CDFs) of ePDRs at rush hours are presented in Figure 3.8. It is shown that OnCAR achieves the best reliability with the largest ePDR.

We further summarize several statistics of ePDRs at rush hours in Table 3.3 (for Berkeley scenario) and Table 3.4 (for San Diego scenario). The statistics include mean, maximum and minimum values of ePDRs, as well as the mean ePDR improvements of OnCAR over other approaches. Compared with JPRA, OnCAR improves the average reliability of DSRC by 21.9% and 23.7%, respectively. Moreover, OnCAR achieves the highest minimum and maximum ePDR among all approaches. This suggests that the improvement in reliability

Table 3.4 Statistics of ePDRs at rush hours of San Diego.

Approach	mean	Improvement by OnCAR	max	min
TPA	0.4631	51.2%	0.8973	0.3507
DRA	0.5636	24.2%	0.8650	0.4628
JPRA	0.5659	23.7%	0.9052	0.4387
OnCAR	0.7002	--	0.9335	0.5728

**Figure 3.9** CDFs of eTPUT in real-life scenarios at rush hours.

benefits every vehicle. In addition, we observe that the joint approach JPRA achieves a lower ePDR than that of the individual approach of DRA. This again confirms that sequential adjustments of power and rates sometimes result in a mismatched pair of these two variables, leading to a compromised DSRC performance. The synchronous control adopted by OnCAR address this issue by embracing the strong coupling with a MIMO control model. It enables OnCAR to select the optimal choices of power and rates. Hence, OnCAR addresses **Challenge 1**, and greatly enhances DSRC reliability of all vehicles

3.4.4 DSRC Efficiency in Real-life Scenarios

We further evaluate the efficiency of OnCAR in terms of eTPUT. We present the CDFs of eTPUT for all approaches during rush hours in Figure 3.9. It is shown that OnCAR achieves the largest eTPUT and thus the best efficiency of DSRC. Therefore, we conclude that among all the approaches, OnCAR provides the highest efficiency of DSRC.

We also summarize the mean, minimum and maximum of eTPUT, as well as the mean eTPUT improvement by OnCAR over other approaches, in Table 3.5 and Table 3.6. Note

Table 3.5 Statistics of eTPUT at rush hours of Berkeley.

Approach	mean	Improvement by OnCAR	max	min
TPA	1.4287	70.3%	1.8768	0.6808
DRA	1.9280	26.2%	0.7364	3.0836
JPRA	1.8869	28.9%	0.6840	2.9088
OnCAR	2.4324	--	0.9816	3.4264

Table 3.6 Statistics of eTPUT at rush hours of San Diego.

Approach	mean	Improvement by OnCAR	max	min
TPA	1.3986	88.9%	1.6732	1.1120
DRA	2.0479	29.0%	2.6728	1.0512
JPRA	2.0307	30.1%	2.9300	1.1288
OnCAR	2.6416	--	3.5072	1.1040

that the unit of eTPUT in Table 3.5 and Table 3.6 is Mbps. Compared with the state-of-the-art joint approach JPRA, OnCAR enlarges the overall efficiency of DSRC by 28.9% and 30.1%, respectively. Furthermore, we find that OnCAR’s improvements in eTPUT is larger than that in ePDR (in terms of percentage). In other words, OnCAR further enlarges the eTPUT beyond the increment brought by an enhanced ePDR.

3.4.5 DSRC Fairness in Real-life Scenarios

The metric of fairness, i.e., the CV of ePDRs, is presented in Figure 3.10. It is shown that, in both scenarios, OnCAR achieves the lowest CV and hence the best fairness among all approaches. To quantify the improvement in fairness, we summarize the decreases in CV of ePDRs brought by OnCAR in Table 3.7. Compared to JPRA, OnCAR significantly improves the fairness across all vehicles by up to 44.0% and 40.1%, respectively. These improvements are mainly brought by the receiver-side measurement mechanism of OnCAR. This mechanism establishes an implicit feedback loop, which forces vehicles to consider the performance of their neighbors. Therefore, OnCAR helps vehicles achieve enhanced reliability and improved fairness simultaneously, and indeed addresses **Challenge 3**.

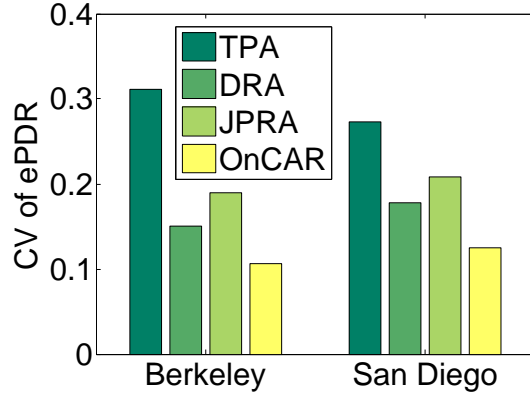
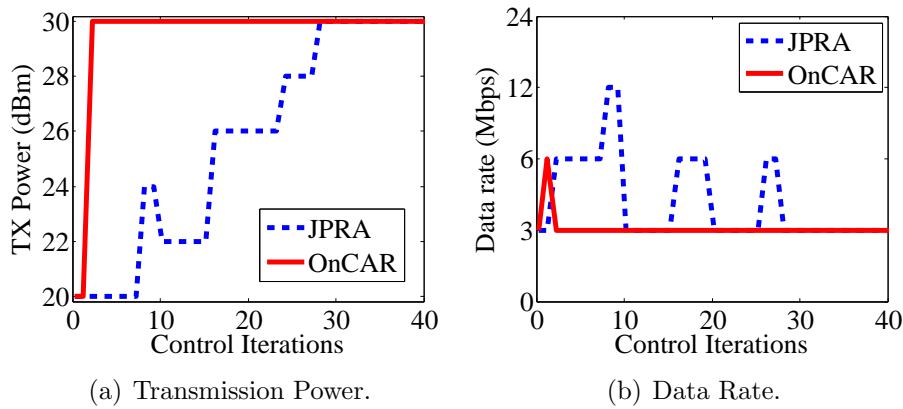


Figure 3.10 CV of ePDR in real-life scenarios.

Table 3.7 OnCAR’s improvements in fairness over others.

Fairness Improvement	Berkeley	San Diego
Over TPA	65.8%	54.2%
Over DRA	29.4%	29.8%
Over JPRA	44.0%	40.1%



(a) Transmission Power.

(b) Data Rate.

Figure 3.11 Convergence in San Diego Scenario.

Table 3.8 Traffic densities of ten synthetic scenarios.

Scenario	T_1	T_2	T_3	T_4
#1	0.025	0.05	0.075	0.1
#2	0.1	0.075	0.05	0.025
#3	0.025	0.075	0.05	0.1
#4	0.025	0.1	0.025	0.1
#5	0.025	0.125	0.05	0.15
#6	0.025	0.2	0.025	0.2
#7	0.05	0.1	0.025	0.15
#8	0.05	0.025	0.15	0.1
#9	0.1	0.025	0.05	0.15
#10	0.1	0.15	0.025	0.05

3.4.6 Convergence Speed in Real-life Scenarios

We further evaluate the convergence speed of different approaches. We compare OnCAR with JPRA, while omitting TPA and DRA as they only adjust one individual variable. We extract the results at the very beginning of the simulations, when all vehicles just start to adapt their power and rates. Figure 3.11 presents the selections of power and rates across time. It is demonstrated that power and rates of OnCAR converge much faster than those of JPRA. While OnCAR achieves a convergence of both variables in only 3 control iterations, JPRA requires almost 30 control iterations. This is because the sequential adaptation procedure in JPRA is sensitive and vulnerable to the dynamics in the environment. Changes in one variable sometimes evoke cascading oscillations across two variables for a relatively long period. OnCAR avoids this problem with a synchronous control of both variables. In this way, OnCAR addresses **Challenge 2** and significantly increases the convergence speed.

3.4.7 Evaluation in Synthetic Scenarios

In this section, we demonstrate that OnCAR achieves large improvements during not only rush hours but also other time periods. To this end, we establish ten synthetic scenarios, each of which is generated with an unique synthetic traffic density trace. These synthetic scenarios allow us to evaluate OnCAR in a more comprehensive manner. Each trace is divided into four periods denoted by T_1 , T_2 , T_3 and T_4 , respectively. Traffic density in each

Table 3.9 OnCAR’s improvements over others in the synthetic scenarios.

Density	Approach	$\Delta ePDR$	$\Delta eTPUT$	ΔCV
0.075	TPA	39.7%	53.9%	65.8%
	DRA	12.9%	17.4%	39.1%
	JPra	18.8%	21.0%	44.1%
0.1	TPA	63.7%	78.1%	62.8%
	DRA	21.0%	25.6%	27.2%
	JPra	21.6%	31.0%	48.4%
0.15	TPA	87.0%	98.5%	45.3%
	DRA	42.4%	30.8%	26.9%
	JPra	29.0%	35.7%	38.5%

period is different from the previous one. The traffic densities of ten synthetic scenarios are summarized in Table 3.8. The unit of traffic density is vehicles per meter.

To better compare the approaches, we group simulation results into five density sets. For example, we group the ePDRs during T_3 of scenario #1, T_2 of scenario #2 and T_2 of scenario #3 as the set of density 0.075. For better clarity, we focus on the results of a low density set (i.e., density 0.075), one medium density set (i.e., density 0.1), and one high density set (i.e., density 0.15). We summarize OnCAR’s improvements in mean ePDRs, mean eTPUT and CV of ePDRs over other approaches in Table 3.9. It is confirmed that OnCAR delivers the most reliable, efficient and fair performance across different traffic densities.

3.5 Evaluating OnCAR on a Testbed

In this section, we implement OnCAR on a testbed, and compare OnCAR with several cutting-edge approaches in the existence of hidden terminals. These experiments serve as a compliment to the trace-driven simulations.

3.5.1 Testbed Setup

Testbed Overview

Our testbed consists of three Universal Software Radio Peripheral (USRP) B210 boards, one USRP X310 motherboard, one USRP CBX 120 daughterboard, three iRobot-Creat

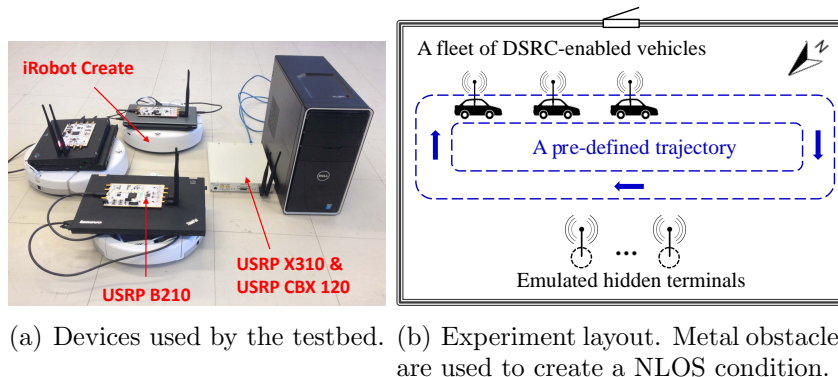


Figure 3.12 A testbed to evaluate OnCAR.

robots, three laptops and one desktop as shown in Figure 3.12(a). With this testbed, we conduct experiments in emulated scenarios as shown in Figure 3.12(b). There are three DSRC-enabled vehicles driving together as a car fleet. The car fleet follows a pre-defined trajectory. None-Line-of-Sight (NLOS) scenarios are emulated by introducing several metal obstacles between antennas. This setting simulates common real-life traffic scenarios, where LOS paths between two vehicles are often blocked by other vehicles or road-side buildings. The vehicles are constantly communicating with each other on DSRC Channel 172 (i.e., the 10 MHz DSRC channel centered at 5.86 GHz). Furthermore, since hidden terminals are one of the major reasons of performance degradation in DSRC, we also emulate a number of hidden terminals on Channel 172.

DSRC Radios Setup

DSRC radios are implemented on USRP B210 boards, where DSRC protocols are realized in GNU radio³. To enable DSRC capabilities, we have revised and extended the GNU radio code of IEEE 802.11p developed by Bloessl et al. in [104]. Each DSRC radio broadcasts safety messages on DSRC Channel 172 with a period of 0.1 seconds. The data encapsulated in each packet is of 500 bytes. The packet headers are then added based on IEEE 802.11p protocols. Moreover, we implement OnCAR and other power/rate adaptation approaches in GNU radio. The options of data rates include *3Mbps*, *6Mbps*, *12Mbps*, and *24Mbps*. Note that the implemented approaches adjust the virtual power gain in GNU radio instead of real transmission power of B210 boards. The manufacturers of B210 boards do not

³GNU radio: <http://gnuradio.org>



Figure 3.13 The components of a DSRC-enabled vehicle and their connections.

provide any official calibrated mapping. As a result, we resort to an unofficial calibration of USRP B210⁴ to map the virtual power gain in GNU radio to real transmission power as follows

$$P_{real} = \begin{cases} 0, & 0 \leq P_{vir} < 50, \\ (P_{vir} - 80) \text{ dBm}, & 50 \leq P_{vir} < 90, \\ 10 \text{ dBm}, & 90 \leq P_{vir} \leq 100, \end{cases} \quad (3.22)$$

where P_{real} represents the real transmission power and P_{vir} denotes the virtual power gain in GNU radio. This unofficial mapping certainly introduces some calibration errors (In fact, even an official mapping yields some errors due to the device diversity). These errors are treated as disturbances by OnCAR, and can be cancelled by the adaptive controller effectively as discussed in Section 3.3.4.

DSRC-Enabled Vehicles Setup

Each DSRC-enabled vehicle consists of a DSRC radio, a laptop and an iRobot-Crete robot as illustrated by Figure 3.13. Packets successfully received by the DSRC radio are transmitted to the laptop via a USB 3.0 cable. Based on the information capsulated in these packets (e.g., sender IDs, sequential numbers in the MAC header and etc.), the laptop applies OnCAR (as well as other approaches) to adjust transmission power and data rates. These adjustments are then fed to the USRP B210 board through the USB 3.0 cable. In

⁴Transmission power calibration of USRP Bus series: http://forums.ni.com/ni/attachments/ni/500/1420/1/b200_rev4_TX_FE1.pdf

addition to power and rate adjustments, the laptop also controls the movement of the iRobot-CREATE robot. The movement commands are sent to the robot via a USB-serial conversion cable. The laptop and the radio board are mounted on top of the robot for the ease of movement.

Interference from Hidden Terminals

In our testbed, we emulate the communication behaviors of hidden terminals. Each hidden terminal works as a DSRC radio, except that it neither adjusts its power/rate nor follows the CSMA/CA mechanism (because they are hidden from the three DSRC radios). The interference from hidden terminals is implemented with one USRP X310 motherboard and one USRP CBX 120 daughterboard. To emulate multiple hidden terminals with a limited number of devices, we design the message generation procedure of the USRP X310 motherboard as follows. For each hidden terminal, the testbed generates an i.i.d. random numbers between $0ms$ to $99ms$ as the starting time of packet transmission in every $100ms$ time slot. If the transmissions of multiple hidden terminals overlap, the overlapped packets will be merged into one packet with extended size, so that the transmission time of this large packet equals the total transmission time of all these overlapped packets. The transmission power of this large packet will then be multiplied by the number of overlapped packets. Note that, in this way (i.e., aggregating the power of overlapped transmissions from hidden terminals), we emulate the worst-case situation of the hidden terminal problem. This allows us to conduct worst-case analysis of experiment results and derive reasonable insights.

3.5.2 Experiment Results

For each approach, we repeat experiments five times with the same setting. To evaluate the impact of hidden terminals, we vary the number of hidden terminals and collect a group of experiment results.

DSRC Reliability

We first evaluate DSRC reliability in terms of ePDR. Figure 3.14 compares the ePDRs of approaches with different number of hidden terminals. In addition to the mean value of ePDRs, the error bars in Figure 3.14 demonstrate the deviations of ePDRs across five experiment instances. As expected, ePDRs decrease with the increase of the number of

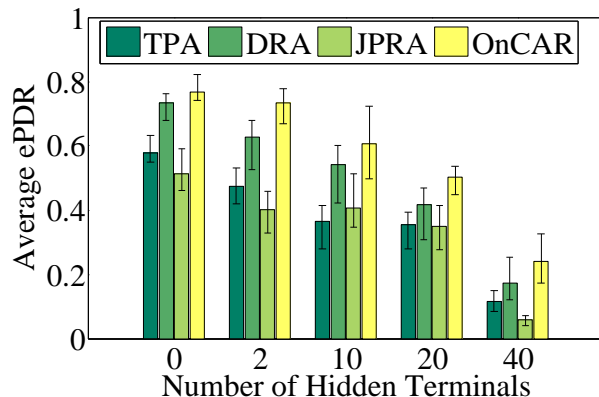


Figure 3.14 Average ePDRs of DSRC-enabled vehicles in the existence of hidden terminals.

hidden terminals. Compared with the second best approach, OnCAR improves the average ePDR by up to 40.1%.

Furthermore, we observe that the joint approach JPRA performs worse than DRA. This phenomenon again suggests that the coupling between transmission power and data rate must be properly addressed. JPRA selects transmission power before data rate, thus it fails to capture this important coupling. Its selection of transmission power sometimes does not match its selection of data rate. As a result, JPRA provides a suboptimal reliability that is even worse than an individual approach. On the contrary, OnCAR utilizes a MIMO model to characterize the relation between system inputs (i.e., transmission power and data rate) and system outputs (i.e., ePDR and eTPUT). The coupling of power and rate is implicitly captured by this model. Therefore, OnCAR produces a synchronous pair of power and rate, achieving a better reliability than existing individual and joint approaches.

DSRC Efficiency

We next evaluate another equivalently important goal of OnCAR - the efficiency of DSRC. Figure 3.15 compares CDFs of eTPUTs provided by different approaches. It is shown that OnCAR always achieves a higher eTPUT than all other approaches under different numbers of hidden terminals. In addition, when there exist hidden terminals (e.g., the cases shown by Figure 3.15(b)-(d)), the maximum eTPUTs provided by OnCAR are always higher than that of other approaches. Therefore, we conclude that OnCAR handles the hidden terminal problem much better than existing approaches.

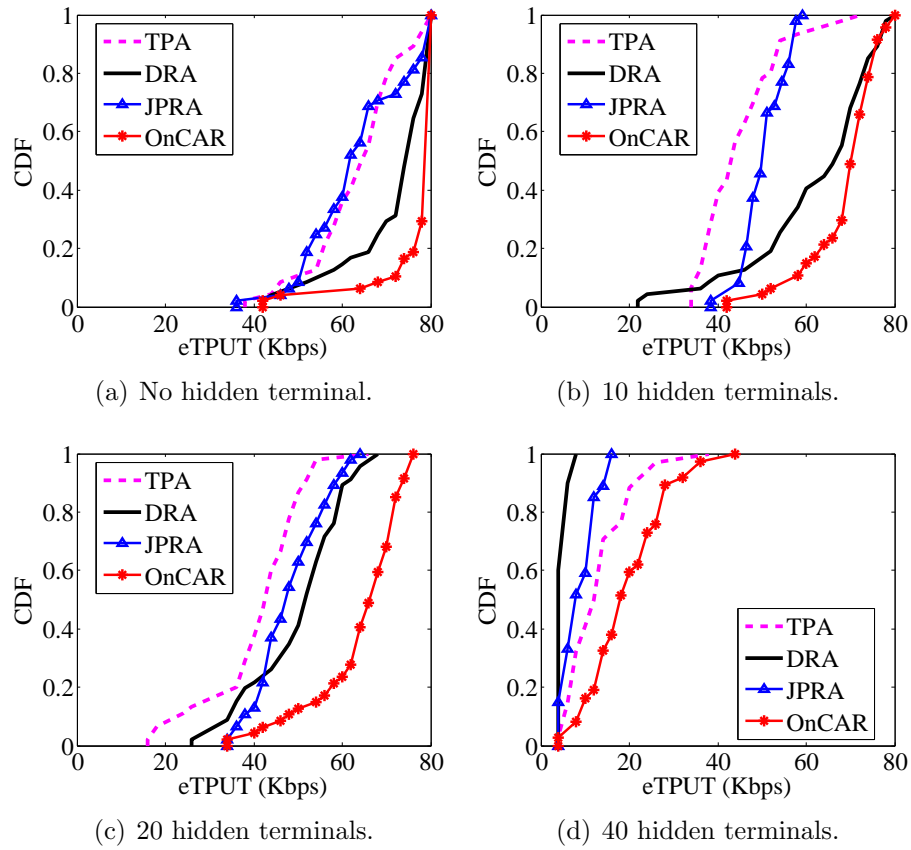


Figure 3.15 CDFs of eTPUTs of DSRC-enabled vehicles.

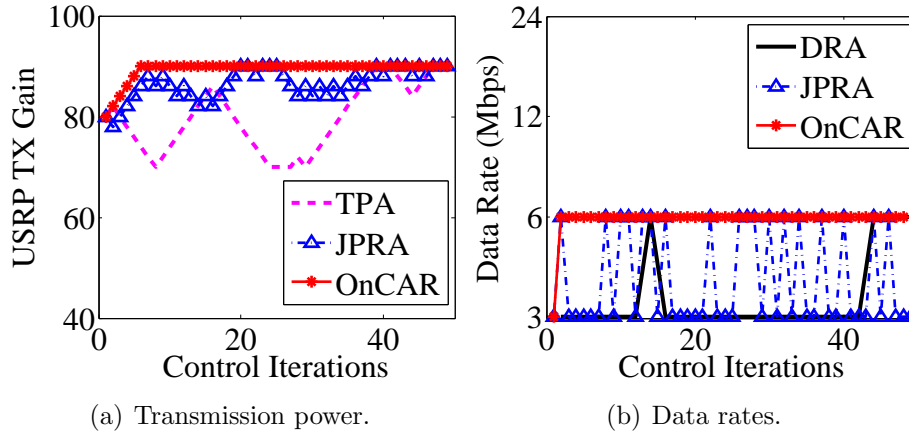


Figure 3.16 Convergence of power and rate adaptations when there are 10 hidden terminals.

Convergence

The convergence is an important consideration for approaches in dynamic environments. Therefore, we further evaluate the convergence of OnCAR and other approaches. We take the case of 10 hidden terminals as an example. Figure 3.16 demonstrates the convergence of power and rate adaptations. As DRA does not adjust transmission power, we do not include its curve of transmission power in Figure 3.16(a). For a similar reason, we do not include TPA in Figure 3.16(b). It is shown in Figure 3.16 that the adaptations of DRA, TPA and JPRA oscillate and fail to converge. This is because that they are essentially heuristic solutions and cannot guarantee the convergence of system in noisy environments. Furthermore, JPRA is the most unstable one among all heuristic solutions. The reason is that JPRA adjusts transmission power before data rate. When the selection of transmission power oscillates, the selection of data rate is affected and thus magnifies the oscillations. On the contrary, OnCAR converges quickly to the optimal pair of power and rate, and provides the most stable performance. This is because OnCAR is developed based on systematic control theories. The smooth control law Eq. (3.16) of OnCAR not only adjusts power and rate adaptively, but also guarantees the convergence of the controller.

3.6 Strictly Distributed Coordination

In order to further improve DSRC performance, we need to go beyond the boundary of a single vehicle, and accomplish the mission from a network perspective. Besides optimizing the selections of communication variables locally, vehicles must further coordinate these variables to achieve a global optima. Therefore, in this section, we study how to improve DSRC performance at the network level.

In large-scale vehicular networks, the overhead of coordination messages could be tremendous. This overhead grows even larger during rush hours. Hence, a strictly distributed coordination scheme with no coordination message is desirable. 1) It completely eliminates the overhead of coordination. 2) It aligns with the distributed nature of vehicular networks, where centralized control units such as Road-Side Units (RSUs) are sparse, especially in the early stage of DSRC deployment. 3) It is fully compatible with current DSRC protocols, requiring no modification. However, this mission, i.e., *developing a strictly distributed scheme to coordinate transmission power of DSRC units with zero coordination overhead*, seems unachievable, and was never fulfilled previously.

To accomplish this apparently impossible mission, in this section, we develop a series of strictly distributed coordination schemes, namely DisCo. To better illustrate the design of DisCo, we adopt transmission power as an example of the communication variable being coordinated, and use the reliability and fairness of DSRC as the target metrics being optimized.

The baseline DisCo scheme is called DisCo with Fixed Targets (DisCo-FT). A fairness assumption of DisCo-FT is that all DSRC units are aiming at the same ePDR target (although they may not end up with the same ePDR). It enables the strictly distributed coordination with an efficient distributed control technique, assuming that all units targets an ePDR of 100%. However, this assumption is greedy, and sometimes makes the DisCo-FT overly aggressive in the coordination. This is because, by assuming all neighbors are greedy, a DSRC unit may become reluctant to coordinate with others. On the contrary, if every unit reduces its targeted ePDR slightly, the DSRC channels can become less congested, leading to more reliable DSRC for all. In order to achieve better coordination between individual DSRC units, we release the assumption and develop an advanced scheme named DisCo with Adaptive Targets (DisCo-AT). By applying an online control loop, DisCo-AT adaptively estimates the optimal ePDR target, and its transmission power accordingly to

further enhance DSRC reliability and fairness.

3.6.1 Problem Statement and Challenges

Consider a vehicular network where N DSRC units are within the carrier sense range of each other. Unit i , $i = 1, 2, \dots, N$, aims to adjust its ePDR $x_i(t)$ to achieve its ePDR target $x_{mi}(t)$. Meanwhile, it would like to improve the fairness of DSRC to avoid being endangered by some uninformed vehicles. To this end, unit i would coordinate its transmission power u_i with its $N - 1$ neighbors. As an example, we focus on the strictly distributed power coordination problem, where each unit i has no knowledge of the transmission power (i.e., $u_j(t), j \neq i$), the ePDRs (i.e., $x_j(t), j \neq i$) and the ePDR targets (i.e., $x_{mj}, j \neq i$) of others.

There exist two major challenges in designing strictly distributed power coordination schemes in DSRC.

Challenge 4. *With absolutely no message exchange (i.e., neither feedback, handshaking nor probing), it seems impossible to coordinate the power of individual DSRC units.*

Challenge 5. *A strictly distributed coordination may sometimes yield overly aggressive or conservative coordination decisions.*

3.6.2 DisCo with Fixed Coordination Targets

To address Challenge 4, we first develop a strictly distributed power controller and adopt it in the design of DisCo. In this section, all DSRC units targets the maximum possible ePDR, i.e., a ePDR of 100%. Under this rule, each DSRC units aims to maximize its own ePDR. The corresponding DisCo scheme is called DisCo-FT, of which the architecture is illustrated in Figure 3.17. The distributed power controller is the core of DisCo-FT. It considers the ePDR $x_i(t)$ as the control output vector to be adaptively controlled by the control input of transmission power vector $u_i(t)$. The detailed design is presented as follows.

We first describe the subsystem of unit i , $i = 1, 2, \dots, N$ as

$$\dot{x}_i(t) = A_i x_i(t) + \zeta_i \left[\sum_{j=1, j \neq i}^N l_{ij}^T(t) x_j(t) + u_i(t) \right], \quad (3.23)$$

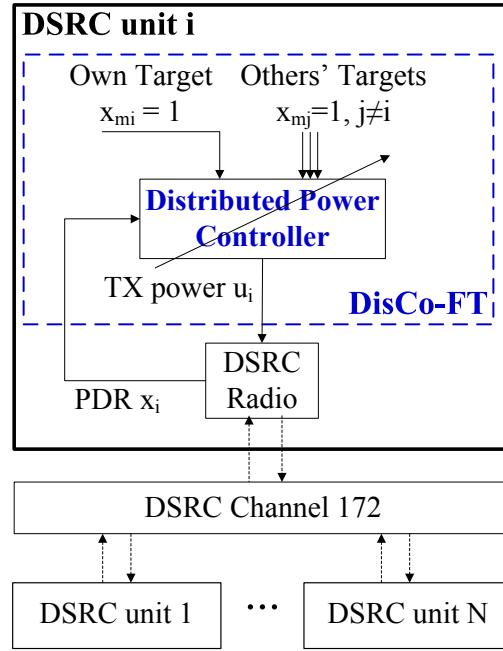


Figure 3.17 The architecture of DisCo-FT.

where $l_{ij}(t)$ are parameter vectors that capture the interconnection between units i and j , $l_{ij}(t)x_j(t)$ correspond to the impacts of units j , ($j \neq i$) on unit i , A_i are unknown parameter matrices to be determined, ζ_i are scaling constant vectors. (This model can be extended to capture non-linear systems [105] as well).

Suppose the reference model of unit i , $i = 1, 2, \dots, N$, is given by

$$\dot{x}_{mi}(t) = A_{mi}x_{mi}(t) + \zeta_i r_i(t), \quad (3.24)$$

where A_{mi} is a stable matrix, and $r_i(t)$ is a (known) bounded reference input vector. This reference model describes the desired output of each DSRC unit. This reference model represents the desired behavior that we would like each unit to follow. It acts as a guideline for the actual output (i.e., ePDR in our case).

Given A_{mi} , A_i , and ζ , we can find a constant vector k^* that satisfies the following linear equation

$$A_{mi} = A_i + \zeta_i k_i^{*T}, i = 1, 2, \dots, N. \quad (3.25)$$

The objective of the distributed power controller is to assure that the actual ePDR of unit

i follows that of the reference model with zero error. The tracking error is defined as

$$e_i(t) = x_i(t) - x_{mi}(t). \quad (3.26)$$

Then the objective of each distributed power controller is expressed as

$$\lim_{t \rightarrow \infty} \|x_i(t) - x_{mi}(t)\| = 0. \quad (3.27)$$

Lemma 1. *A straightforward solution to achieve this objective would be*

$$u_i(t) = r_i(t) + k_i^T x_i(t) - \sum_{j=1, j \neq i}^N \hat{l}_{ij}^T(t) x_j(t), \quad (3.28)$$

where k_i is an estimate of k^* , and $\hat{l}_{ij}(t)$ is an estimate of $l_{ij}(t)$, both of which can be adaptively updated by the controller.

Proof. Substitute Eq. (3.25) into Eq. (3.24), we have

$$\dot{x}_{mi}(t) = A_i x_{mi}(t) + \zeta_i k_i^{*T} x_{mi}(t) + \zeta_i r_i(t). \quad (3.29)$$

Combining Eq. (3.29) and Eq. (3.23), we have

$$\dot{x}_{mi}(t) - \dot{x}_i(t) = (A_i + \zeta_i k_i^{*T}) [x_{mi}(t) - x_i(t)] + \zeta_i \left[r_i(t) + k_i^{*T} x_i(t) - \sum_{j=1, j \neq i}^N \hat{l}_{ij}^T(t) x_j(t) - u_i(t) \right]. \quad (3.30)$$

We reorganize the above equation and obtain

$$\dot{e}_i(t) + Z_1 e_i(t) = Z_2, \quad (3.31)$$

where

$$Z_1 = -(A_i + \zeta_i k_i^{*T}), \quad (3.32)$$

and

$$Z_2 = \zeta_i \left[r_i(t) + k_i^{*T} x_i(t) - \sum_{j=1, j \neq i}^N \hat{l}_{ij}^T(t) x_j(t) - u_i(t) \right]. \quad (3.33)$$

Assume that the control system starts from stationary state with a zero tracking error,

then we have $e_i(0) = 0$ as the initial condition. Take the Laplace transform of Eq. (3.31), we have

$$sE_i(s) + Z_1E_i(s) = Z_2, \quad (3.34)$$

where $E_i(s)$ is the L-transform of $e_i(t)$, and s is a non-zero complex number. Hence,

$$E_i(s) = \frac{Z_2}{s + Z_1}. \quad (3.35)$$

In this case, minimizing $\|e_i(t)\|$ in the time domain is equivalent to minimizing $\|E_i(s)\|$ in the s -domain. And $\|E_i(s)\|$ is minimized when $Z_2 = 0$. Therefore, by setting Eq. (3.33) to zero, we obtain Eq. (3.28). \square

However, the solution given by Lemma 1 and Eq. (3.28) cannot deal with Challenge 4, where the state information $x_j(t), j \neq i$, is not available at unit i .

To achieve the objective without any knowledge of $x_j(t), j \neq i$, a revised solution is given as [106]

$$u_i(t) = r_i(t) + k_i^T x_i(t) - \gamma_i e_i^T(t) \mathbb{P}_i \zeta_i - \sum_{j=1, j \neq i}^N \hat{l}_{ij}^T(t) x_{mj}(t), \quad (3.36)$$

where γ_i is a gain factor to be determined, and \mathbb{P}_i is a symmetric positive-definite matrix and is the solution to the Lyapunov equation

$$A_{mi}^T \mathbb{P}_i + \mathbb{P}_i A_{mi} = -I, \quad (3.37)$$

where I is an identity matrix. However, the solution given by Eq. (3.36) requires all units to exchange their targets $x_{mi}, i = 1, 2, \dots, N$, in advance, which is impractical in a dynamic vehicular environment.

Therefore, **to tackle Challenge 4**, we propose to adopt the control input as

$$u_i(t) = r_i(t) + k_i^T x_i(t) - \gamma_i e_i^T(t) \mathbb{P}_i \zeta_i - \sum_{j=1, j \neq i}^N \hat{l}_{ij}^T(t) \hat{x}_{mj}(t), \quad (3.38)$$

where $\hat{x}_{mj}(t)$ is an estimate of $x_{mj}(t)$. DisCo-FT avoids the exchange of either $x_j(t)$ or

$x_{mj}(t)$, by applying an aggressive estimate as $\hat{x}_{mj}(t) = 1, j \neq i$. In addition, every DisCo-FT controller sets its own ePDR target as $x_{mi}(t) = 1$. Hence, there is no estimation error in $\hat{x}_{mj}(t)$. The adaptation of $x_{mi}(t)$ and the corresponding adaptive estimation of $\hat{x}_{mj}(t)$ is to be presented in Section 3.6.4. The subsystem of unit i is then described as

$$\begin{aligned} \dot{x}_i(t) &= A_i x_i(t) + \zeta_i k_i^T x_i(t) + \zeta_i r_i(t) - \gamma_i \zeta_i e_i^T(t) \mathbb{P}_i \zeta_i \\ &+ \zeta_i \sum_{j=1, j \neq i}^N l_{ij}^T(t) x_j(t) - \zeta_i \sum_{j=1, j \neq i}^N \tilde{l}_{ij}^T(t) \hat{x}_{mj}(t). \end{aligned} \quad (3.39)$$

The tracking error $e_i(t)$ is described as

$$\begin{aligned} \dot{e}_i(t) &= A_{mi} e_i(t) + \zeta_i \tilde{k}_i^T x_i(t) - \gamma_i \zeta_i e_i^T(t) \mathbb{P}_i \zeta_i \\ &+ \zeta_i \sum_{j=1, j \neq i}^N \tilde{l}_{ij}^T(t) \hat{x}_{mj}(t) + \zeta_i \sum_{j=1, j \neq i}^N \hat{l}_{ij}^T(t) e_j(t), \end{aligned} \quad (3.40)$$

where

$$\tilde{k}_i(t) = k_i - k_i^*, \quad (3.41)$$

$$\tilde{l}_{ij}(t) = l_{ij}(t) - \hat{l}_{ij}(t), j \neq i. \quad (3.42)$$

By applying control input as Eq. (3.38), DisCo-FT minimizes the tracking error. Note that in Eq. (3.38), $r_i(t)$, \mathbb{P}_i , and ζ_i are known parameters given by the reference model. Parameters $k_i(t)$, $\hat{l}_{ij}(t)$, and $\gamma_i(t)$ need to be adaptively updated. For $i = 1, 2, \dots, N$, the adaptive laws of these three parameters are given by

$$\dot{k}_i(t) = -e_i^T(t) \mathbb{P}_i \zeta_i x_i(t), \quad (3.43)$$

$$\dot{\hat{l}}_{ij}(t) = e_i^T(t) \mathbb{P}_i \zeta_i \hat{x}_{mj}(t), \quad (3.44)$$

$$\dot{\gamma}_i(t) = e_i^T(t) e_i(t). \quad (3.45)$$

Theorem 2. *DisCo-FT described by Eqs. (3.38), (3.43), (3.44) and (3.45) guarantees the global stability of the overall system.*

Proof. We first choose a Lyapunov candidate function as

$$V(e, \tilde{k}, \tilde{l}) = \sum_{i=1}^N \left[e_i^T \mathbb{P}_i e_i + \tilde{k}_i^T \tilde{k}_i \right] + \sum_{i=1}^N \sum_{j=1, j \neq i}^N \tilde{l}_{ij}^T \tilde{l}_{ij}. \quad (3.46)$$

Then we have

$$\dot{V} = \sum_{i=1}^N \left[-e_i^T Q_i e_i - 2\gamma_i (e_i^T \mathbb{P}_i \zeta_i)^2 \right] + \sum_{i=1}^N \sum_{j=1, j \neq i}^N 2e_i^T \mathbb{P}_i \zeta_i l_{ij}^T e_j, \quad (3.47)$$

where

$$Q_i = 2\mathbb{P}_i A_{mi}, \quad (3.48)$$

and $\psi_{\min}(Q_i)$ is the smallest eigenvalue of Q_i . Take the norm of \dot{V} , we have

$$\|\dot{V}\| \leq \sum_{i=1}^N \left[-\psi_{\min}(Q_i) \|e_i\|^2 - 2\gamma_i \|e_i^T \mathbb{P}_i \zeta_i\|^2 \right] + \sum_{i=1}^N \sum_{j=1, j \neq i}^N \|2e_i^T \mathbb{P}_i \zeta_i l_{ij}^T e_j\|. \quad (3.49)$$

By inequality (3.49), a sufficient condition for \dot{V} to be negative-semidefinite is

$$\gamma_i > \frac{1}{2}(N-1) \max_j \left[\frac{\|l_{ij}\|^2}{\psi_{\min}(Q_j)} \right]. \quad (3.50)$$

Therefore, there exist a $\bar{\gamma}_i$ such that whenever $\gamma_i(t) \geq \bar{\gamma}_i$, \dot{V} is negative-semidefinite. Thus, V is a Lyapunov function for the overall system. \square

3.6.3 Discretization of the Controller

To implement DisCo-FT on a digital device where time is slotted into control periods of length T , we need to discretize the continuous control laws described in Eqs. (3.38), (3.43), (3.44) and (3.45). By applying implicit the Euler method, the discretized control input is

$$u_i[n] = r_i[n] + k_i^T[n] x_i[n] - \gamma_i[n] e_i^T[n] \mathbb{P}_i \zeta_i - \sum_{j=1, j \neq i}^N \tilde{l}_{ij}^T[n] \hat{x}_{mj}[n], \quad (3.51)$$

where n denotes the n th control period. And the corresponding adaptive laws of parameters are discretized as, for $n = 0, 1, 2, \dots$,

$$k_i[n+1] = k_i[n] - Te_i^T[n+1]\mathbb{P}_i\zeta_i x_i[n+1], \quad (3.52)$$

$$\hat{l}_{ij}[n+1] = \hat{l}_{ij}[n] - Te_i^T[n+1]\mathbb{P}_i\zeta_i \hat{x}_{mj}[n+1], \quad (3.53)$$

$$\gamma_i[n+1] = \gamma_i[n] - Te_i^T[n+1]e_i[n+1]. \quad (3.54)$$

The adaptations of these parameters, as well as the adjustments of the control inputs $u_i[n]$, are conducted at the end of each control period. Meanwhile, the control outputs $x_i[n]$ are measured at the beginning of each control period. Note that, for digital controllers, there is a one-step delay between the current control inputs and the corresponding control outputs. This means: $u_i[n]$ is responsible for $x_i[n+1]$. As a result, when $u_i[n]$ is being calculated, $x_i[n]$ and $e_i[n]$ are already measured. In order to initiate the control input and the adaptive laws of each node i , we provide the initiation conditions as $u_i[0] = u_0$, $k_i[0] = k_0$, $\hat{l}_{ij}[0] = \hat{l}_0$, and $\gamma_i[0] = \gamma_0$, where u_0 , k_0 , \hat{l}_0 and γ_0 are all small constant vectors.

To prove that the discretized DisCo-FT is stable, we adopt the following lemma [100].

Lemma 2. *When the implicit Euler method is applied, a stable continuous-time system will always be transferred into a stable discrete-time system.*

Then combining Theorem 2 and Lemma 2, we have the following corollary.

Corollary 1. *The discretized DisCo-FT described by Eqs. (3.51), (3.52), (3.53) and (3.54) guarantees the global stability of the overall system.*

3.6.4 DisCo with Adaptive Coordination Targets

The design of DisCo-FT follows a rule that all DSRC units targets a ePDR of 100%. This could be overly aggressive and encounter Challenge 5. In this case, an individual unit may be reluctant to coordinate with others that are also greedy. To allow more freedom for coordinate, each DSRC unit could reduce its target ePDR slightly. This reduction could be beneficial by alleviating the congestions in the dedicated channel, and thus may improve the overall reliability and fairness. However, an overly conservative reduction may decrease the ePDR targets too much, leading to compromised reliability. Therefore, the ePDR targets should be estimated appropriately. In addition, considering the dynamics in vehicular environments, these targets should be controlled in an online manner.

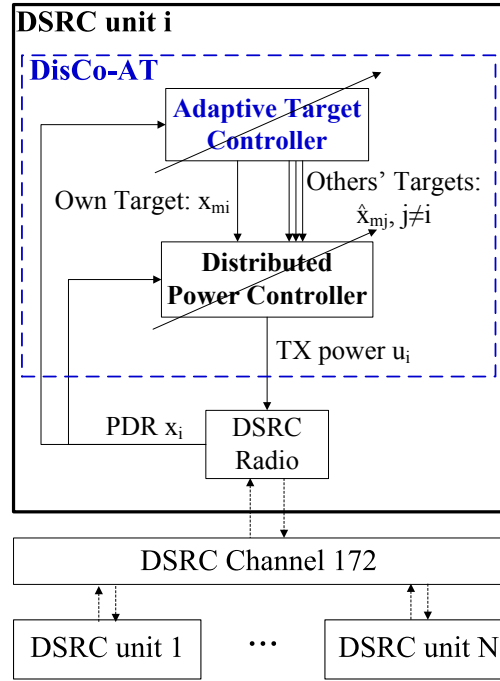


Figure 3.18 The architecture of DisCo-AT.

Therefore, to further address **Challenge 5**, we develop DisCo with adaptive coordination targets (DisCo-AT), whose architecture is presented in Figure 3.18. DisCo-AT also aims to maximize its own reliability (i.e., ePDR x_i). To achieve this objective in the presence of other interrelated DSRC units, DisCo-AT targets a ePDR x_{mi} that is less than 100%, which is different from DisCo-FT. In addition, DisCo-AT would like to assure that such an overall improvement is never based on sacrifices of some of the units. To sum up, DisCo-AT would like all DSRC units to have an optimal ePDR x^* fairly, i.e., to achieve the following objective together

$$x_i = x_{mi} = x^*, i = 1, 2, \dots, N. \quad (3.55)$$

An adaptive target controller is designed to online adjust its own ePDR target x_{mi} , as well as the estimated targets $\hat{x}_{mj}, j \neq i$. The architecture of the adaptive target (AT) controller in DisCo-AT is demonstrated in Figure 3.19. The detailed design of this AT controller is presented as follows.

The AT controller takes the own target x_{mi} and the estimations of others' targets

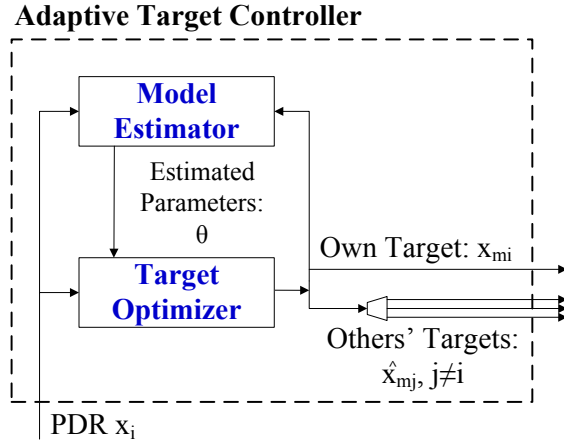


Figure 3.19 The architecture of the adaptive target controller.

$\hat{x}_{mj}, j \neq i$, as control inputs, while considering the ePDR x_i as the control output. In other words, the AT controller optimizes the actual ePDR x_i by adjusting ePDR targets x_{mi} and $\hat{x}_{mj}, j \neq i$. According to the objective of DisCo-AT in Eq. (3.55), the AT controller follows a rule as $\hat{x}_{mj} = x_{mi}, j \neq i$ in its control operation. In this way, the control of x_i is solely based on one parameter, i.e., x_{mi} . In this section, we present a discrete-time design that is ready for implementation in digital systems. Time is divided into control periods with an identical duration. Due to the one-step delay of digital implementations, the control input at control period $n - 1$ (i.e., $x_{mi}[n - 1]$) will affect the control output at control period n (i.e., $x_i[n]$).

As illustrated in Figure 3.19, the AT controller first estimates an auxiliary model, which captures the relation between the control input $x_{mi}[n]$ and the control output $x_i[n]$. Based on the estimated model parameters $\theta[n]$, the AT controller further maximize $x_i[n]$. Note that this auxiliary model is different from the reference model presented in Section 3.6.2. While the reference model defines the desired behaviors of the overall system, this auxiliary model is used to capture the relation between the ePDR target and the actual ePDR.

In our design, we develop this auxiliary model as a linear regression model, which is described by a time-difference equation as

$$G(q^{-1})x_i[n] = H(q^{-1})x_{mi}[n] + z[n], \quad (3.56)$$

where

$$G(q^{-1}) = 1 - g_1q^{-1} - \dots - g_wq^{-w}, \quad (3.57)$$

$$H(q^{-1}) = h_0q^{-1} - \dots - h_{w-1}q^{-w}, \quad (3.58)$$

q^{-1} is the back shift operator, w is the order of the regression model, and $z(n)$ is the i.i.d. zero-mean noise. To estimate this model in an online manner, we again apply an RLS scheme [100] described as follows. We first convert the model of Eq. (3.56) into a RLS-friendly form as

$$x_i[n] = \phi^T[n]\theta[n], \quad (3.59)$$

where

$$\phi^T[n] = \{x_i[n-1], \dots, x_i[n-w], x_{mi}[n-1], \dots, x_{mi}[n-w]\}^T, \quad (3.60)$$

$$\theta[n] = \{g_1[n], \dots, g_w[n], h_0[n], \dots, h_{w-1}[n]\}^T. \quad (3.61)$$

Therefore, the parameters of the auxiliary model is captured by $\theta[n]$, and are estimated by RLS scheme as

$$\theta[n] = \theta[n-1] + S[n-1]\phi[n]\epsilon[n], \quad (3.62)$$

where

$$S[n-1] = S[n-2] - (\phi^T[n]S[n-2]\phi[n] + 1) \cdot S[n-2]\phi[n]\phi^T[n]S[n-2], \quad (3.63)$$

$$\epsilon[n] = x_i[n-1] - \phi^T[n-1]\theta[n-1]. \quad (3.64)$$

To initialize the RLS scheme, we adopt $S[-1] = s_0I$, where $s_0 > 0$ is a constant and I is an identity matrix.

Based on the auxiliary model parameter $\theta[n]$, the target optimizer calculate the control input $x_{mi}[n-1]$ to maximize the expected ePDR $\hat{x}_i[n]$ by solving the following optimization problem

$$\max_{x_{mi}[n-1]} \hat{x}_i[n] = \phi^T[n]\theta[n], \quad (3.65)$$

$$s.t. \quad x_{mi}[n-1] \in [x_{min}, 1], \quad (3.66)$$

where $x_{min} > 0$ is the minimum ePDR target. Note that the current control input $x_{mi}[n-1]$

is encapsulate in $\phi[n]$ as defined by Eq. (3.60). There exist a number of approaches to solve the optimization problem Eq. (3.65) in polynomial time. We thus skip the description of the solution.

Then $\hat{x}_{mj}, j \neq i$, are estimated according to Eq. (3.55). These updated targets (both x_{mi} and $\hat{x}_{mj}, j \neq i$) are passed to the distributed power controller for power coordination. The design of the distributed power controller in DisCo-AT is identical to that in DisCo-FT as described in Section 3.6.2.

3.6.5 Estimation of Neighbor Number

To implement DisCo schemes, the number of neighbor vehicles $N_b = N - 1$ is required. To estimate N_b , every DSRC unit counts the unique transmitter MAC addresses in the MAC header of its received packets. This estimation is refreshed in every control period.

3.6.6 Estimation of ePDR

Due to the lack of feedback messages, we propose to approximate the transmitting ePDR with the receiving ePDR by leveraging the channel reciprocity in DSRC. Concretely, every MAC header of DSRC packets contains a sequence number with a size of 12 bits. By subtracting the minimum sequence number from the maximum, every DSRC unit estimates the expected number of packets sent by a specific transmitter. Then, the ePDR is calculate by dividing the number of received packets with the number of expected packets.

3.7 Evaluation of DisCo

Next, we demonstrate the large improvements provided by the proposed DisCo schemes over the state of the art, and discuss the reasons behind the improvements.

3.7.1 Evaluation Setup

We conduct extensive ns-2 simulations to evaluate the proposed DisCo schemes. The simulation setup is described in this subsection.

DisCo Implementation

To implement DisCo, we first design the reference model that determines the desired output behavior of each DSRC unit. For the sake of system stability and low complexity, we adopt a time-invariant and lightweight reference model⁵. Concretely, the reference input stays stable as a constant value of $20dBm$, i.e., $\forall t, r_i(t) = r_i = 20dBm$. We also would like the ePDR target to stay stable during each control period, which yields $\dot{x}_{mi}(t) = 0$ and $x_{mi}(t) = x_{mi}, \forall t$. As we have only one control output, the matrices A_{mi} and \mathbb{P}_i degenerate to constants. In our lightweight design, we adopt $A_{mi} = -1$, and thus $\mathbb{P}_i = 1/2$. We substitute the above conditions into Eq. (3.24), and have

$$\zeta_i = \frac{-A_{mi}x_{mi}}{r_i}. \quad (3.67)$$

For DisCo-FT, we have $x_{mi} = 1$ as described in its design. For DisCo-AT, x_{mi} also stays the same during each control period, and is updated by the adaptive target controller at the beginning of every control period.

Traffic and Vehicle Settings

Our traffic scenario is built on a two-way four-lane highway, of which the length is 2000 meters. The number of vehicles varies from 40 to 400 in different simulation runs. The vehicle dynamics, such as direction, speed and acceleration, are generated by the tool of SUMO⁶. The speed limit is $100km/h$ (corresponding to roughly $62mph$). A vehicle reaching the end of one lane will rejoin the traffic in another lane. Each vehicle is equipped with a DSRC OBU. In addition, we consider a completely decentralized scenario where there is no DSRC RSU.

Communication Settings

Each DSRC OBU broadcasts its routine safety packets in DSRC Channel 172 (5.855 GHz to 5.865 GHz) with a period of 0.05 seconds. The size of data section in each packet is 500 bytes. Headers are added according to the IEEE 802.11p protocols. The header section

⁵The design presented in Section 3.6.2 also generalizes more sophisticated reference models. The reference model used here satisfies the requirements of safety-critical applications with good stability and low complexity.

⁶SUMO – Simulation of Urban Mobility: <http://www.dlr.de/ts/sumo>

uses the modulation of BPSK (i.e., a bit rate of 3 Mbps), while the data section employs the modulation of 64QAM (i.e., a bit rate of 24 Mbps). The minimum and maximum transmission power settings are 10 dBm and 30 dBm, respectively. The adjustment step of transmission power is 2 dBm.

3.7.2 Schemes Studied

We focus on comparing DSRC reliability provided by fully distributed schemes. The following schemes are considered.

- **DisCo-FT** and **DisCo-AT**: are proposed in this thesis. The transmission power is initialized as 10 dBm for both schemes.

- **ACO-based**: is a scheme based on fully local measurement of Average Channel Occupancy (ACO) [49]. It is a representative of the state of the art in strictly distributed power adaptation (but not coordination).

- **Min-Power**: always adopts the minimum transmission power of 10 dBm.

- **Max-Power**: always adopts the maximum transmission power of 30 dBm.

3.7.3 DSRC Reliability

We first evaluate the DSRC reliability in terms of ePDR. Figure 3.20 compares the average ePDRs of different schemes under different traffic densities. It is shown that the DisCo schemes (both DisCo-FT and DisCo-AT) always outperform other schemes in all traffic density conditions. This confirms that the proposed DisCo schemes significantly enhance overall reliability by appropriately coordinating the transmission power of individual DSRC units. In addition, DisCo-AT always achieves high ePDRs than that of DisCo-FT. This suggests that an adaptive ePDR target control is beneficial, and helps DisCo-AT further boost DSRC reliability greatly.

To demonstrate the improvements brought by DisCo, we take the Max-Power scheme as the baseline, and calculate the improvements in ePDR brought by other schemes. The ePDR improvements are presented in Figure 3.21. Compared with the baseline, DisCo-AT doubles the ePDR at traffic density 0.1 vehicles per meter, and achieves an ePDR that is almost 2.5 times higher at traffic density 0.2 vehicles per meter. Moreover, compared to the state-of-the-art approach ACO-based, DisCo-FT and DisCo-AT improve DSRC reliability by 13.1% and 30.3% at density 0.1 vehicles per meter, respectively. The corresponding im-

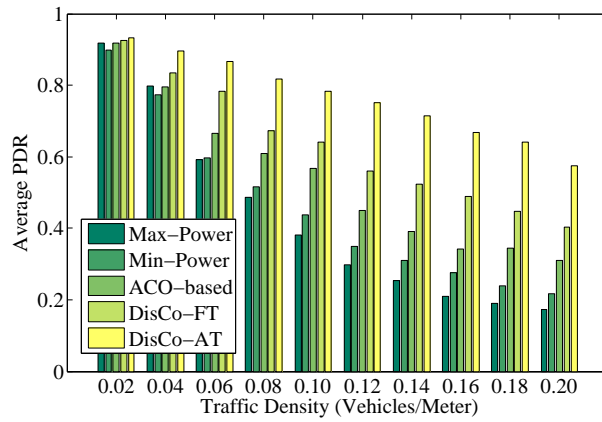


Figure 3.20 The average ePDRs of different schemes.

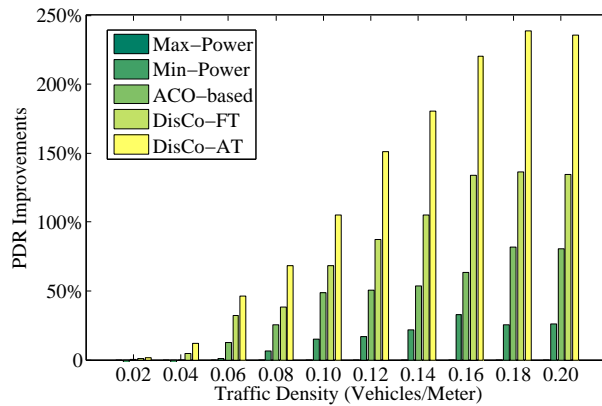


Figure 3.21 The ePDR improvements of all schemes over the Max-Power scheme.

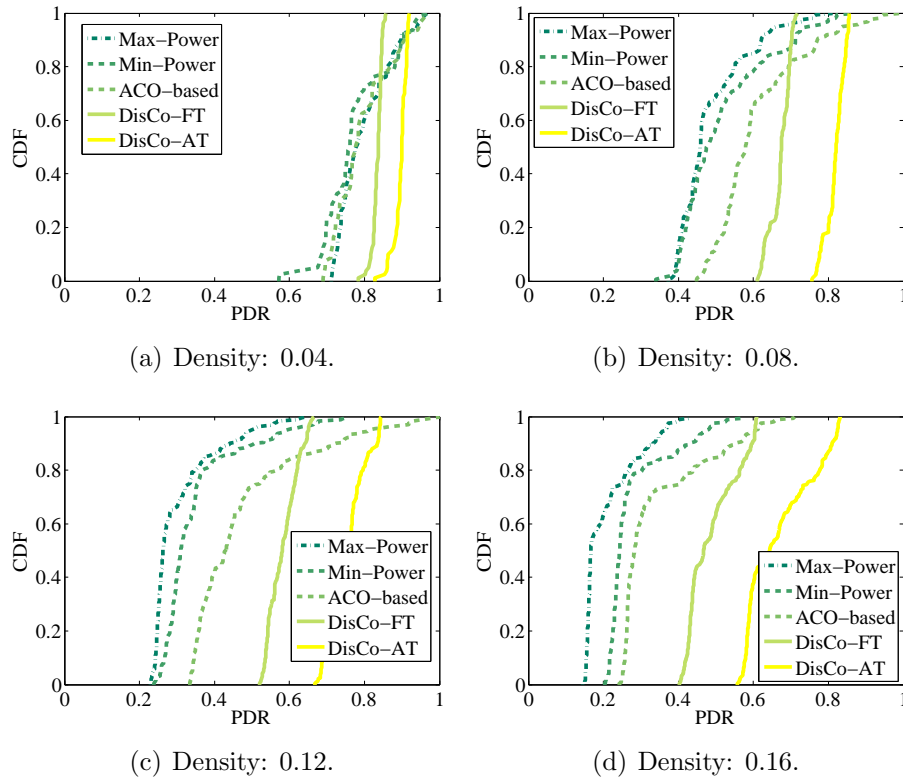


Figure 3.22 CDF of ePDRs under different traffic densities.

improvements over the state of the art are 30.3% and 85.8% at density 0.2 vehicles per meter, respectively. Furthermore, from Figure 3.21, we observe that the improvements brought by the DisCo schemes increases with traffic density. While other schemes degrade significantly when the traffic is becoming congested, the DisCo schemes resolve the communication collision and interference with exactly zero coordination overhead.

3.7.4 DSRC Fairness

In order to evaluate the ePDR fairness achieved by different schemes, we first investigate the CDF of ePDRs. Figure 3.22 presents the CDF of ePDRs under four different traffic densities. It is demonstrated that the ePDRs achieved by both DisCo schemes concentrate around their mean values, while the ePDRs brought by the ACO-based scheme are more scattered. Although the ACO-based scheme provides high ePDRs to some DSRC units, it largely sacrifices the ePDRs of others, leading to a jeopardized fairness and a degraded

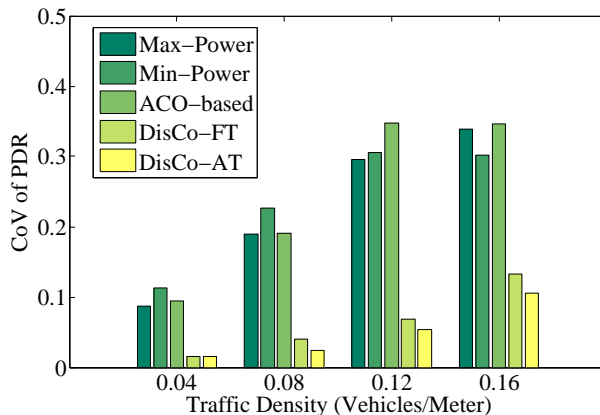


Figure 3.23 CoV of ePDRs under different traffic densities.

overall performance as shown previously in Figure 3.20.

To quantify the fairness, we adopt the CV of ePDR as the fairness metric. A smaller CV denotes a better fairness among all DSRC units. The CV of ePDRs under four different traffic densities is depicted in Figure 3.23. Generally, the CV values decrease with the traffic density, as it is increasingly hard to achieve fairness when there are more participants in the system. The DisCo schemes achieve lower CV (i.e., better fairness) than all other schemes, while the DisCo-AT always provides the best fairness across all DSRC units. Compared with the state-of-the-art ACO-based scheme, the DisCo-AT scheme improves the fairness by 69.4% to 83.7%.

Another interesting finding is that, although the Min-Power and Max-Power schemes adopt identical transmission power (i.e., 30dBm and 10dBm respectively), their fairness performance is unsatisfactory. This is because the traffic density varies along the highway even when the total number of vehicles stays the same. As a result, the optimal coordination power in different road sections is different. Applying identical transmission power leads to largely different ePDRs for vehicles in different sections, resulting in a poor overall fairness.

Selections of Transmission Power

To understand how the DisCo schemes outperform the state-of-the-art scheme ACO-based, we investigate the selections of transmission power. We focus on the traffic density of 0.2 vehicles per meter, where the DisCo schemes achieve their largest improvements in this case. We skip Max-Power and Min-Power in this section, as their transmission power is fixed.

For the other three schemes, their occurrence rates of transmission power are illustrated in Figure 3.24. In all the cases, the ACO-based concentrate its transmission power on only low-power settings (i.e., 14dBm and 18dBm). This is because the ACO-based scheme tends to apply identical transmission power for vehicles in proximity. However, this solution is suboptimal in a practical scenario where traffic and channel condition varies drastically in different road sections. Even vehicles in proximity can experience different channel quality due to issues such as hidden terminals, fading and shadowing.

Different from the ACO-based scheme, the DisCo-FT adopts low power in 66% of the time, and applies high power in rest of the time. This allows DisCo-FT to cope with the ever-changing traffic and channel conditions. However, DisCo-FT assumes that all DSRC units are greedy and target a ePDR of 100%. Therefore, it sometimes becomes overly aggressive and adopts the highest transmission power to grab more channel resource. In some other cases, it becomes overly conservative, and reduces its transmission power to the lowest level to avoid interference with others. On the contrary, DisCo-AT addresses this issue by adaptively estimating the ePDR targets. As a result, DisCo-AT obtains more freedom in power coordination across all DSRC units, and is able to approach the optimal transmission power under time-varying communication conditions. It is illustrated that the power settings of DisCo-AT mainly fall into three levels, i.e., low-power (10 to 14 dBm), medium-power (18 to 22 dBm) and high-power (26 to 30 dBm) levels. This also suggests that DisCo-AT is able to automatically classify the channel conditions into roughly three levels, and make coordination decisions correspondingly.

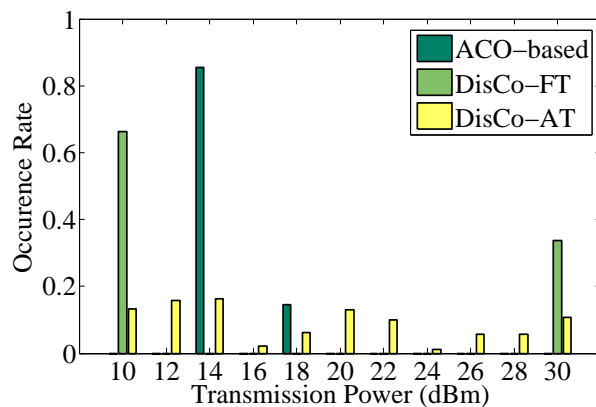


Figure 3.24 Occurrence rates of transmission power when density is 0.2 vehicles per meter.

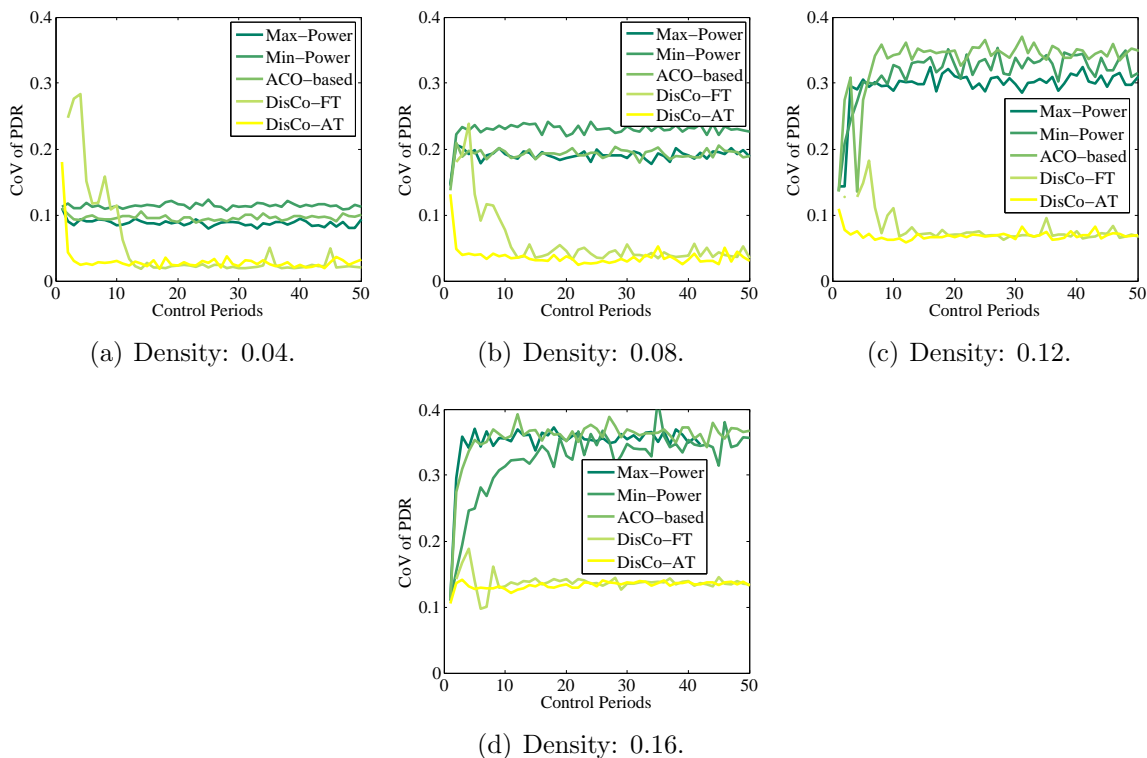


Figure 3.25 Convergence of CV.

3.7.5 Convergence

A fast convergence is required in the presence of various dynamics in vehicular networks.

We first evaluate the convergence of fairness in Figure 3.25, which presents the CV of ePDRs across time. In Figure 3.25, while DisCo schemes converge to low CV values eventually, the other three schemes fail to achieve a convergence of CV. Their CV values keep oscillating as time goes by. This demonstrates the superiority of systematic control techniques developed for DisCo over the heuristics adopted by existing schemes. In addition, compared with DisCo-AT, DisCo-FT requires a longer fluctuation period to converge, mainly due to the aggressive estimation of ePDR targets. DisCo-AT avoids this issue and increases the convergence speed by encouraging deeper coordination with appropriately adjusted the ePDR targets.

To further evaluate the convergence of reliability, Figure 3.26 presents the average ePDRs of all vehicles across time. Although all approaches manage to converge, the DisCo schemes converge to higher ePDRs than that of others. Moreover, the ePDR convergence

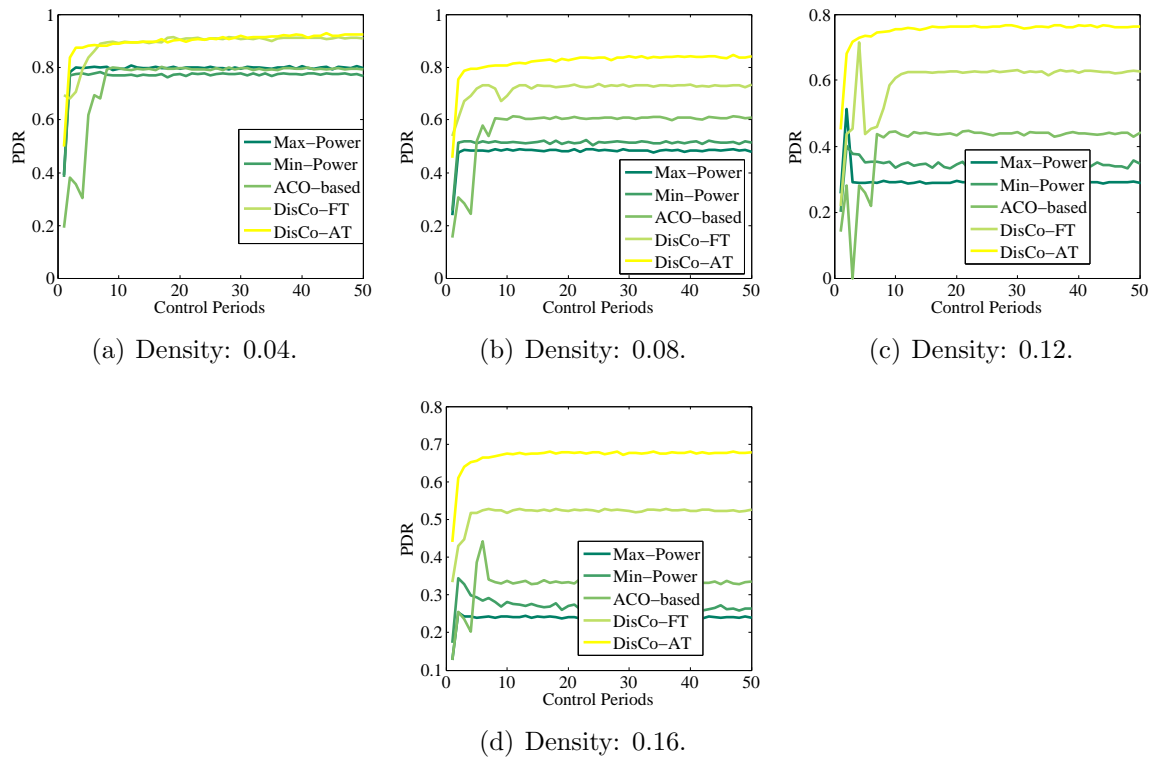


Figure 3.26 Convergence of ePDRs.

speed of DisCo-AT is at least 2 times faster than that of ACO-based scheme. Concretely, DisCo-AT achieves a fast convergence of ePDR using only 3 control iterations, while The state-of-the-art ACO-based scheme needs at least 9 control periods to converge. Therefore, from Figure 3.25 and Figure 3.26, we conclude that the convergence performance of DisCo-AT is much faster and more consistent than others.

3.8 Concluding Remarks

In this chapter, we study the DSRC technologies, which are designed, developed and implemented to enhance the driving safety. To guarantee this safety, it is of critical importance to improve the reliability, efficiency and fairness of DSRC, by adapting and coordinating the communication variables to the ever-changing environments. In order to achieve this goal, we address two major issues, i.e., the strong coupling between communication variables, and the huge overhead introduced by coordination messages. We develop two new approaches, OnCAR and DisCo, to tackle these two issues, respectively. We utilize experiments and simulations to evaluate OnCAR and DisCo, demonstrate the large improvement in DSRC performance brought by them over the state of the art. The evaluation study also illustrates the fast convergence of both OnCAR and DisCo, even in the cases where the state-of-the-art approaches fail to converge.

Chapter 4

Providing Infotainment Services to Connected Vehicles

4.1 Overview

With an increased driving safety, travellers feel more secure in their trips, and thus are more likely to enjoy IVI services. Driven by the huge IVI market, automotive manufacturers are trying to upgrade their vehicles to reinvent the driving experience. To this end, the so-called in-cabin Wi-Fi system is recently developed. It is a mobile Wi-Fi system provides a wireless network that allows a driver and passengers to connect to the Internet using a smartphone, a laptop, or a car-embedded infotainment system. This system adopts a built-in Wi-Fi AP, which provides a car the ability to become an Internet hotspot and powers Wi-Fi devices throughout the vehicle. In this way, cars become portable offices and homes, providing a shared mobile experience for all passengers in a vehicle.

In this chapter, we first discuss the newly deployed in-cabin Wi-Fi system and services, and investigate their unique features. We then try to fully understand the in-cabin Wi-Fi system, and develop cross-layer models to describe the features of this system in a mathematical way. After that, we proceed forward to improve the QoS provided by this system. We focus on the most popular and most bandwidth-consuming service, i.e., video streaming, and design a new scheduling framework to boost the streaming QoS.

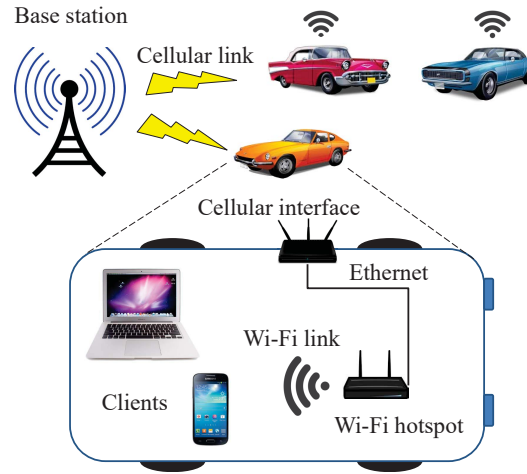


Figure 4.1 An example of the in-cabin Wi-Fi system.

4.1.1 In-cabin Wi-Fi Services

As shown in Figure 4.1, the in-cabin Wi-Fi service is provided through two wireless links. The long-range cellular link carries the data from base stations to the built-in cellular interface, while the short-range Wi-Fi link delivers the data to the in-vehicle clients directly. There is an Ethernet connection relaying the data from the cellular interface to the in-cabin Wi-Fi AP. When a client wants to access the Internet, it first sends a request to the in-cabin Wi-Fi AP. This request is then relayed to the cellular interface via the Ethernet connection. Based on the request, the cellular interface communicates with the base station, and receives the corresponding data from the Internet. The data is then delivered back to the in-cabin Wi-Fi AP and finally the client. By doing the above, the in-cabin Wi-Fi AP is able to provide passengers services including streaming video for entertainment, as well as services like real-time traffic updates and navigation driving directions. The in-cabin Wi-Fi system framework not only allows consumers to bring in and connect to personal mobile devices, but also lets the vehicle act as its own mobile device, enabling embedded vehicle capabilities.

Comparing with LTE connected smart devices, the in-cabin Wi-Fi service offers distinct advantages including a more powerful antenna array to improve signal quality, a constant energy source to power this service, and an integrated design that is optimized for in-vehicle use. Meanwhile, compared to other vehicular communication technologies (e.g.,

DSRC [11]), the in-cabin Wi-Fi technology provides a much higher service. The long-range cellular link utilizes 4G LTE technology, and provides a peak download rate of up to 299.6 Mbps. The short-range Wi-Fi link adopts IEEE 802.11n or the newly deployed IEEE 802.11ac, and offers a maximum downlink speed of 433 Mbps for single antenna devices.

In this thesis, we mainly focus on the in-cabin Wi-Fi links. Compared to the long-range cellular links, the Wi-Fi links are more likely to become the bottleneck of the whole system. While the long-range cellular links are controlled and scheduled by the base stations, the Wi-Fi links contend for the channel based on the CSMA schemes. Further, we do not consider the interference of cellular signals on in-cabin Wi-Fi links, since LTE and Wi-Fi use different carrier frequencies.

4.1.2 Differences from Other Communication Techniques

The in-cabin Wi-Fi system is specially designed to meet the requirements of high-speed vehicular communications. As a new communication technique, in-cabin Wi-Fi communication technique has a number of differences from existing communication techniques.

Differences Between In-Cabin Wi-Fi Communications and Traditional Cellular Communications

Although the in-cabin Wi-Fi system employs LTE communications, the in-cabin Wi-Fi communications are essentially different from traditional cellular communications. 1) Unlike traditional cellular communications, the in-cabin Wi-Fi communications do not require any cellular interface in the client side. Such a cellular interface is missing in most of potential in-cabin Wi-Fi client devices (e.g., laptops and tablets). Without the in-cabin Wi-Fi communications, these client devices can hardly access the high-speed cellular networks in a mobile scenario. 2) Compared to client devices directly connected to a cellular network, client devices served by an in-cabin Wi-Fi system consume less battery energy. The reason is that, instead of connecting to a distant cellular tower, in-cabin Wi-Fi client devices connects to a nearby onboard Wi-Fi hotspot, which largely reduces the energy consumption [107].

Differences Between In-Cabin Wi-Fi Communications and Traditional VANET Communications

1) The primary objective of traditional VANET communications is to enhance the safety, while the in-cabin Wi-Fi system aims to equip vehicles with the capability to provide in-entertainment services to passengers. To achieve this goal, compared to traditional VANET systems (e.g., IEEE 802.11p based systems), the in-cabin Wi-Fi system has a larger bandwidth in both the Wi-Fi and LTE links. 2) At the same time, the in-cabin Wi-Fi network has a unique layout. An in-cabin Wi-Fi AP serves only the passengers inside the vehicle. Therefore, the communication distance between an in-cabin Wi-Fi AP and its clients (typically 0.5m - 2m) is much smaller than the communication distance. 3) Moreover, the vehicle cabin introduces a path loss to the interference signals from hotspots on other vehicles.

4.1.3 Unique Features and Their Impacts

In this section, we discuss some unique features and their impacts of in-cabin Wi-Fi communications, comparing with conventional Wi-Fi communications.

Feature 1. (*space layout*) *Each in-cabin Wi-Fi AP is very close to its users.*

The ultimate goal of in-cabin Wi-Fi communications is to provide high-quality Internet access for drivers and passengers in the vehicles. The distance between the in-cabin Wi-Fi AP and passengers ranges from 0.5m to 2m, typically.

Impact of Feature 1: Due to Feature 1, the desired coverage of an in-cabin Wi-Fi AP is much smaller than those in conventional scenarios. To cover a very small area such as a vehicle, each Wi-Fi device only requires a small transmission power to provide a high-quality wireless service. Any signal beyond the vehicle cabin becomes interference to passengers on other vehicles.

Moreover, due to the unique space layout, the number of hidden terminals and exposed terminals are very limited in an in-cabin Wi-Fi system. Take Figure 4.2 as an example. One client C1 is 1m away from its in-cabin Wi-Fi AP A1. The sensing range is set to 400m, which is a typical value for Wi-Fi communications. The transmission range is smaller than the sensing range, which follows the practice in the industry. If a node is outside the sensing range of C1, then the signal from that node to C1 is very weak and is deemed as noise.

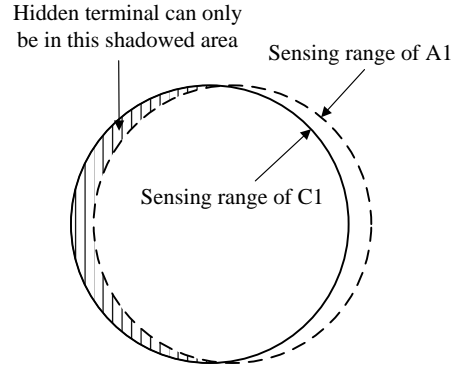


Figure 4.2 An example for in-cabin Wi-Fi hidden terminals

If a node is inside the sensing ranges of both A1 and C1, then that node will not collide with A1. Therefore, any other node can be a hidden terminal to A1, only if that node is inside the sensing range of C1 and at the same time outside the sensing range of A1 [108]. Equivalently, one node can be a hidden terminal to C1, only if it is in the shadowed area in Figure 4.2. The corresponding probability is less than 0.0025. A more practical example would be a bi-directional highway, which has four lanes on each direction. The width of such a highway is typically less than 40m. In this case, the probability that a node would become the hidden terminal of C1 is again less than 0.0025. In a congested scenario where there are 10 vehicles per 100m in each lane, the expected number of hidden terminals of C1 is less than 1.6. Compared to the interference and collisions of other nodes, the interference of the hidden terminals is very limited. Similar conclusions can be made to exposed terminals in the in-cabin Wi-Fi system. Therefore, we do not discuss hidden and exposed terminals in this thesis.

Feature 2. (*power loss*) *The vehicle cabin introduces a 5dB to 10dB power loss to the in-cabin Wi-Fi transmission signals [109, 110].*

Impact of Feature 2: Due to this feature, the interference range of in-cabin Wi-Fi AP shrinks significantly. Therefore, when small transmission power is used, interference signals are restricted in a very local area. For the same deployment density, an in-cabin Wi-Fi AP usually causes less communication interferences (hence less collisions) compared with a conventional Wi-Fi. However, along with the bursty traffic on different roads, the deployment density of in-cabin Wi-Fi APs can vary a lot, ranging from a very small number

to a very large number. Hence, it is not intuitive to understand the performance of in-cabin Wi-Fi communications.

Feature 3. (*mobility*) *All in-cabin Wi-Fi APs are moving on wheels.*

Impact of Feature 3: Due to this feature, in-cabin Wi-Fi communications are highly dynamic. The mobility feature not only indicates that the speed of each vehicle is varying, but also suggests that the traffic density around a vehicle is ever-changing. Each in-cabin Wi-Fi AP needs to adapt itself to the surrounding environments. It is worth noting that the density of in-cabin Wi-Fi APs can be very high on a congested road. During busy hours, there can be hundreds of vehicles at a single crossing. With the popularity of the in-cabin Wi-Fi technology, every vehicle may become a hotspot. Even considering about Feature 1 and Feature 2, the loss of communication quality can be severe due to fading and interference. Although the speed of vehicles is low on a congested road, the variation of density can be highly dynamic. Thus, we need to extensively analyze in-cabin Wi-Fi communication performance under different traffic conditions.

4.2 Metrics

The in-cabin Wi-Fi systems are primarily deployed for in-vehicle infotainment services. Therefore, in this chapter, we focus on the QoS provided by these systems. Accordingly, we defined the following metrics of QoS.

4.2.1 The average queueing delay and delay jitter

The queueing delay $D^{(p)}$ of a packet p is defined as

$$D^{(p)} = \begin{cases} t_{end} - t_{arr}, & p \text{ is received or dropped,} \\ t_{cur} - t_{arr}, & p \text{ is waiting for transmission,} \end{cases} \quad (4.1)$$

where t_{arr} is the time that packet p arrives at an in-cabin Wi-Fi AP, t_{end} is the time that packet p is received by a client or is dropped by the AP, and t_{cur} is the current time. Then the average queueing delay \bar{D} is defined as

$$\bar{D} = \frac{1}{N_p} \sum_{p=1}^{N_p} D^{(p)}, \quad (4.2)$$

where N_p is the number of packets being considered in the calculation. N_p is can be adjusted to meet different application requirements and functionalities.

There are different definitions of delay jitter (we call it jitter for short) in the literature. In this thesis, we use the definition of jitter in the IP network [111], and define the jitter J as the average deviation of delays from the average delay, i.e.,

$$J = \frac{1}{N} \sum_{i=1}^N \left[\frac{1}{N_r(i)} \sum_{p=1}^{N_r(i)} |D^{(p)} - \bar{D}| \right], \quad (4.3)$$

where N is the total number of clients, $N_r(i)$ is the number of video packets received by client i .

4.2.2 The deadline missing ratio

Suppose the video buffer of a client device is going to drain at time t_{pre} , and the next packet p is going to arrive at t_{arr} . If $t_{arr} > t_{pre}$, then we consider that packet p misses its deadline. The deadline missing ratio ξ_i is then defined as the portion of packets that miss their deadlines, i.e.,

$$\xi_i = N_d(i)/N_r(i), \quad (4.4)$$

where $N_d(i)$ is the number of packets that arrive at client i and miss their deadlines.

4.2.3 The average and regional throughput

Regional throughput S_{reg} is defined from the view of a reference region d_{ref} . It sums up the throughput of every node inside d_{ref} :

$$S_{reg} = \sum_{i \in d_{ref}} N_r(i) \eta_i / T, \quad (4.5)$$

where T is the time period we are interested in, and η_i the average size of packets received by client i .

The average throughput S_{avg} is then defined as follows,

$$S_{avg} = S_{reg} / N_c, \quad (4.6)$$

where N_c is the total number of clients inside d_{ref} .

4.2.4 The average and regional goodput

While the throughput captures the rate of transmitting packets, the goodput features the speed of receiving packets. The transmitted packets may either be corrupted in the wireless channels or miss their deadlines. These packets do not contribute to the in-cabin Wi-Fi services, and thus should be excluded in the goodput.

The regional goodput R_{reg} sums up the goodput of all nodes inside a reference region d_{ref} :

$$R_{reg} = \sum_{i \in d_{ref}} [N_r(i) - N_d(i)] \eta_i / T, \quad (4.7)$$

The average goodput R_{avg} is then defined as follows,

$$R_{avg} = R_{reg} / N_c. \quad (4.8)$$

4.3 Modelling the In-Cabin Wi-Fi Communications

In order to fully understand the new system of in-cabin Wi-Fi, in this section, we present our theoretical modelling. We establish a cross-layer framework to capture the in-cabin Wi-Fi communications. In the MAC layer, the proposed framework employs a two-dimension (2D) Markov chain model, which is similar to but more accurate than previous models. In the PHY layer, the proposed framework is the first to take the unique features of in-cabin Wi-Fi communications into consideration. Based on this framework and its analytical models, we are able to accurately calculate the in-cabin Wi-Fi performance under different conditions.

4.3.1 MAC Layer Modelling

We discuss the MAC layer model from the view of a single in-cabin Wi-Fi device. We establish a 2D Markov chain, which is similar to but more accurate than previous 2D Markov chain models. The improvements made in our MAC layer model are summarized as follows. (1) Unlike previous MAC layer models of IEEE 802.11, our MAC layer model works interactively with our PHY layer model, to capture the unique features of in-cabin Wi-Fi

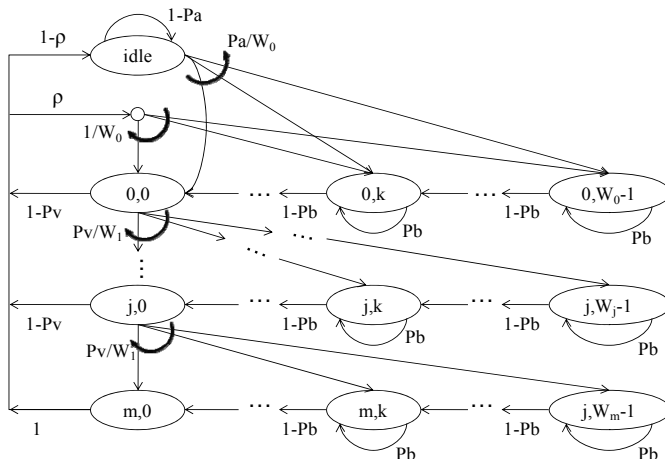


Figure 4.3 2D Markov chain for in-cabin backoff process

communications. (2) Unlike previous models of saturated communications (e.g., the model proposed by Bianchi in [9]), our MAC layer model generalizes both saturated and non-saturated communications. (3) Unlike previous models of non-saturated communications (e.g., models proposed by in Malone et al. in [28], and by Daneshgaran et al. in [29]), our MAC layer model captures the limited retransmissions defined in the IEEE 802.11n standard [112]. (4) Unlike the models proposed by Yao et al. in [34] and by Nguyen et al. in [30], our MAC layer model refines the definition of a virtual time slot, hence further improves the model accuracy.

The 2D Markov chain for the backoff process is presented in Figure 4.3. Concretely, in our 2D Markov chain, time is divided into virtual time slots. We call each virtual time slot a time slot for short, if not further specified. We define the length of each time slot as the expected duration E_s that the backoff process spends in each state of the 2D Markov chain. E_s is to be defined in Eq. (4.24). We denote each state in the chain as $\{s(t), b(t)\}$. Here, $s(t)$ stands for the backoff stage, which is determined by the number of transmission attempts of the current packet. $b(t)$ denotes the backoff time counter, which goes down by one if the current time slot is sensed idle. To model the unsaturated throughput, we further append an idle state $\{idle\}$ in the Markov chain to characterize the packet arrival process for real-time Wi-Fi scenarios.

Let ρ be the probability that the queue of the in-cabin Wi-Fi device is not empty. Use W_j to denote the maximum length of contention window for backoff stage j . Let m

be the maximum number of retransmission attempts. Let P_a be the probability that the transmitter leaves the idle state. Let P_b be the probability that the channel is busy at the current time slot. Let P_v denote the probability that a transmission is failed. The cause of a transmission failure is due to both collisions in the MAC layer and signal deteriorations in the PHY layer. Thus, the calculation of P_v is a joint work of both the MAC layer model and the PHY layer model. As a result, these two models are coupled.

Suppose an in-cabin Wi-Fi AP $A1$ starts functioning with no packet in its queue, i.e., it begins from the $\{idle\}$ state. In the next time slot, a packet arrives at $A1$'s queue with probability P_a . This means that $A1$ begins to backoff with probability P_a . In this case, it reaches the backoff stage 0, and uniformly randomly chooses a backoff counter k from $0, 1, \dots, W_0 - 1$. From state $\{0, k\}$, $A1$ goes to state $\{0, k - 1\}$ if the channel is not busy (with probability $1 - P_b$), or stays in state $\{0, k\}$ if the channel is busy (with probability P_b). Once $A1$ reaches state $\{0, 0\}$, it transmits the packet at the head of its queue. If the transmission fails (with probability P_v), $A1$ enters the next backoff stage $\{1, *\}$, and repeats the random backoff procedure again. Upon a successfully transmission (with probability $1 - P_v$), $A1$ goes back to the $\{idle\}$ state if there is no more packet in its queue (with probability $1 - \rho$), or enters the backoff procedure at backoff stage $\{0, *\}$ if its queue is not empty (with probability ρ). If the transmission of a packet has failed m times, $A1$ drops this packet, and goes back to the $\{idle\}$ state or one of the states in backoff stage $\{0, *\}$, depending on the condition of the queue.

Let $\pi_{j,k}$ be the stationary probability of state $\{s(t) = j, b(t) = k\}$, and π_{idle} be the stationary probability of state idle. Then, we can have the following equations:

$$\pi_{idle} = \frac{1 - \rho}{P_a} \cdot \pi_{0,0}, \quad (4.9)$$

$$\pi_{j,0} = (P_v)^j \cdot \pi_{0,0}, \text{ for } j > 0, \quad (4.10)$$

$$\pi_{0,k} = \frac{W_0 - k}{(1 - P_b)W_0} \cdot \pi_{0,0}, \text{ for } k > 0, \quad (4.11)$$

$$\pi_{j,k} = \frac{(W_0 - k) \cdot (P_v)^{j+1}}{(1 - P_b)W_j} \cdot \pi_{0,0}, \text{ for } j, k > 0, \quad (4.12)$$

$$1 = \pi_{idle} + \sum_{j=0}^m \sum_{k=0}^{W_j-1} \pi_{j,k}. \quad (4.13)$$

Thus, we can combine Eq. (4.9)-(4.13) to obtain the following equation:

$$\pi_{0,0} = \left\{ \frac{W_0 P_v [1 - (2P_v^{m+1})]}{(1 - P_b)(1 - 2P_v)} + \frac{[1 - (P_v)^{m+1}]}{(1 - P_v)} + \frac{W_0}{(1 - P_b)} + \frac{(1 - \rho)}{P_a} \right\}^{-1}. \quad (4.14)$$

4.3.2 PHY Layer Modelling

Our PHY layer modelling consists of two analytical models, the propagation model and the packet receiving model. To capture the unique features of in-cabin Wi-Fi communications, we extend existing empirical models accordingly.

The Propagation Model

We improve the dual-scope path loss model in [2] to capture the in-cabin Wi-Fi path loss. Concretely, we adopt a cabin path loss C to represent the unique path loss by vehicle cabins. The in-cabin Wi-Fi path loss $L(d)$ is expressed as follows:

$$L(d) = \begin{cases} -10\tau_1 \log_{10}\left(\frac{d}{d_0}\right) - C, & d_0 \leq d \leq d_c, \\ -10\tau_1 \log_{10}\left(\frac{d_c}{d_0}\right) - 10\tau_2 \log_{10}\left(\frac{d}{d_c}\right) - C, & d \geq d_c, \end{cases} \quad (4.15)$$

where d denotes the transmission distance, d_0 is the reference distance, d_c is the equivalent transmission distance, τ_1 and τ_2 are path loss factors, and C is the cabin loss constant. For propagations within the reference distance d_0 , we assume that they follow a free space propagation. Propagations outside the reference distance d_0 follow the dual-scope model described by Eq. 4.15. According to this model, propagations outside the equivalent transmission distance d_c experience a more server path loss than those with d_c .

The Packet Receiving Model

We adopt empirical waterfall curves (summarized from our extensive simulations) to model the in-cabin Wi-Fi packet receiving process. In this model, the PLR is a non-increasing function of SINR. The empirical SINR-PLR curves in our packet receiving model is depicted in Figure 4.4.

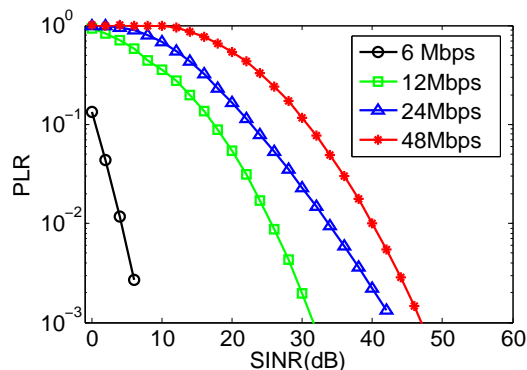


Figure 4.4 Empirical SINR-PLR curves

4.3.3 Calculation of Throughput and PLR

Estimating P_v

The value of P_v (i.e. the probability that a transmission is failed) is determined by data rate and SINR value. Thus, we do not need to solve the MAC layer 2D Markov chain to get P_v . Instead, We take the SINR and data rate as the inputs, and estimate P_v with the SINR-PLR curves (the empirical SINR-PLR curves are illustrated in Figure 4.4). The SINR value can be estimated accurately with many existing techniques (e.g., those proposed in [113–115]).

Estimating Throughput

Define λ as the packet arrival rate, and μ as the average service rate. Then the probability ρ that the queue is not empty can be expressed as follows:

$$\rho = \min \left(1, \frac{\lambda}{\mu} \right). \quad (4.16)$$

Define ς as the probability that the transmitter transmits at current time slot, then the relationship between ς and P_b is:

$$\varsigma = \sum_{j=0}^m \pi_{j,0} = [1 - (P_b)^{m+1}] \cdot \pi_{0,0}, \quad (4.17)$$

$$P_b = 1 - (1 - \varsigma)^{N-1}, \quad (4.18)$$

where N is the total number of vehicles.

We can further express the probability P_{tr} that at least one node is transmitting at current time slot as follows:

$$P_{tr} = 1 - (1 - \zeta)^N. \quad (4.19)$$

And the probability P_s that a transmission is successful can be expressed as follows:

$$P_s = N\zeta(1 - \zeta)^{N-1}. \quad (4.20)$$

The relative throughput S is defined as the fraction of time that the channel is used for transmission [9]:

$$\begin{aligned} S &= \frac{E[\text{Payload information transmitted in a time slot}]}{E_s} \\ &= \frac{P_s T_p}{(1 - P_{tr})\sigma + P_s T_s + (P_{tr} - P_s)T_c}, \end{aligned} \quad (4.21)$$

where E_s is expected length of a virtual time slot in our MAC layer model, σ is the basic slot length defined in the 802.11n standard [112], T_s is the round-trip time for a successful transmission, T_c is the time for a failed transmission, and T_p is the transmission time for the data section in a data packet. T_s and T_c are defined as follows [9]:

$$T_s = H + T_p + SIFS + \sigma + T_{ACK} + DIFS, \quad (4.22)$$

$$T_c = H + T_p + DIFS, \quad (4.23)$$

where H is the time for packet headers transmission, and T_{ACK} is the time for ACK packet transmission, $SIFS$ is the time interval of the Short Interframe Space, and $DIFS$ is the time interval of the DCF Interframe Space. Then the expected length of a time slot E_s is calculated as follows:

$$E_s = (1 - P_{tr})\sigma + P_s T_s + (P_{tr} - P_s)T_c. \quad (4.24)$$

We assume that the packet arrival follows a Poisson process. Then we can express the probability of exiting idle state P_a as follows:

$$P_a = 1 - e^{-\lambda \cdot E_s}. \quad (4.25)$$

And the average service rate of each node is calculated as follows:

$$\mu = \left\{ (1 - P_v)T_s \sum_{j=0}^m \pi_{j,0} + E_s \sum_{j=0}^m \sum_{k=1}^{W_j-1} \pi_{j,k} + P_v T_c \pi_{m,0} \right\}^{-1}. \quad (4.26)$$

By solving the system of nonlinear equations from Eq. (4.14) to Eq. (4.26), we get the value of relative throughput S .

Then we can estimate the average throughput as follows:

$$S_{avg} = \frac{S \cdot r}{N}, \quad (4.27)$$

where r is the data rate.

We further calculate the PLR as follows:

$$PLR = P_v \cdot \pi_{m,0} = (P_v)^{m+1} \cdot \pi_{0,0}. \quad (4.28)$$

4.3.4 Model Validation

Real testbed experiments will be ideal to evaluate this research. However, in practice, it is hard to duplicate identical experiment setups such as traffic conditions. Hence, we resort to simulation studies. In this section, we first describe the setup for the evaluation. We then validate our analytical models by comparing the theoretical results with ns-2 simulations, with vehicle mobility module developed in house at General Motors. We consider a typical simulation scenario as described in Table 4.1 - 4.3.

Evaluation Setup

In this subsection, we describe the highway scenario, the device and cabin settings, the PHY layer model, and the propagation model.

Urban highway scenario: We conduct our analysis in a typical bidirectional urban highway scenario, of which the length is 3000m. The highway contains four lanes, each of which has a width of 4m. Taking the isolation zone into consideration, the total width of the highway is 20m. Vehicles on each lane are deployed according to a Poisson process. The average length of vehicles is set to 4m. Each vehicle is equipped with one in-cabin Wi-Fi

device. As the main purpose is to investigate in-cabin Wi-Fi communication performance under different traffic conditions, we consider a simple case that each in-cabin Wi-Fi device serves one passenger. The reference range d_{ref} for the regional goodput calculation is set to 1000m, which is a typical coverage range of a LTE BS in an urban scenario [116]. Table 4.1 summarizes all the settings for the highway model.

Table 4.1 Settings for the highway scenario

Description	Value
Highway length	3000m
Highway width	20m
# of lanes	4
Lane width	4m
Isolation zone width	4m
Positions of vehicles	Poisson
# of vehicles	$N \in [30, 1200]$
Vehicle length	4m
# of Wi-Fi devices on each vehicle	1
# of users served by each AP	1
Distances between AP and target users	$[0.1m, 0.5m]$

Table 4.2 Settings for in-cabin Wi-Fi device

Description	Value
Center frequency	2.4GHz
Bandwidth	20MHz
Transmission scheme	CBR (unicast)
Network protocol	UDP
Transmission power	0, 10, 20 and 28 dBm
Buffer size	5MB
Packet size	500 bytes
MAC protocol	CSMA/CA
Workload distribution	Poisson
Data Arrival Rate	340Kbps, 2Mbps and 6Mbps

In-cabin Wi-Fi device settings: According to 802.11n protocol [112], we utilize the 2.4GHz frequency, and allocate 20MHz bandwidth for transmissions. Workload arrivals of each user follow the Poisson process, which is commonly used to characterize the Internet bursty traffic [117]. The duration of each workload is an exponential random variable.

Table 4.3 Data rates in this thesis

Data Rate	Modulation	Coding Rate
48Mbps	64QAM	2/3
24Mbps	16QAM	1/2
12Mbps	QPSK	1/2
6Mbps	BPSK	1/2

Table 4.4 Parameters for the propagation model

Description	Value
Reference distance d_0	1m
Equivalent transmission distance d_c	220m
In-cabin constant C	10dB
path loss parameter τ_1	1.9
path loss parameter τ_2	4.0

The interval time between two adjacent workloads is also an exponential random variable. During each transmission interval, the workloads come with a Constant Bit Rate (CBR) manner. The transmission scheme is unicast. Network protocol is UDP. Table 4.2 summarizes the settings for Wi-Fi devices.

Data rates: The perceivable data rates are determined by modulation and coding rates used in transmissions. We consider about four defined transmissions options in IEEE 802.11n illustrated in Table 4.3.

Propagation model: The empirical values of parameters in the propagation model are summarized in Table 4.4. We modify the model parameters in [2], so as to include the path loss caused by vehicle cabin.

Model Validation

In order to illustrate the effectiveness of our proposed analytical model, we compare the theoretical results with simulation results, in terms of both average and regional goodputs. We further compare our proposed model with the model proposed by Yao et al. in [34], so as to illustrate the improvement brought by our model. Yao's model is one of the most accurate and related models that capture the unsaturated throughput of 802.11 based communications. In this subsection, we set transmission power as 20dBm and data arrival rate as 340Kbps. The value of m is set to 6, which means a packet is dropped if the

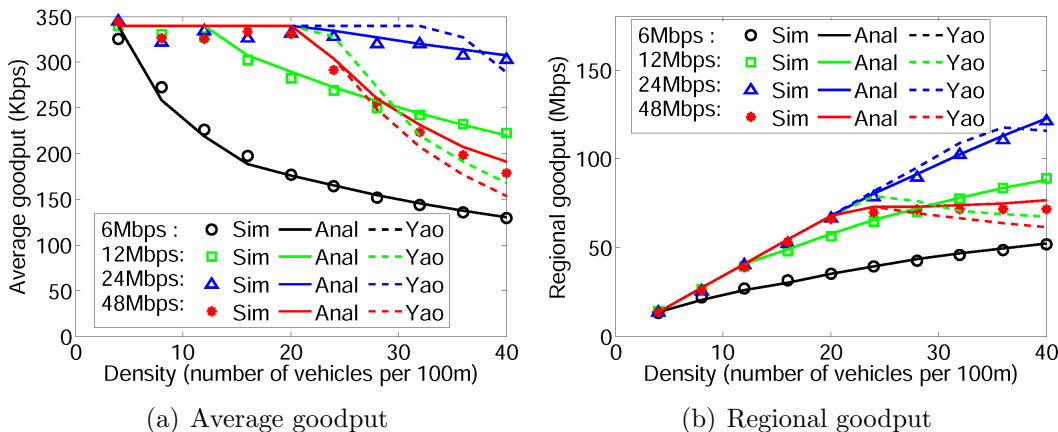


Figure 4.5 Model evaluation via average and regional goodputs. The simulated goodputs are denoted as "Sim" and marked by dots. The modeled goodputs of our model are denoted as "Anal" and marked by solid lines. The modeled goodputs of Yao's model are denoted as "Yao" and marked by dash lines.

transmission attempt has failed for 7 times. As shown in Figure 4.5, we compare the modeled goodputs of our model (denoted as "Anal") with the simulated goodputs (denoted as "Sim"), as well as the modeled goodputs of Yao's model (denoted as "Yao").

In Figure 4.5(a), we can observe that the average goodputs of our analytical model for all four data rates can fit the simulated average goodputs very well. Similarly, in Figure 4.5(b), the regional goodputs with analytical models for all data rates can fit the simulated regional goodputs very well. In contrast, Yao's model sometimes yields a large error in modelling the goodputs in the high density region (i.e., when the vehicle density is larger than 20 vehicles per 100m). This confirms that our model improves the modelling accuracy.

4.3.5 System Analysis based on Extensive Simulations

In this section, we present more simulation study of the in-cabin Wi-Fi communications. We summarize several important observations to show how in-cabin Wi-Fi performance is impacted by traffic density, transmission power and data rate. In-depth analysis of these observations is provided. In order to obtain a certain goodput guarantee under different traffic conditions, we provide important recommendations of default settings of in-cabin Wi-Fi devices to automotive engineers. We further illustrate the impacts of transmission power and data rate on queuing delay, in order to provide useful guidelines for delay-

sensitive applications.

Impacts of Traffic Density on Goodputs

Due to the mobility of vehicles, in-cabin Wi-Fi communication environments change a lot with traffic conditions. To illustrate the impacts of traffic density, we consider an example with transmission power of all vehicle as 20dBm, and data rate of all vehicles as 48Mbps data. The data arrival rate of each vehicle is 340Kbps ($\lambda = 340Kbps$). Figure 4.6 illustrates how the average goodput is affected by the traffic density.

Based on Figure 4.6, we summarize our observation as follows:

Observation 3. *The average goodput decreases with the traffic density. Meanwhile, the average goodput is degrading faster in the high density region than in the low density region.*

We can explain Observation 3 as follows.

1. As the density increases, the number of interference nodes increases. When more interference nodes appear, the interference power increases, leading to a decrease in the SINR value. According to Eq. (4.18), the probability P_b that the channel is sensed busy increases with N . Both PHY-layer and MAC-layer performances degrade with the increasing traffic density. As a result, the average goodput of all the users drops with the traffic density.
2. When the traffic density is low, the impact of interference is low. The wireless channel capacity is larger than the data arrival rate. All the arrived packets can be transmitted immediately. Thus the average goodput shown in Figure 4.6 is approximating the data arrival rate. This explains why the average goodput is degrading very slowly in the low density region.
3. As the traffic density increases, N and P_b increase. Due to the increasing interference, the SINR drops sharply. As a result, the capacity of the wireless channel begins to decrease, and can no longer serve all arrived packets. The average goodput begins to decrease severely with the decreasing channel capacity. This explains why the average goodput is degrading much faster in the high density region than in the low density region.

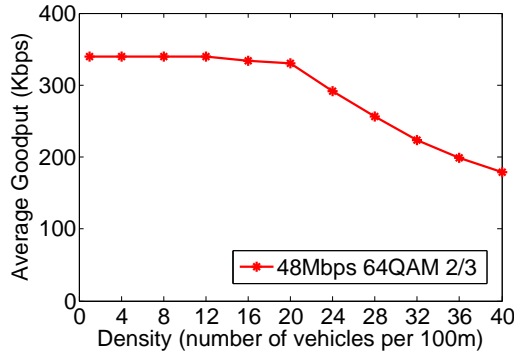


Figure 4.6 Average goodput when transmission power is 20dBm and data rate is 48Mbps

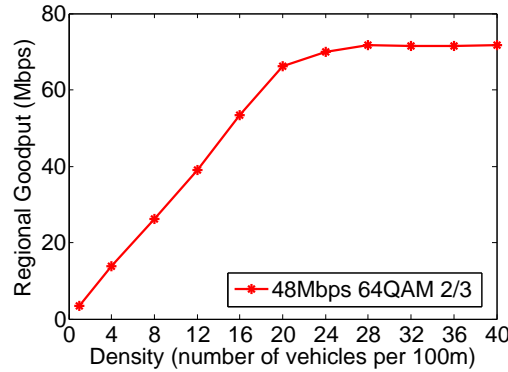


Figure 4.7 Regional goodput when transmission power is 20dBm and data rate is 48Mbps

We also analyze the impact of traffic density on regional goodput. Figure 4.7 illustrates how the regional goodput is affected by the traffic density.

The following observation can be summarized from Figure 4.7.

Observation 4. *The regional goodput increases with the traffic density. Meanwhile, the regional goodput is increasing faster in the low density region than in the high density region.*

We can explain Observation 4 as follows.

1. As the traffic density increases, the number of vehicles in the reference range d_{ref} increases. This explains why the regional goodput increases with the traffic density.
2. The regional goodput is also determined by average goodput of vehicles within d_{ref} . When the average goodput decreases quickly in the high traffic density region, the

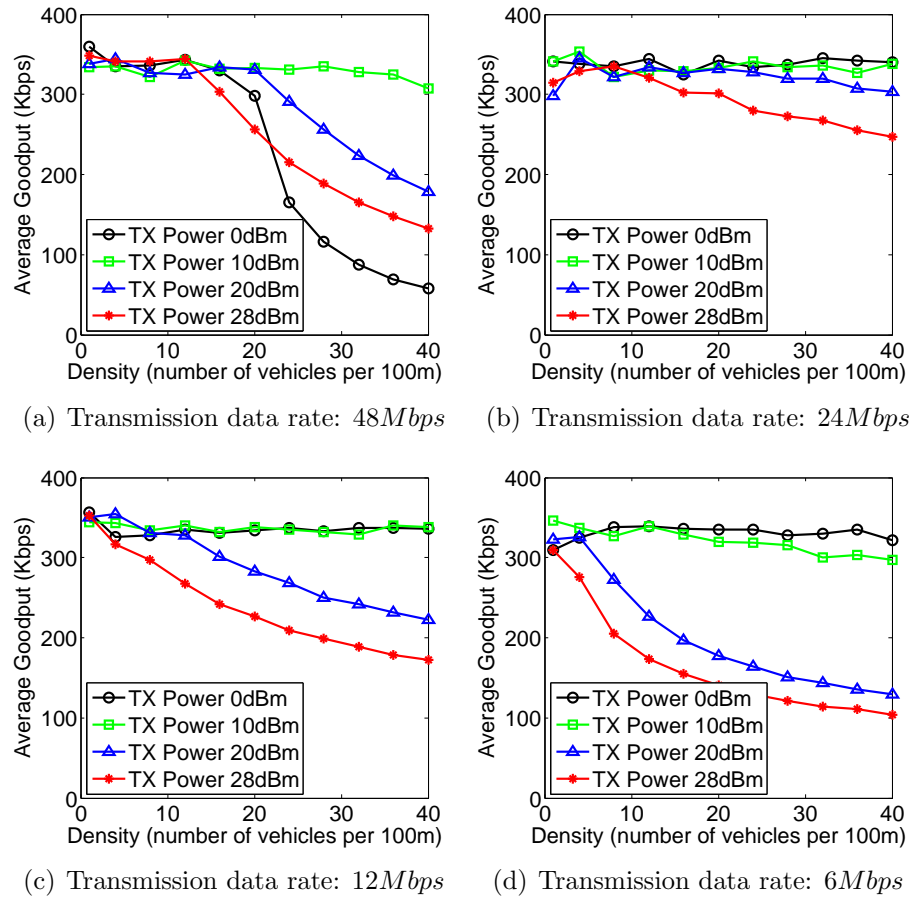


Figure 4.8 Average goodputs of different transmission powers.

regional goodput becomes increasing very slowly even with a larger number of vehicles in the reference range. The wireless channel is saturated.

Impacts of Transmission Power on Goodputs

The transmission power of in-cabin Wi-Fi device not only determines the signal power for passengers in the vehicle, but also affects the interference level of in-cabin Wi-Fi communications outside the vehicle. Usually, a higher transmission power provides a better signal power but introduces more interferences; a lower transmission power provides a worse signal power but introduces less interferences. To see the impact of the transmission power, we use a data arrival rate of 340Kbps as an example. Figure 4.8 shows how the transmission power affects the average goodput.

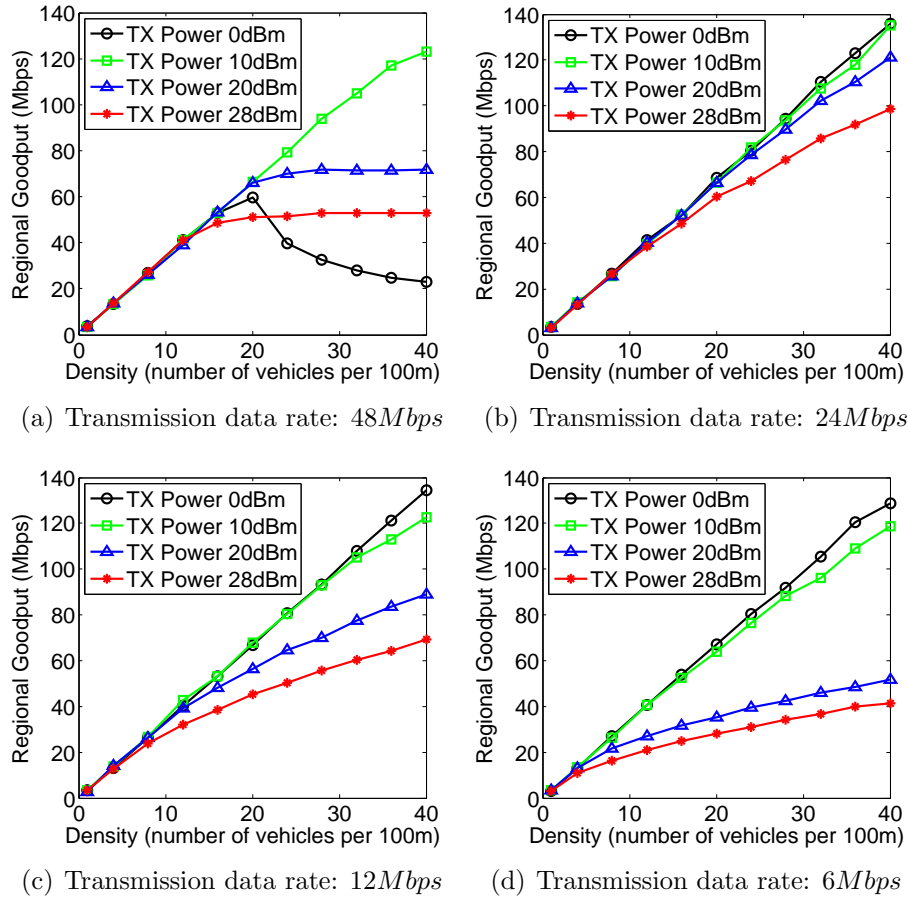


Figure 4.9 Regional goodputs of different transmission powers.

From Figure 4.8, we can summarize the following observation.

Observation 5. *In a lower traffic density region, the transmission power has a very limited impact on the average goodput. The small transmission powers (0 dBm and 10 dBm) usually achieve better average goodputs than that of the large transmission powers (20 dBm and 28 dBm) in a higher traffic density region. In general, the transmission power of 10 dBm provides the best and the most robust performance in average goodput.*

We further compare the regional goodput of different transmission powers in Figure 4.9. And we can summarize the following observation.

Observation 6. *In a lower traffic density region, the transmission power has a very limited impact on the regional goodput. The small transmission powers (0 dBm and 10 dBm)*

provide better regional goodputs than that of the large transmission powers (20 dBm and 28 dBm) in a higher traffic density region. In general, the transmission power of 10 dBm provides the best and the most robust performance in regional goodput.

We can explain Observation 5 and 6 with a tradeoff between PHY-layer performance and MAC-layer performance in terms of transmission power.

1. Usually, the PHY-layer performance increases with transmission power. Meanwhile, the PHY-layer performance is increasing slower in the high power region (20-28 dBm) than in the low power region (0-10 dBm). As the transmission power increases from 0dBm to 10dBm, an increased transmission power provides an increased signal power, leading to a large increase in SINR and a significant improvement of the PHY-layer performance. However, as we further increase the transmission power to over 20 dBm, the channel distortion, as well as the interference power, become the bottleneck. And this change cannot be reflected by the SINR value. In this case, we can only achieve marginal improvement in the PHY-layer performance with a large increase in transmission power.
2. Usually, the MAC-layer performance decreases with transmission power. As the transmission power increases, interference power increases. Thus, the interference range of each in-cabin Wi-Fi increases, leading to an increase in the number of interference vehicles $N - 1$. According to Eq. (4.18), as N increases, collisions are more likely to happen. Thus, the MAC-layer performance degrades with the increasing transmission power.
3. With the largest transmission power (28 dBm), in-cabin Wi-Fi hotspots impose a large interference power to each other, making the MAC-layer performance degenerates largely. With the smallest transmission power (0 dBm), in-cabin Wi-Fi hotspots may fail to deal with channel fading and path loss efficiently, resulting in a huge loss in the PHY-layer performance, especially when the data rate of 48Mbps is used. Therefore, both the largest and the smallest transmission power can not achieve the best performance.
4. The transmission power of 10 dBm provides the best and the most robust performance in terms of average goodput and regional goodput. It achieves a good tradeoff between the PHY-layer performance and the MAC-layer performance: it provides a well

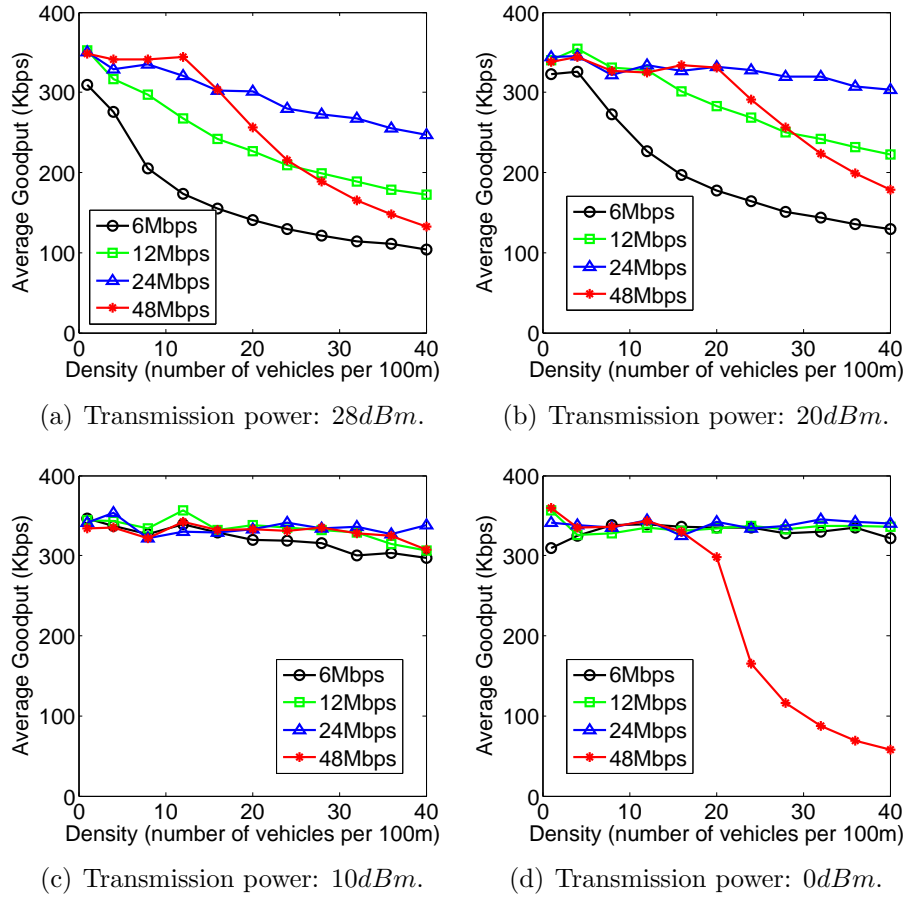


Figure 4.10 Average goodputs of different transmission data rates.

enough signal power such that P_v approximates to 0; the transmission interference is limited in a local area, and the number of interference nodes N is small.

Impacts of Data Rate on Goodputs

The Adaptive Modulation and Coding (AMC) technique [118] has been widely studied and applied in wireless communications. It is still necessary to analyze the impacts of data rate, as we have a completely different application with many distinct features. To focus on the data rate, we fix the data arrival rate as 340 Kbps. Figure 4.10 illustrates the average goodputs with different data rates.

From Figure 4.10, we summarize the following observation.

Observation 7. *In general, the data rate of 24 Mbps provides the largest and the most robust average goodput for in-cabin Wi-Fi communications. Both the highest and the lowest data rates provide poor average goodputs.*

We explain Observation 7 with a tradeoff between the PHY-layer performance and MAC-layer performance in terms of the data rate.

1. The PHY-layer performance decreases with the data rate. A higher data rate corresponds to a higher order modulation, thus is more vulnerable to noise and interference. To achieve the same PLR performance, a higher data rate requires a higher SINR value (i.e. a better channel condition). In other word, when the PHY-layer condition is fixed, PLR increases with the data rate. This suggests that each packet experiences a larger number of retransmissions when a higher data rate is used.
2. The MAC-layer performance increases with the data rate. A higher data rate can transmit more packets when the channel is clear. Meanwhile, the transmission duration of each packet reduces with data rate. For example, for a 500-byte packet, the transmission duration with 6Mbps and 48Mbps is 6.7 msec and 0.8 msec, respectively. With a higher data rate, each packet goes through the wireless channel faster, and experiences less collision in transmission.
3. According to the above explanations, there is a tradeoff between the PHY layer performance and MAC layer performance in terms of the data rate. For the data rate range of 6 Mbps to 24 Mbps, the decrease of the average goodput due to the channel fading and interference is complemented by the increase of the transmission rate. Hence, the average goodput increases with the data rate in this range. For the data rate range of 24 Mbps to 48 Mbps, the impact of channel fading and interference overshadows the increase of the data rate. As a result, the average goodput decreases with the data rate in this range.

Figure 4.11 illustrates regional goodputs of different data rates. We can summarize the following observation from Figure 4.11.

Observation 8. *In general, the data rate of 24 Mbps provides the largest and the most robust regional goodput for in-cabin Wi-Fi communications.*

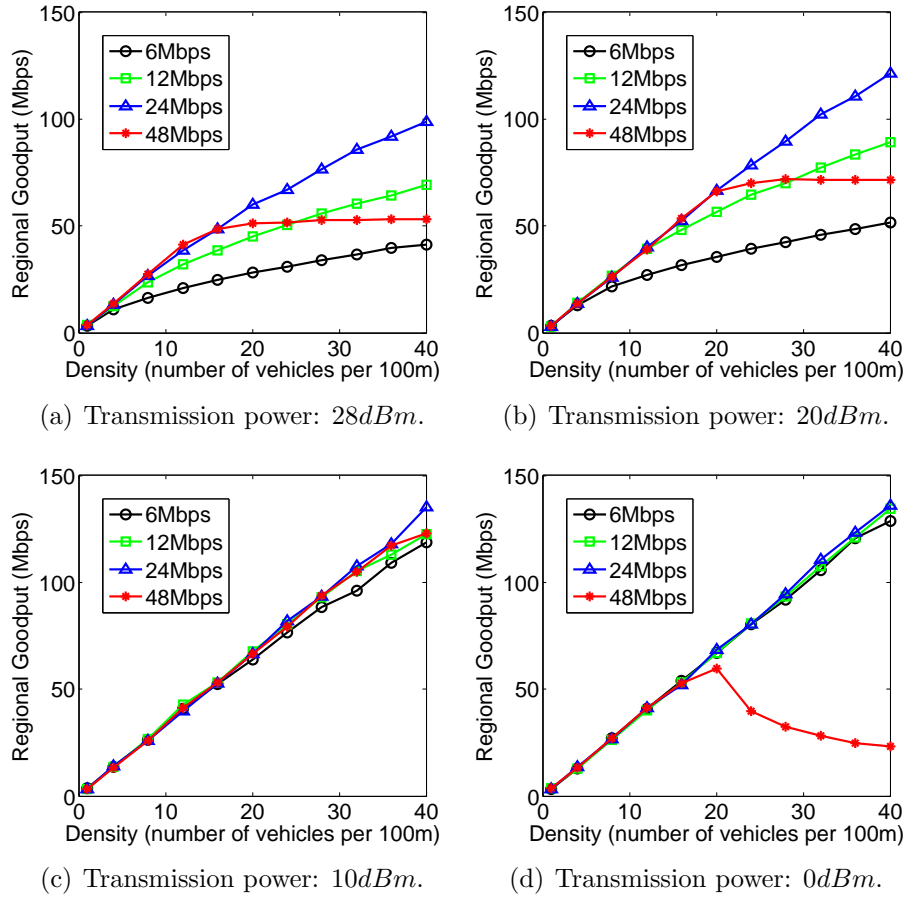


Figure 4.11 Regional goodputs of different transmission data rates.

As the explanation for Observation 8 is similar to that of Observation 7, we skip the explanation. We also notice that the tendency of the goodput of 48 Mbps is different from those of 6 Mbps, and 12 Mbps. The goodput of 48 Mbps decreases rapidly in the high density region. The reason is explained as follows. For the data rates of 6 Mbps and 12 Mbps, the goodput decreases mainly due to the increasing collisions. The impact of collisions on goodput grows gradually with the traffic density. For the data rate of 48 Mbps, the goodput reduces mainly due to the decreasing channel SINR. According to the empirical packet receiving model (i.e., the SINR-PLR curves in 4.4), the packet loss increase dramatically with the decreasing channel SINR, resulting in a fast-reducing goodput. Consequently, the goodput of 48 Mbps decreases much faster than that of other data rates.

Figure 4.10 and Figure 4.11 also confirm Observation 5 and Observation 6. For example, by comparing Figure 4.10(a) with Figure Figure 4.10(b), (c) and (d), we can see that the transmission power of 10dBm can support all the data rates well, while other transmission powers result in performance degeneration of one or several data rates. Similarly, we can use Figure 4.8 and Figure 4.9 to confirm that the transmission power of 10 dBm is superior to other power options.

4.4 In-cabin Wi-Fi Video Streaming and its Challenges

With a good understanding of the in-cabin Wi-Fi systems, we can now move forward and try to improve the QoS of these systems. In fact, the adaptation and control approaches of communication variables developed for DSRC in Chapter 3 can also be applied to in-cabin Wi-Fi systems in achieving better QoS. However, in this chapter, we will not try to reinvent the wheels. Instead of adaptive communication variables, we utilize and develop adaptive protocols to achieve our goal. To understand the motivations of our design of adaptive protocols, we next discuss the major traffic consuming service of in-cabin Wi-Fi systems - the video streaming service, as well as the challenges in supporting this service.

Mobile video streaming is one of the most popular but also most bandwidth hungry mobile services. Along with the deployment of in-cabin Wi-Fi systems, the penetration of mobile video streaming in vehicular communications will soar. To provide a satisfactory video viewing experience, video packets should be delivered with low delays and small delay jitters. This mission is non-trivial, as we are dealing with a wireless system that is very different from existing ones.

Figure 4.12 illustrates the differences between our in-cabin Wi-Fi scenario and a traditional one. (1) The in-cabin Wi-Fi APs are deployed on personal vehicles, and thus are fully distributed and non-cooperative. There is no message exchange among the APs. Meanwhile, in-cabin Wi-Fi APs are rapidly moving, resulting in a frequently varying AP topology. (2) Video streaming requires low delivery delay and small jitters. (3) The clients only use on-the-shelf mobile devices. (4) The BS never makes scheduling decisions for video content distributions at in-cabin Wi-Fi APs. Considering the above differences, a new scheduling scheme is needed for the novel service of in-cabin Wi-Fi video streaming.

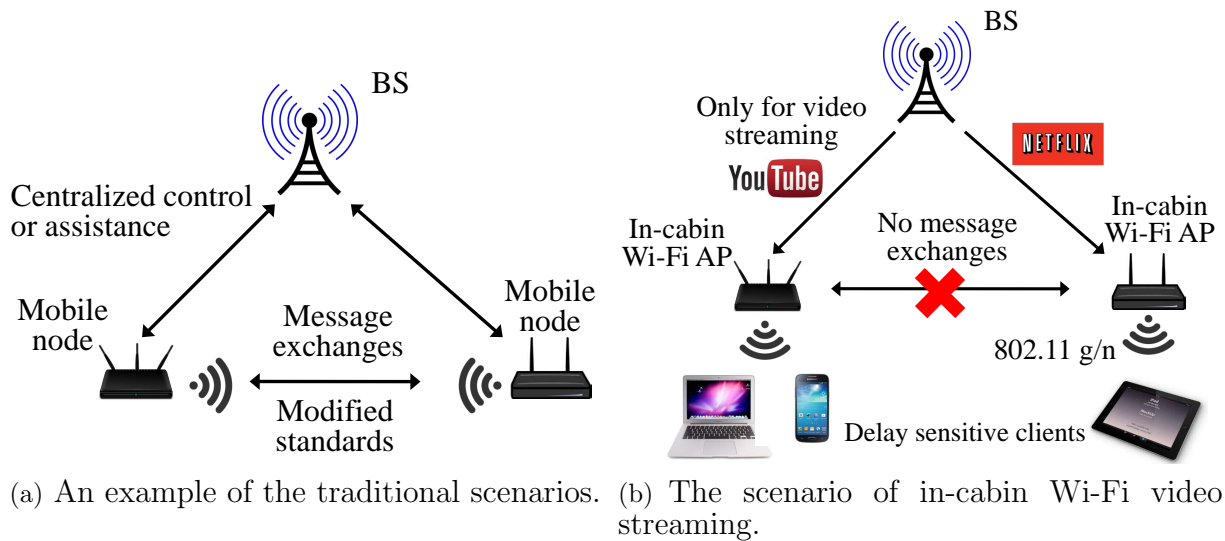


Figure 4.12 Differences between a traditional scenario and the in-cabin Wi-Fi scenario.

4.4.1 Challenges

The design of a scheduling scheme for in-cabin Wi-Fi video streaming faces the following challenges.

Challenge 6. *The scheduling scheme should be fully distributed. Due to the large communication delay, a cellular BS is not suitable to control the dynamic in-cabin Wi-Fi transmissions. Meanwhile, it is inefficient to select a centralized controller from all the constantly moving in-cabin Wi-Fi APs.*

Challenge 7. *At the same time, this distributed scheduling scheme should be delay-aware to serve video streaming. Existing delay-aware scheduling algorithms are mainly designed for centralized networks, and thus are not suitable for in-cabin Wi-Fi systems.*

Challenge 8. *The scheduling scheme should be robust to the fast-changing topology of APs in vehicular environments.*

Challenge 9. *The scheduling scheme should be compatible with the commodity client and AP devices. For the ease of deployment, the scheduling scheme should introduce little modification to the on-the-shelf AP and client devices.*

4.5 Design of the DRIVING Framework

To address the aforementioned challenges, we propose the **Delay-awaRe DIstributed Video schedulING** (DRIVING) framework.

4.5.1 Overall Design

The core idea of DRIVING is to assign high transmission priorities to packets with large queueing delays. DRIVING supports K levels of priorities. Level 0 represents the highest priority while level $K - 1$ denotes the lowest priority. To realize the priorities, a small Contention Window (CW) size is assigned to a high-priority packet. DRIVING consists of three modules, and is summarized as follows.

The DRIVING framework

1. **The delay measurement** module measures the queueing delay of the head-of-line packet, and saves this delay as D_{head} . If the queue is empty, D_{head} is set to 0.
2. **The priority evaluation** module evaluates the priority level of the head-of-line packet according to D_{head} , and set the corresponding priority as k , where $k = 0, 1, \dots, K - 1$.
3. **The scheduling decision** module sets the CW size of the upcoming backoff procedure as $W_{i,k}$, according to the priority level k and a number i . This i denotes the number of transmission attempts that have been made for the head-of-line packet. The scheduling decision module then instructs the backoff handler of the CW size $W_{i,k}$.

The procedure of DRIVING is summarized as in Figure 4.13

4.5.2 Solving the Challenges with DRIVING

The delay measurement module measures the local queueing delay D_{head} of the head-of-line packet. This information is measured locally by APs (while acquiring the deadline information requires extra message exchanges between APs and clients). This delay serves as a fully distributed criterion of scheduling. In this way, DRIVING solves **Challenge 6**.

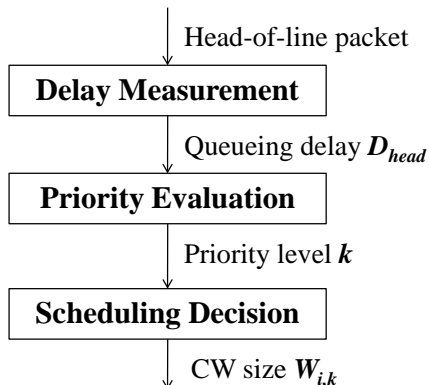


Figure 4.13 The block diagram of DRIVING.

The *priority evaluation module* evaluates the transmission priority level of each head-of-line packet, according to the queueing delay D_{head} . A large queueing delay indicates an approaching deadline. Thus, a high transmission priority is assigned to the packet. In this way, transmissions are scheduled by delay-aware priorities. Hence, DRIVING is delay-aware and solves **Challenge 7**.

The detailed implementation of the priority evaluation module is summarized as follows. Each priority level k corresponds to a continuous set β_k of the queueing delay. The queueing delay of a packet with a higher priority is always larger than the queueing delay of a packet with a lower priority. Let D_k denotes the queueing delay of a packet in priority level k . For two priority levels i and j , we have

$$\max(D_j | D_j \in \beta_j) < \min(D_i | D_i \in \beta_i), 0 \leq i < j \leq K - 1. \quad (4.29)$$

Further, the union of all the delay sets covers all the non-negative real numbers, i.e.,

$$\bigcup_{k=0}^K \beta_k = \mathbf{R}^+ \cup \{0\}. \quad (4.30)$$

Note that the DRIVING framework generalize different designs of the delay sets.

The *scheduling decision module* realizes the scheduling decision based on the priority passed down from the priority evaluation module. To achieve this, this module sets the minimum CW size of the upcoming backoff procedure as $W_{0,k}$ according to the priority k .

A packet with a high priority has a small minimum CW size, i.e.,

$$W_{0,0} \leq W_{0,1} \leq \cdots \leq W_{0,K-1}. \quad (4.31)$$

For a packet that has been transmitted i times, this module further sets the CW size as $W_{i,k}$. According to the IEEE 802.11 backoff process, we have

$$W_{i,k} = W_{0,k} \cdot 2^i. \quad (4.32)$$

This CW size is then passed to the backoff handler. In this way, DRIVING utilizes the backoff process to realize its scheduling decisions. As the backoff process runs independently of the network topology, the scheduling decision remains valid even when the network topology changes frequently. Hence, DRIVING solves **Challenge 8**. In addition, it only requires a software upgrade to integrate the scheduling decision module into commodity APs. Thus, DRIVING solves **Challenge 9**.

4.6 Analytical Modeling of DRIVING

In order to theoretically analyze and optimize the DRIVING framework, we establish new analytical models.

4.6.1 Analytical Models in Two Levels

We establish one packet level model for the backoff process and two queue level models for the queuing process. These two levels of models are correlated through their inputs and outputs, as presented in Figure 4.14.

4.6.2 The Packet Level Model

The packet level model is identical to the model developed in Section 4.3. Thus, we skip the details for brevity. With this model, given the video packet arriving rate λ_k , we can derive the average service rate μ_k .

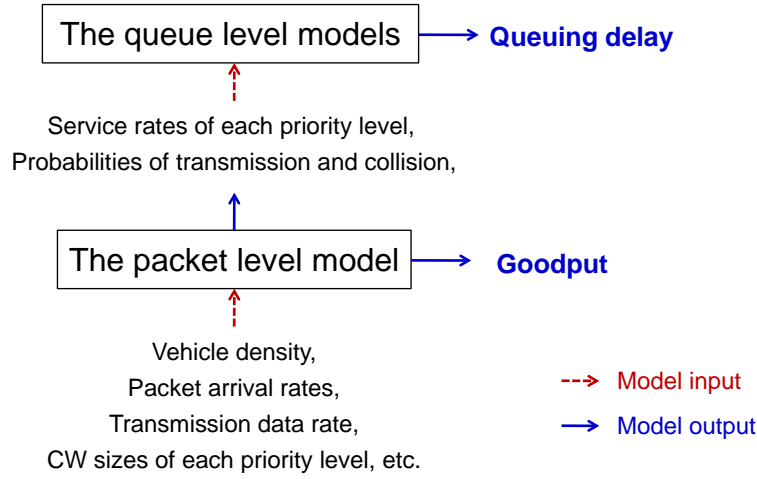


Figure 4.14 The two-level models.

Interactions among Markov Chains in the Packet Level Model

Denote the number of nodes with priority k as N_k . In real deployment, an indicator can be appended to the packet header to indicate the priority k of the packet. Then, N_k can be estimated by monitoring this indicator and the distinct MAC addresses encapsulated in headers of received packets [119]. The total number of nodes is then $N = \sum_{k=0}^{K-1} N_k$. We assume that all these N nodes are within the carrier sensing range of each other¹. For a node at the priority level k , it not only contends with other $N_k - 1$ nodes in the same priority level, but also experiences collisions from $N - N_k$ nodes in other priority levels. Let ς_k denote the probability that a node in priority level k attempts to transmit in the current virtual slot. Then, the probability P_{C_k} that the channel is busy is

$$P_{C_k} = 1 - (1 - \varsigma_k)^{N_k - 1} \prod_{i \neq k} (1 - \varsigma_i)^{N_i}, k = 0, \dots, K - 1. \quad (4.33)$$

The probability P_{S_k} that a node in priority level k successfully transmits a packet in the current virtual slot is [9]

$$P_{S_k} = \varsigma_k (1 - P_{C_k}), k = 0, 1, \dots, K - 1. \quad (4.34)$$

¹To capture the presence of hidden terminals, existing models (e.g. models in [108] and [120]) can be integrated into our model.

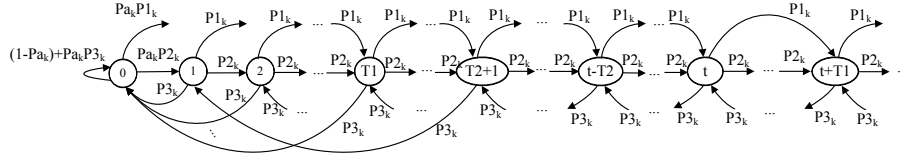


Figure 4.15 The DTMC for the queueing process of each node in priority level k when $\lambda_k < \mu_k$

Further, the probability P_{tr} that at least one of the nodes is transmitting at current virtual slot is defined as [9]

$$P_{tr} = 1 - \prod_{k=0}^K (1 - \varsigma_k)^{N_k}. \quad (4.35)$$

4.6.3 The Queue Level Models

The queue level model consists of another set of DTMCs. For each priority level, we establish one DTMC to model the queueing process of each node in this priority level. We notice that queues with $\lambda_k < \mu_k$ evolve differently from queues with $\lambda_k \geq \mu_k$. In the case of $\lambda_k < \mu_k$, the queueing process can be characterized with the stationary distribution of its corresponding DTMC. In the case of $\lambda_k \geq \mu_k$, the stationary distribution does not exist, and features of the queueing process are time-dependent. Thus, we separate the discussions of these two cases, and establish two different kinds of DTMCs. Note that the input μ_k is an output of the packet level model. Meanwhile, λ_k is determined by the resolution of the requested videos, hence λ_k is known to each node in priority level k .

The Queue Level Model of $\lambda_k < \mu_k$

The DTMC for this case is presented in Figure 4.15.

There are three one-step transition probabilities for each state except state 0.

(a) Let $P1_k$ denote the probability that the channel is busy and the head-of-line packet does not reach its re-transmission limit (thus is not dropped). In this case, no matter the current node transmits or not, it has to freeze its backoff counter and wait for T_1 time slots. Thus, the queueing delay increases by T_1 time slots.

(b) Let $P2_k$ denote the probability that the channel is idle. In this case, no one transmits in the current time slot, and the queueing delay increases by 1 time slot.

(c) Let $P3_k$ denote the probability that the head packet is successfully transmitted or is dropped after $m + 1$ transmission attempts. In this case, the head packet leaves the queue and the succeeding packet becomes the head packet. And arrival time of the new head packet is Ta_k/σ time slots less than that of the former head packet. Meanwhile, the new head packet needs to wait T_S/σ time slots when the previous packet is being transmitted. Thus, the queueing delay of the head packet decreases by $\min[D, T_2]$ time slots, where D is the current queueing delay.

For the special case of state 0, we have the following rules. From state 0, the DTMC stays in state 0 if no packet arrives in the current time slot or the newly arrival is successfully transmitted. Then the transition probability from state 0 to state 0 is $(1 - Pa_k) + Pa_k P3_k$. From state 0, the DTMC transits to state 1 with probability $Pa_k P2_k$, if there is a newly arrived packet and the channel is idle. From state 0, the DTMC transits to state T_1 with probability $Pa_k P1_k$, if there is a newly arrived packet and the channel is busy.

Taking the outputs from the packet level model, we determine $P1_k$, $P2_k$, and $P3_k$ as follows

$$P1_k = Pc_k(1 - Pc_k^m \pi_{0,0,k}), \quad (4.36)$$

$$P2_k = (1 - \varsigma_k)(1 - Pc_k), \quad (4.37)$$

$$P3_k = \varsigma_k(1 - Pc_k) + Pc_k \cdot Pc_k^m \pi_{0,0,k}, \quad (4.38)$$

where $\pi_{0,0,k}$ is the stationary probability of the state (0,0) in the DTMC of priority k from the packet level.

The Queue Level Model of $\lambda_k \geq \mu_k$

To model the queueing process of this case, we use a M/M/1 queue with an arrival rate of λ_k and a service rate of μ_k , as shown in Figure 4.16. Each state in the DTMC in Figure 4.16 represents a queue length. M/M/1 queues have been extensively studied. However, we still need a ready-to-use queueing delay analytical model for the case of $\lambda_k \geq \mu_k$.

4.6.4 Average Queueing Delay

Given the queue level model, λ_k and μ_k , we next derive the average queueing delay \bar{D} . Note that μ_k is derived by the packet level model.

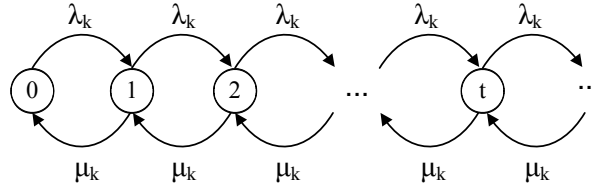


Figure 4.16 The DTMC for the queueing process of each node in priority level k when $\lambda_k \geq \mu_k$.

The Average Queueing Delay of $\lambda_k < \mu_k$

We focus on the DTMC shown in Figure 4.15. Let $\bar{e}_k(t)$ denote the stationary distribution of this DTMC, where t is the index of state. Then we have the following recurrence equations

$$\bar{e}_k(t) = \begin{cases} P1_k \bar{e}_k(t - T_1) + P2_k \bar{e}_k(t - 1) + P3_k \bar{e}_k(t + T_2), t \geq T_1 + 1, \\ P_a P1_k \bar{e}_k(t - T_1) + P2_k \bar{e}_k(t - 1) + P3_k \bar{e}_k(t + T_2), t = T_1, \\ P2_k \bar{e}_k(t - 1) + P3_k \bar{e}_k(t + T_2), 2 \leq t \leq T_1 - 1, \\ P_a P2_k \bar{e}_k(t - 1) + P3_k \bar{e}_k(t + T_2), t = 1, \\ \frac{P3_k}{P_a k (1 - P3_k)} \sum_{i=1}^{T_2} \bar{e}_k(i), t = 0. \end{cases} \quad (4.39)$$

The next lemma characterizes $\bar{e}_k(t)$ when $t \geq T_1 + 1$.

Lemma 3. *The stationary distribution of the DTMC shown in Figure 4.15 satisfies*

$$\bar{e}_k(t) = A_1 r^t, \quad t \geq T_1 + 1, \quad (4.40)$$

where A_1 is a constant, $0 < r < 1$, and r is a root of the following characteristic function

$$P1_k u + P2_k u^{T_1} + P3_k u^{T_1 + T_2 + 1} - u^{T_1 + 1} = 0. \quad (4.41)$$

Proof. We first proof this lemma when $t \geq 2T_1 + 1$. When $t \geq 2T_1 + 1$, we have $\bar{e}_k(t - T_1) = P1_k \bar{e}_k(t - 2T_1) + P2_k \bar{e}_k(t - T_1 - 1) + P3_k \bar{e}_k(t - T_1 + T_2)$. Thus, all stationary probabilities involve in the recurrence equations of $\bar{e}_k(t), t \geq 2T_1 + 1$, are in the same form. Therefore,

for $\bar{e}_k(t), t \geq 2T_1 + 1$, we have

$$\bar{e}_k(t) = A_1 r^t, t \geq 2T_1 + 1, \quad (4.42)$$

where A_1 is a constant and $0 < r < 1$ is a root of the characteristic function (4.41). When the queue is stable ($\lambda_k < \mu_k$), this root r exists. Next, we proof the lemma when $T_1 + 1 \leq t \leq 2T_1$. With Eq. (4.42), we have

$$\begin{cases} A_1 r^{2T_1+1} = P1_k \bar{e}_k(T_1 + 1) + P2_k A_1 r^{2T_1} + P3_k A_1 r^{2T_1+T_2+1}, \\ A_1 r^{2T_1+2} = P1_k \bar{e}_k(T_1 + 2) + P2_k A_1 r^{2T_1+1} + P3_k A_1 r^{2T_1+T_2+2}, \\ \vdots \\ A_1 r^{3T_1} = P1_k \bar{e}_k(2T_1) + P2_k A_1 r^{3T_1-1} + P3_k A_1 r^{3T_1+T_2}. \end{cases} \quad (4.43)$$

Summing up all the equations in Eq. (4.43), we have

$$\sum_{t=T_1+1}^{2T_1} \bar{e}_k(t) = A_1 r^{T_1} (r + r^2 + \dots + r^{T_1}). \quad (4.44)$$

Therefore, we can conclude that

$$\bar{e}_k(t) = A_1 r^t, t \geq T_1 + 1.$$

□

With *Lemma 1* and Eq. 4.39, we can further derive equations (4.45), (4.46) and (4.47).

$$\begin{aligned} \bar{e}_k(0) &= \frac{P3_k}{P_a(1-P3_k)} \left\{ \frac{1}{(1-P2_k)} \left[A_1 P3_k - k r^{T_2+1} \left(\frac{1-r^{T_1}}{1-r} \right) \right. \right. \\ &\quad \left. \left. + P_a(P1_k + P2_k) \bar{e}_k(0) - \bar{e}_k(T_1) \right] + A_1 r^{T_1+1} \left(\frac{1-r^{T_2-T_1}}{1-r} \right) \right\}, \end{aligned} \quad (4.45)$$

$$\bar{e}_k(T_1) = \frac{A_1}{P2_k} r^{T_1+1} - P1_k P_a \bar{e}_k(0) - \frac{P1_k P3_k}{P2_k} A_1 r^{T_2+1} - \frac{P3_k}{P2_k} A_1 r^{T_1+T_2+1}, \quad (4.46)$$

$$1 = \left[1 + \frac{P_a(1-P3_k)}{P3_k} \right] \bar{e}_k(0) + \frac{A r^{T_2+1}}{1-r}. \quad (4.47)$$

By solving Eq. (4.45), (4.46) and (4.47), we obtain the values of $\bar{e}_k(0)$, $\bar{e}_k(T_1)$, and the

constant A_1 . All the $\bar{e}_k(t), t = 0, 1, \dots$, can be explicitly expressed by $\bar{e}_k(0)$, $\bar{e}_k(T_1)$, and A_1 . Thus, the stationary distribution of the DTMC in Figure 4.15 is achieved.

Denote the average queueing delay of packets transmitted by any node in priority level k as \bar{D}_k . Given the stationary distribution, \bar{D}_k is estimated as

$$\bar{D}_k = \sigma \cdot \sum_{t=0}^{\infty} t \cdot \bar{e}_k(t). \quad (4.48)$$

The Average Queueing Delay of $\lambda_k \geq \mu_k$

We focus on the DTMC shown in Figure 4.16. We number the arrival packets by $1, 2, \dots$, in the order of their arrival time. Denote the arrival time of the n th packet as a_n , and the departure time of the n th packet as c_n . We focus on the case where the queue begins to evolve with no packet. (An initially non-empty queue can be easily modeled by changing the initial conditions of our model.) Then we have the following lemma on the expectations of a_n and c_n .

Lemma 4. *Let $\mathbf{E}(a_n)$ and $\mathbf{E}(c_n)$ be the expectations of arrival and departure time of the n th packet, respectively. When $\lambda_k \geq \mu_k$, we have the following equations for the queueing process presented in Figure 4.16*

$$\lim_{n \rightarrow \infty} \mathbf{E}(a_n)/n = (\lambda_k + \mu_k)/\lambda_k, \quad (4.49)$$

$$\lim_{n \rightarrow \infty} \mathbf{E}(c_n)/n = (\lambda_k + \mu_k)/\mu_k. \quad (4.50)$$

Proof. Suppose the n th client arrives at time slot x , i.e., $a_n = x$. Then n follows a Binomial distribution with parameters x and $\lambda_k/(\mu_k + \lambda_k)$. Let random variable $Y \sim \text{Bin}(x, \lambda_k/(\mu_k + \lambda_k))$. Hence, we have

$$\mathbf{P}\{a_n = x\} = \mathbf{P}\{Y = n\}. \quad (4.51)$$

Next, we will prove that there exists a constant A_2 , such that

$$\lim_{n \rightarrow \infty} \mathbf{P}\{a_n \geq (1 + \epsilon)A_2n\} = 0, \quad (4.52)$$

$$\lim_{n \rightarrow \infty} \mathbf{P}\{a_n \leq (1 - \epsilon)A_2n\} = 0, \quad (4.53)$$

where $\epsilon > 0$ is an arbitrarily small number.

We first prove Eq. (4.52). Since a_n is a discrete variable, proving Eq. (4.52) is equivalent to proving the following equation

$$\lim_{n \rightarrow \infty} \mathbf{P}\{a_n \geq \lceil (1 + \epsilon)A_2n \rceil\} = 0, \quad (4.54)$$

where $\lceil \cdot \rceil$ is the ceiling operator. From Eq. (4.51) and Eq. (4.54), we have

$$\mathbf{P}\{a_n \geq \lceil (1 + \epsilon)A_2n \rceil\} = \mathbf{P}\left\{Bin\left(\lceil (1 + \epsilon)A_2n \rceil, \frac{\lambda_k}{\lambda_k + \mu_k}\right) \leq n\right\}. \quad (4.55)$$

Let $X \sim Bin\left(\lceil (1 + \epsilon)A_2n \rceil, \frac{\lambda_k}{\lambda_k + \mu_k}\right)$. By Hoeffding's inequality, we have the following bound

$$\mathbf{P}\{X \leq n\} \leq \exp\left(\frac{-2\left[\lceil (1 + \epsilon)A_2n \rceil \frac{\lambda_k}{\lambda_k + \mu_k} - n\right]^2}{\lceil (1 + \epsilon)A_2n \rceil}\right). \quad (4.56)$$

Taking $A_2 = \frac{\lambda_k + \mu_k}{\lambda_k}$ and $n \rightarrow \infty$, Eq. (4.56) can further express as follows

$$\lim_{n \rightarrow \infty} \mathbf{P}\{X \leq n\} \leq \lim_{n \rightarrow \infty} \exp\left(\frac{-2\epsilon n^2 - \frac{2\lambda_k}{\lambda_k + \mu_k}}{(1 + \epsilon)A_2n - 1}\right) = 0 \quad (4.57)$$

Therefore, taking $A_2 = \frac{\lambda_k + \mu_k}{\lambda_k}$, we prove Eq. (4.52) and Eq. (4.54), and further have

$$\lim_{n \rightarrow \infty} \mathbf{P}\{a_n \geq (1 + \epsilon)\frac{\lambda_k + \mu_k}{\lambda_k}n\} = 0. \quad (4.58)$$

The proof of Eq. (4.53) is similar to the above proof of Eq. (4.52). We skip it for brevity and directly give the following result

$$\lim_{n \rightarrow \infty} \mathbf{P}\{a_n \leq (1 - \epsilon)\frac{\lambda_k + \mu_k}{\lambda_k}n\} = 0. \quad (4.59)$$

Combining Eq. (4.58) and Eq. (4.59), we have

$$\lim_{n \rightarrow \infty} \mathbf{E}(a_n)/n = \frac{\lambda_k + \mu_k}{\lambda_k}.$$

Similarly, for c_n , we have

$$\lim_{n \rightarrow \infty} \mathbf{E}(c_n)/n = \frac{\lambda_k + \mu_k}{\mu_k}.$$

□

When $\lambda_k \geq \mu_k$, the average queueing delay keeps increasing as time goes by. Therefore, we focus on the average queueing delay of packets that are transmitted before a constant time slot T ($T < \infty$). To capture the delay up to T , we first need to calculate the number of clients transmitted before T . We have the following lemma for the average number of transmitted packets before time slot T .

Lemma 5. *Let N_T be the number of packets that are transmitted before T . When $\lambda_k \geq \mu_k$, we have the following equation for the queueing process presented in Figure 4.16*

$$\lim_{T \rightarrow \infty} N_T/T = \mu_k/(\lambda_k + \mu_k). \quad (4.60)$$

Proof. By definition of N_T , we have $N_T = \max\{n | c_n \leq T\}$. Therefore, we have

$$c_{N_T} \leq T. \quad (4.61)$$

Then, there exists a value $\delta \geq 0$ such that $c_{N_T} = T - \delta$. As the $(N_T + 1)$ th client is served after T , it is true that

$$c_{N_T+1} - c_{N_T} > T - c_{N_T} = \delta. \quad (4.62)$$

Hence, we have

$$\begin{aligned} \mathbf{E}[c_{N_T+1}] &= T - \mathbf{E}[\delta] \\ &> T - \mathbf{E}[c_{N_T+1} - c_{N_T}] = T - \frac{\lambda_k + \mu_k}{\mu_k}. \end{aligned} \quad (4.63)$$

Combining inequalities (4.61), (4.63) and Lemma 2, we have

$$\lim_{T \rightarrow \infty} \mathbf{E}[c_{N_T}]/T = \lim_{T \rightarrow \infty} \frac{\frac{\lambda_k + \mu_k}{\mu_k} N_T}{T} = 1. \quad (4.64)$$

Rearranging the terms in Eq. (4.64), we conclude our proof with

$$\lim_{T \rightarrow \infty} N_T/T = \frac{\mu_k}{\lambda_k + \mu_k}.$$

□

Given *Lemma 2* and *Lemma 3*, we can characterize the average queueing delay for the case of $\lambda_k \geq \mu_k$ with the following theorem.

Theorem 3. *Let $\bar{D}_k(T)$ denote the average queueing delay (in seconds) of packets transmitted by a priority k node before time slot T . When $\lambda_k \geq \mu_k$, we have the following equation for the queueing process presented in Figure 4.16*

$$\bar{D}_k(T) \xrightarrow{a.s.} \frac{\sigma T}{2} \cdot \frac{\lambda_k - \mu_k}{\lambda_k}, \quad (4.65)$$

where $\xrightarrow{a.s.}$ means “converges almost surely”.

Proof. By *Lemma 2*, we have the following equation for the queueing delay $c_n - a_n$ of the n th packet

$$\mathbf{E}[c_n - a_n] = \mathbf{E}[c_n] - \mathbf{E}[a_n] \xrightarrow{a.s.} \frac{\lambda_k + \mu_k}{\mu_k} n - \frac{\lambda_k + \mu_k}{\lambda_k} n = \frac{\lambda_k^2 - \mu_k^2}{\lambda_k \mu_k} n. \quad (4.66)$$

And by *Lemma 3*, we have the following equation for the number of packets transmitted before T

$$\mathbf{E}[N_T] \xrightarrow{a.s.} \frac{\mu_k}{\lambda_k + \mu_k} T. \quad (4.67)$$

Take the length of each time slot as σ . Then combining Eq. (4.66) and Eq. (4.67), we have

$$\begin{aligned} \bar{D}_k(T) &= \sigma \mathbf{E} \left[\frac{\sum_{i=1}^{N_T} i \cdot \frac{\lambda_k^2 - \mu_k^2}{\lambda_k \mu_k}}{N_T} \right] \\ &\xrightarrow{a.s.} \sigma \cdot \frac{\mathbf{E}[N_T] + 1}{2} \cdot \frac{\lambda_k^2 - \mu_k^2}{\lambda_k \mu_k} \\ &\xrightarrow{a.s.} \frac{\sigma T}{2} \cdot \frac{\lambda_k - \mu_k}{\lambda_k}. \end{aligned}$$

□

With *Theorem 3*, we can estimate the average queueing delay of all packets in any given period. A brief example to apply *Theorem 3* is as follows. Suppose the system initiates at 0 second with empty queues. Then after running for 50 seconds, we would like to estimate the average queueing delay of nodes at priority level 2. Applying *Theorem 3*, we will set $k = 2$ and $T = 50$ in Eq. (4.65). We also collect λ_2 and μ_2 from the packet level model, and supply them to Eq. (4.65) as well. Also, recall that σ is the basic slot length defined in the 802.11n standard. Then we can estimate the average queueing delay as $[25\sigma \cdot \frac{\lambda_2 - \mu_2}{\lambda_2}]$.

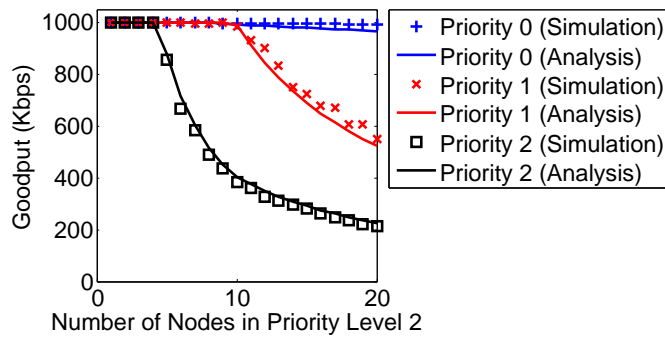
4.6.5 Model Validation

We next use ns-2 simulations to validate the proposed models of DRIVING. In our model validation, there are 3 priority levels, i.e., $k = 0, 1, 2$. The minimum CW sizes are $W_{0,0} = 3$, $W_{0,1} = 7$, and $W_{0,2} = 15$, respectively. To present the validation results clearly, we fix the numbers of nodes in priority levels 0 and 1, and change the number of nodes in priority level 2. Concretely, we fix $N_0 = 2$ and $N_1 = 2$, and change N_2 from 1 to 20. The packet size is set to 500B. For all the nodes, the packet arrival rate is 1Mbps, which matches the standard bit rate of YouTube 360p videos². Each run of simulations lasts for a duration of 50 seconds, i.e., $T = 50$. All the queues are empty at the beginning of this 50-second duration. We use a transmission data rate of 24Mbps as an example.

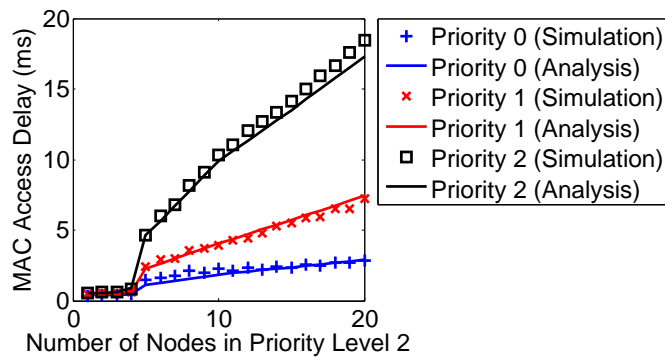
We validate our packet level model with the goodput and the MAC access delay in Figure 4.17(a) and (b), respectively. We also validate our queue level models with queueing delay in Figure 4.17(c). Generally, it is shown that both packet level and queue level metrics are well captured by our two-level models. Therefore, we conclude that the performance of DRIVING is accurately captured by our cross-layer modelling.

One interesting observation is that, the average MAC access delay of all nodes experiences a sudden jump at the point of $N_2 = 5$. The reason is explained as follows. When $N_2 \leq 4$, the probability ρ_k that a node has at least one packet to transmit is less than 1. This means the channel is sometimes idle. Video packets are transmitted quickly without queueing in the nodes. Yet, this situation suddenly disappears when $N_2 = 5$, where ρ_k increases to its upper limit 1. In this case, there is always at least one packet in the queue of each node in priority level 2. All the nodes in priority level 2 are constantly contending for the channel. As a result, the channel becomes very busy, and the MAC access delay (as

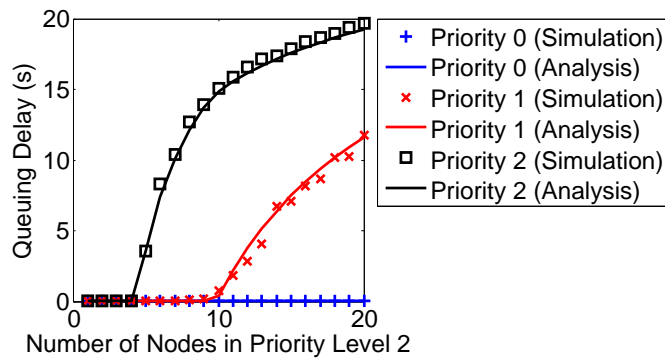
²YouTube Advanced Encoding Settings. [Online]. Available: <https://support.google.com/youtube/answer/1722171?hl=en>



(a) Average Goodput.



(b) Average MAC access delay.



(c) Average queuing delay.

Figure 4.17 The model validation results.

well as the queuing delay) of every node soars high. This again complies with our packet level model.

Table 4.5 Candidate delay sets for DRIVING.

Setting	β_2	β_1	β_0
1	[0, 1)	[1, 2)	[2, $+\infty$)
2	[0, 1)	[1, 4)	[4, $+\infty$)
3	[0, 2)	[2, 4)	[4, $+\infty$)
4	[0, 2)	[2, 10)	[10, $+\infty$)
5	[0, 4)	[4, 10)	[10, $+\infty$)

4.7 Tuning DRIVING with the Models

One important application of our analytical models is to tune the DRIVING for better performance before real deployment. There are three kinds of parameters to be tuned, i.e., the number of priority levels, their corresponding delay sets, and their corresponding minimum CW sizes. Due to the limited space, we only present the tuning of the delay sets while fixing the number of priority levels and the corresponding minimum CW sizes. Concretely, we use 3 priority levels, and set their minimum CW sizes as 3, 7, and 15, respectively. We compare five candidate delay sets as presented in Table 4.5, and select the best one from them.

Based on our two-level models, we calculate the evolution of queueing delays under these five settings. As an example, we set set packet size as $500B$, and the packet arrival rate as $1Mbps$. Fig. 4.18 illustrate how the queueing delays increase with time. It is shown that Setting 3, which is neither the most aggressive nor the most conservative, achieves the lowest queueing delay at all time. The reason is two-fold. On one hand, an aggressive setting tends to push all nodes to the highest priority level quickly. As a result, the CW sizes of all nodes become too small to avoid packet collisions. On the other hand, a conservative setting tends to retain all nodes in at the lowest priority level. Consequently, the CW sizes of all nodes remain too large, and thus the channel utilization remains low.

4.8 Evaluation of DRIVING

In this section, we conduct comprehensive simulation studies to illustrate the improvements brought by DRIVING. We first present the setup of our ns-2 evaluation platform. We then evaluate the performance of DRIVING in terms of delay, jitter, deadline missing ratio and

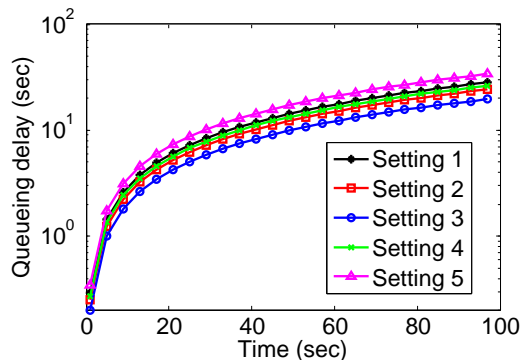


Figure 4.18 The queuing delays under different settings of DRIVING.

Table 4.6 Settings for the highway scenario.

Description	Value
Highway length	3000m
Highway width	20m
# of lanes	4
Lane width	4m
Isolation zone width	4m
Positions of vehicles	Poisson
# of vehicles(n)	$n \in [8, 80]$
Distances between AP and target users	$[0.1m, 0.5m]$

goodput.

4.8.1 Evaluation Setup

The Highway Scenario

We conduct our simulations in an urban bidirectional highway section. This highway section is of 3000m long. It has 2 lanes in each direction and an isolation zone in the middle. We assume that the distance between two neighbour vehicles on the same lane follows an exponential distribution [34, 120]. We further assume that the whole highway section is covered by a cellular network. Table 4.6 summarizes the settings for the highway scenario. We change the density of vehicles in this highway section to study how the video streaming performance is impacted by traffic condition.

Table 4.7 Settings for in-cabin Wi-Fi device.

Description	Value
Center frequency	2.4GHz
Bandwidth	20MHz
Transmission power	10dBm
# of in-cabin Wi-Fi APs on each vehicle	1
# of clients served by each AP	1
Buffer size of each AP	16MB
Packet size	500 bytes

In-cabin Wi-Fi Settings

Each vehicle on the highway is equipped with an in-cabin Wi-Fi AP, which runs on the 2.4GHz band. We assume that all APs are working in the same 20MHz Wi-Fi channel. The transmission power of the APs is set to 10dBm, as Observation 7 and Observation 8 (in Section 4.3.5) already demonstrated that 10dBm provides the best and the most robust performance in general. Each in-cabin Wi-Fi AP has a 16MB buffer for video streaming. We focus on the case where each Wi-Fi AP serves one client. Table 4.7 summarizes these settings.

Propagation Model

Details of this model has already been described in Section 4.3.2. The parameters used in evaluation is given in Table 4.4.

Video Streaming Settings

The video bit-rate in our simulations is 3.3Mbps (High-Definition video streaming). Each video packet carries 500 bytes of video data. Multiple packets are grouped into one large video chunk [121], which represents around 10 seconds of video. Video chunks arrive at in-cabin Wi-Fi APs periodically [78].

Table 4.8 Settings for the propagation model.

Description	Value
Packet size	500 <i>B</i>
Chunk size	4 <i>MB</i>
Video bit-rate	3.3 <i>Mbps</i>
Chunk arrival process	Periodic ON/OFF [78]
Video length in a chunk	10 <i>s</i>

Scheduling Algorithms

We focus on distributed algorithms, as centralized algorithms are impractical in the in-cabin Wi-Fi scenarios. We compare the following three distributed algorithms.

1. The **DRIVING** algorithm supports 3 levels of priorities (in consistence with the industrial practice, e.g., 802.11 EDCA.). The minimum CW sizes of transmissions in priorities 0, 1 and 2 are $W_{0,0} = 3$, $W_{0,1} = 7$ and $W_{0,2} = 15$, respectively. The DRIVING algorithm assigns the highest priority (i.e., priority 0) to the head-of-line packets whose queuing delays are larger than 4 seconds (i.e., 40% of the playtime of a video chunk). The DRIVING algorithm assigns priority 1 to the head-of-line packets whose queuing delays are between 2 seconds and 4 seconds (i.e., 20 – 40% of the playtime of a video chunk). For the rest of the head-of-line packets, DRIVING algorithm assigns the lowest priority (i.e., priority 2).
2. The **Q-based** algorithm is an extension from the queue-length based CSMA algorithms in [75–77]. To compare with the DRIVING algorithms, we update existing queue-length based CSMA algorithms into the Q-based algorithm as follows. The Q-based algorithm also supports 3 levels of priorities. The minimum CW sizes of transmissions in priorities 0, 1 and 2 are $W_{0,0} = 3$, $W_{0,1} = 7$ and $W_{0,2} = 15$, respectively. If the length of a queue is larger than 6.4*MB* (i.e., 40% of the AP’s buffer size), the Q-based algorithm assigns the highest priority (i.e., priority 0) to the head-of-line packet in this queue. If the length of a queue is between 3.2*MB* and 6.4*MB* (i.e., 20 – 40% of the AP’s buffer size), the Q-based algorithm assigns priority 1 to the head-of-line packet in this queue. Otherwise, the head-of-line packet is with priority 2.

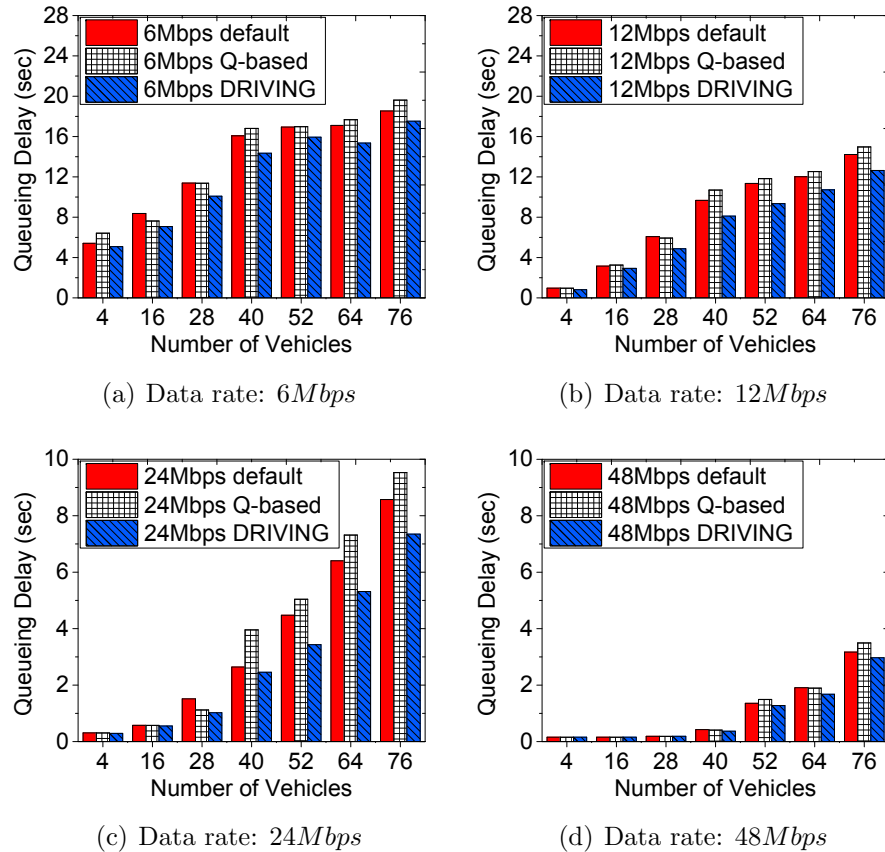


Figure 4.19 The average queuing delays.

3. The **default** algorithm follows the default settings of Wi-Fi Multimedia (WMM). WMM prioritizes traffic according to four Access Categories (AC): voice, video, best effort, and background. However, it does not further specify priorities for different video packets. We consider this algorithm as the baseline.

4.8.2 The Queuing Delay and Jitter Performance

We next evaluate the performance of in-cabin Wi-Fi video streaming in terms of the average queuing delay and jitter.

Figure 4.19 compares the average queuing delays of the three algorithms. Compared to the default algorithm, the DRIVING algorithm reduces the average queuing delay by up to 18.6%, 19.8%, 49.3% and 20.8% (for transmission data rates of 6Mbps, 12Mbps, 24Mbps

and $48Mbps$), respectively. Furthermore, even with the highest traffic density, DRIVING still results in the lowest queueing delay. This demonstrates that DRIVING is robust to the changes of traffic and AP topology.

Another observation from Figure 4.19(c) is worth noticing. The Q-based algorithm yields the largest average queueing delay when the number of vehicles is larger than 40. This indicates that the Q-based algorithm is not suitable for delay sensitive services such as video streaming. The reason is as follows. When the scheduling decision is made based on the queue length, the packets in a large queue always has a higher priority than those in a small queue. Let's consider the following example. Upon the arrival of a new video chunk to an AP Z_1 , the queue length of this AP suddenly rises up. Meanwhile, there is another AP Z_2 , who has only one largely delayed packet p . By the Q-based algorithm, packet p in AP Z_2 has a lower priority than that of the newly arrived packets in AP Z_1 . Therefore, the largely delayed packet p has to wait for almost all the newly arrived packets in AP Z_1 , leading to a significant increased delay for packet p . This problem would happen frequently, if the Q-based algorithm is used to schedule periodic ON/OFF Internet traffics, such as those of video streaming. On the contrary, the DRIVING algorithm avoids this problem by assigning higher priorities to packets with larger delays, and thus outperforms the other two algorithms.

Figure 4.20 compares the three algorithms in terms of the delay jitter. A smaller jitter of the queueing delay indicates a smoother video streaming, thus a better video viewing experience. Compared to the second best algorithm, the DRIVING algorithm reduces the jitter by up to 15.6%, 24.1%, 38.4% and 22.4% (for the transmission data rates of $6Mbps$, $12Mbps$, $24Mbps$ and $48Mbps$), respectively. Therefore, the DRIVING algorithm provides the most robust video streaming service.

It is also interesting to notice that, in terms of percentage, the increment of jitter with the $24Mbps$ data rate is much larger than that with the $6Mbps$ data rate. The reason is as follows. The data rate of $24Mbps$ employs the 16QAM modulation, which is much more vulnerable to the channel degeneration than the BPSK modulation utilized by $6Mbps$ data rate. Therefore, the jitter with the $24Mbps$ data rate is sensitive to the channel degeneration brought by the congested traffic. Compared to the other two algorithms, the DRIVING algorithm has the smallest degradation in jitter. This suggests that the DRIVING algorithm scales with the traffic density much better than the other two algorithms.

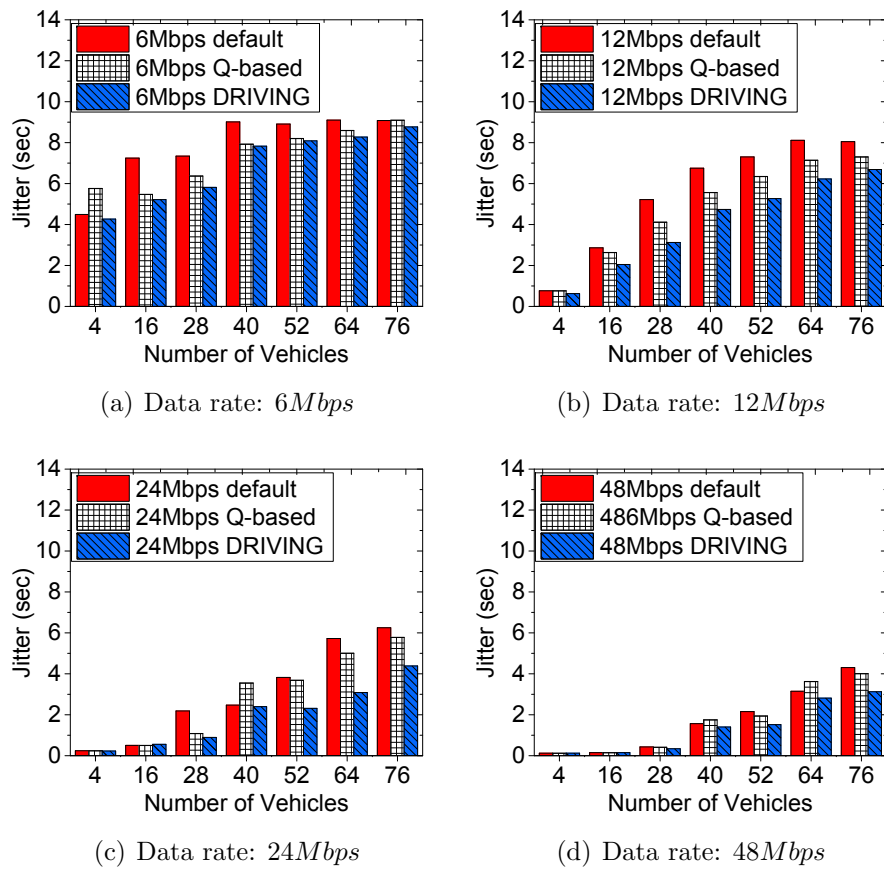


Figure 4.20 The delay jitters.

4.8.3 The Deadline Missing Ratio Performance

In this section, we evaluate the performance of in-cabin Wi-Fi video streaming in terms of the deadline missing ratio.

Figure 4.21 compares the average deadline missing ratios of the three algorithms. It is illustrated that the deadline missing ratios increase with traffic density. With the support of the DRIVING algorithm, the deadline missing ratio of in-cabin Wi-Fi video streaming is largely reduced. Compared to the default algorithm, the DRIVING algorithm reduces the deadline missing ratio by up to 33.5%, 32.9%, 40.8 and 38.9% (for transmission data rates of *6Mbps*, *12Mbps*, *24Mbps* and *48Mbps*), respectively. By using the queueing delay as the criterion of scheduling, the DRIVING algorithm is able to assign smaller CW sizes to packets that are approaching their deadlines. On average, these deadline-approaching packets are transmitted faster than others. In this way, the DRIVING algorithm reduces the deadline missing ratio. The Q-based algorithm cannot guarantee to schedule the deadline-approaching packets before other packets, and thus result in a higher deadline missing ratio. Figure 4.21 also illustrates that DRIVING always achieves the lowest deadline missing ratios in all traffic conditions. This again confirms that DRIVING is capable of working consistently with a varying density of vehicles and a changing topology of APs.

4.8.4 The Goodput Performance

In this section, we evaluate the performance of in-cabin Wi-Fi video streaming in terms of the goodput.

Figure 4.22 compares the average goodputs of the three algorithms. It is shown that the DRIVING algorithm achieves the highest average goodput. Compared to the default algorithm, the DRIVING algorithm enlarges the average goodput by up to 41.3%, 32.8%, 24.3% and 8.8% (for the transmission data rates of *6Mbps*, *12Mbps*, *24Mbps* and *48Mbps*), respectively. More importantly, the gap between DRIVING's average goodput and those of the other two algorithms increases with traffic density. Take the data rate of *24Mbps* for example: DRIVING increases the goodput by 7.1% when there are 8 vehicles. The improvement increases to 24.3% when there are 80 vehicles. This suggests that, compared to the other two algorithms, the DRIVING algorithm is more sustainable in a high-density traffic condition. The goodput performance improvement brought by the DRIVING algorithm is explained as follows. Compared to the default algorithm, the DRIVING algorithm

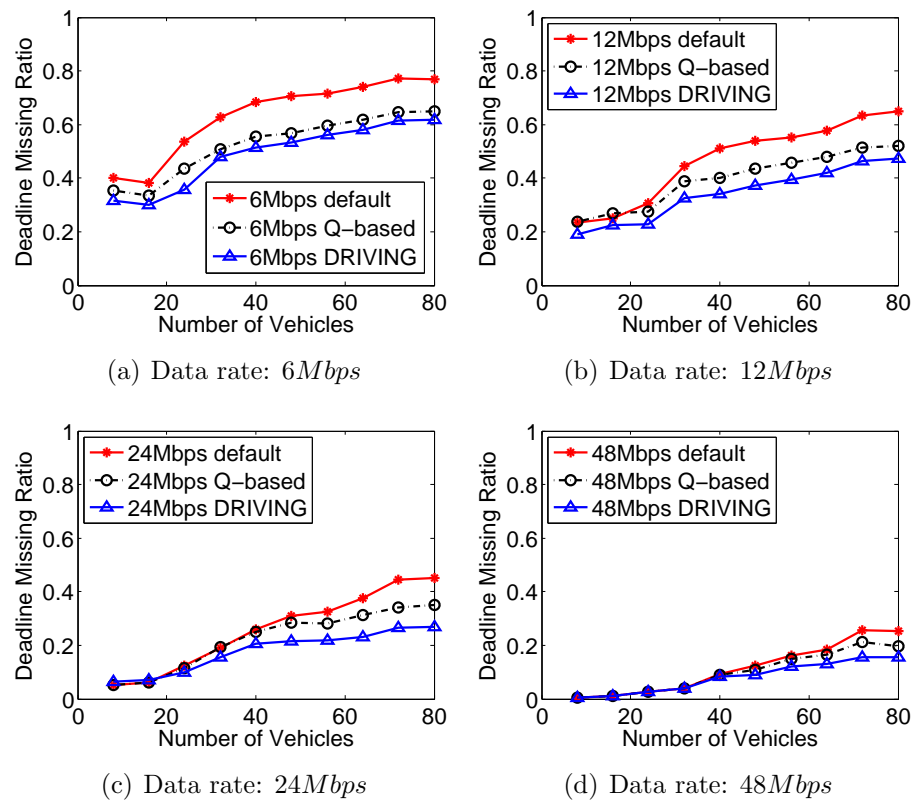


Figure 4.21 The average deadline missing ratios.

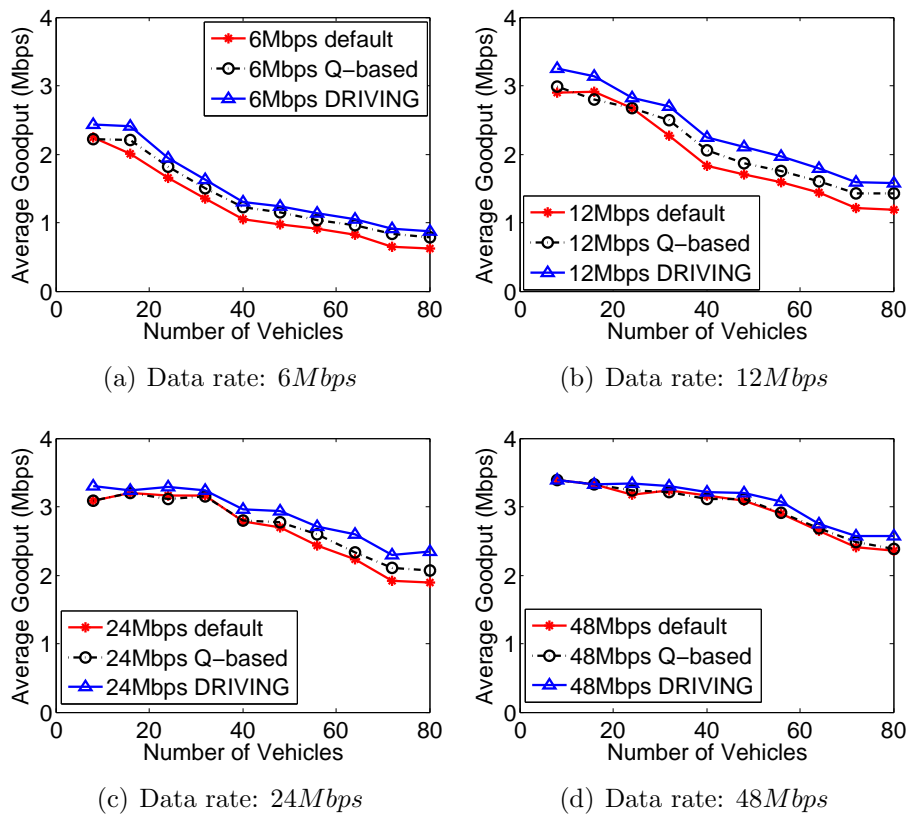


Figure 4.22 The average goodputs of four different data rates.

employs 3 levels of priorities. This increases the efficiency in resolving collisions. Compared to the Q-based algorithm, the DRIVING algorithm assigns priorities according to queueing delays. This policy allows the DRIVING algorithm to utilize the periodic pattern of video traffic to reduce collisions.

Another interesting observation from Figure 4.22 is that the goodput improvement brought by the DRIVING algorithm decreases with the increasing transmission data rates. For example, the maximum goodput improvement (compared to the default algorithm) decreases from 41.3% for 6Mbps to 8.8% for 48Mbps. The reason is that, when the transmission data rate is higher, the queueing delays of packets become smaller. In this case, the highest priority in the DRIVING algorithm (as well as that in the Q-based algorithm) are used less frequently. Therefore, advantage of the DRIVING algorithm in resolving collisions (as well as that of the Q-based algorithm) begins to shrink. However, the DRIVING algorithm still outperforms the other two algorithms. Moreover, due to the severe channel condition in a vehicular scenario, high transmission data rates such as 48Mbps can hardly be used. As a result, the goodput improvement brought by the DRIVING algorithm is still considerable in most of the time. In addition to the average goodput, in Figure 4.23, we also present the CDF of goodput when the number of vehicles is 80 (due to the space limitation, we skip the results of other scenarios). It is confirmed in Figure 4.23 that DRIVING enlarges the goodput of in-cabin Wi-Fi video streaming.

4.9 Concluding Remarks

In this chapter, we study the in-cabin Wi-Fi system, which are designed, developed and implemented to deliver enriched IVI services. We first develop cross-layer analytical models to describe this newly deployed system. Unlike existing models, our models are able to capture the unique features of the in-cabin Wi-Fi enabled vehicles and the vehicular environments. Simulations illustrate that our models achieve much higher modelling accuracy than the existing ones. We then further analyze the most dominating service, i.e., the video streaming service, in the in-cabin Wi-Fi system. We investigate two major challenges of in-cabin Wi-Fi video streaming - the delay/deadline awareness and the decentralized topology. In order to address these two challenges and provide better QoS to video streaming users in vehicles, we develop the DRIVING framework. DRIVING is able to schedule in-cabin Wi-Fi video packets in a delay-aware and fully distributed manner. With extensive simu-

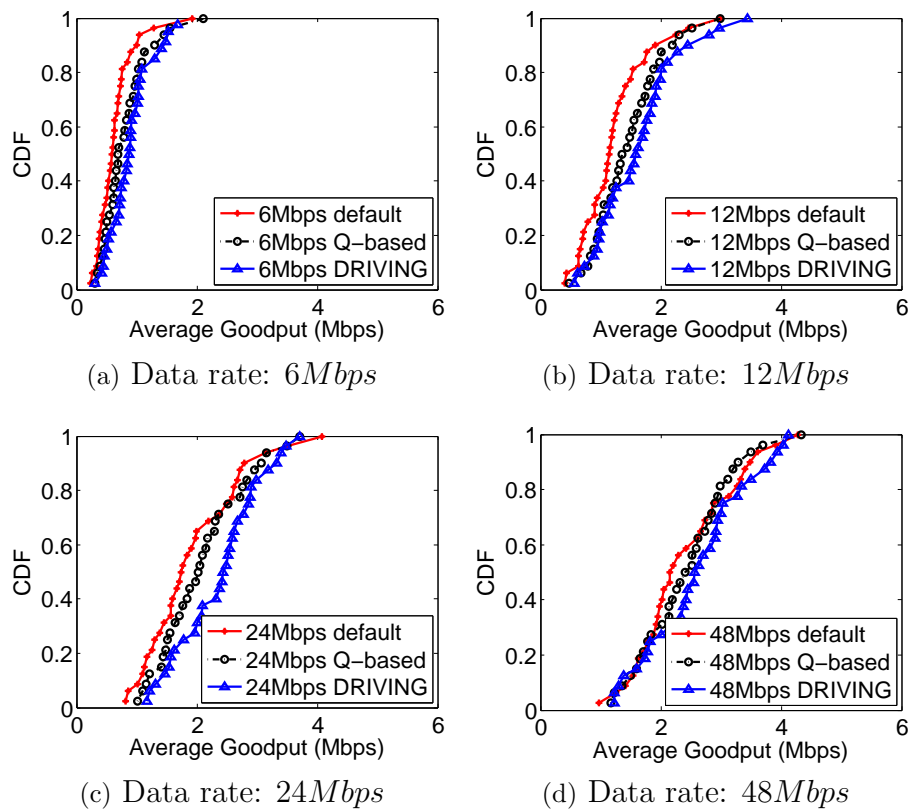


Figure 4.23 The CDFs of goodputs with 80 vehicles.

lations, we demonstrate that DRIVING significantly improves the performance of in-cabin Wi-Fi video streaming, in terms of streaming goodput, delay, jitter, deadline missing ratio and fairness.

Chapter 5

Conclusion and Future Work

5.1 Conclusion

The connected vehicles are envisioned as the pioneers of a far-reaching revolution in our society, fundamentally changing the way people travel and live. Safety, being the biggest concern of modern transportation systems, will be significantly enhanced by reliable communications between vehicles, as well as stable communications between vehicles and traffic infrastructure. Traffic information will be shared among all vehicles and infrastructure units, and will enable safety critical applications such as collision avoidance and blind spot assist. The DSRC technology is the key technology of these safety critical applications, connecting all parities of traffic in a reliable, efficient and fair manner.

In-vehicle infotainment, which makes the travel easier for everyone, becomes another important consideration of automotive manufacturers. An always-connected Internet experience will change the vehicles into portable offices and homes. To fulfill this, the newly deployed in-cabin Wi-Fi system adopts a built-in Wi-Fi hotspot to bridge the communication between the Internet and devices onboard, powering all Wi-Fi devices in a vehicle cabin.

The DSRC and the in-cabin Wi-Fi technologies are not only complementary to but also beneficial to each other. As the driving safety is enhanced by DSRC, passengers are more reassured to enjoy the onboard infotainment services. In return, as the vehicular infotainment becomes popular, more and more vehicles will become connected for infotainment services. With more connected vehicles sharing their safety-related information, the driving safety will be improved.

However, to fill the gap between the future and the present, we still need to enhance the performance of DSRC and improve the QoS of in-cabin Wi-Fi. This is non-trivial, especially in the highly violative and distributed vehicular environments. In this thesis, we identify and address several major challenges in this mission.

To enhance the performance of DSRC in a dynamic network, communication variable adaptation is required. We first tackle the strong coupling between communication variables, which has been overlooked by the state of the art. We propose to embrace the strong coupling with synchronous variable control, so as to avoid the potentially large errors in sequential variable adjustment process. The proposed OnCAR approach jointly adjust multiple variables of a connected vehicle at the same time. We then go further from the vehicle level to the network level, and study the communication coordination between vehicles. To avoid the huge overhead introduced by coordination messages, we develop a series of strictly distributed coordination schemes - DisCo. Based on advanced control techniques, DisCo is able to coordinate communication variables between vehicles with zero exchange of coordination information.

To improve the QoS of the in-cabin Wi-Fi systems, we first extensively investigate its features and differences from existing wireless communication systems. To capture these features and differences, we develop analytical models to show how an in-cabin Wi-Fi system performs under different traffic and communication conditions. We then try to improve the QoS of in-cabin Wi-Fi by looking at the dominating mobile service, i.e., the video streaming. Two major requirements of in-cabin Wi-Fi video streaming, i.e., the fully distributed nature and the delay sensitivity, are identified. Targeting at these two requirements, we propose the DRIVING framework that greatly boosts the QoS of in-cabin Wi-Fi video streaming.

5.2 Future Work

5.2.1 Interaction between Cellular and Wi-Fi Links

In the discussion of the in-cabin Wi-Fi systems, we mainly focus on bottleneck, i.e., the low-cost but low-speed Wi-Fi links, and leave the high-cost but high-speed cellular links untouched. Considering the relatively high cost of cellular data, it is desired to analyze the impact of the bottleneck to the whole system, in terms of overall bandwidth efficiency and cost effectiveness. A joint scheduling framework embracing both kinds of links is expected

to provide much better overall QoS.

5.2.2 Enabling 3D GPS with FM signals

Localization is another critical service for connected vehicles. Location information is the most basic and vital information for vehicle safety applications and beyond. Existing localization technologies, such as GPS, is unable to provide 3D information of vehicles. Yet, the 3D information is of critical importance for applications such as navigation at overpasses and collision avoidance around underground parking lots and inside tunnels. One candidate solution is to adopt FM signal fingerprints at places where 3D information is needed or where the GPS signals are unavailable. As each vehicle has a FM radio, this solution can be easily adopted. However, a major challenge lies in the varying Doppler shifts caused by the changing speed and directions of vehicles.

Appendix A

Acronyms, Abbreviations and Samples

For the convenience of the readers, we summarize the acronyms, abbreviations and mathematical samples used in this thesis.

A.1 Acronyms and Abbreviations

Table A.1: Acronyms and Abbreviations.

Acronym/ Abbv.	Term
3G	the Third Generation
4G	the Fourth Generation
AC	Access Category
ACK	Acknowledgement
ACO	Average Channel Occupancy
AMC	Adaptive Modulation and Coding
AP	Access Point
BS	Base Station
bps	bits per second
BPSK	Binary Phase-Shift Keying
CBR	Constant Bit Rate

CCH	Control Channel
CDF	Cumulative Distribution Function
CSMA	Carrier Sense Multiple Access
CSMA/CA	Carrier Sense Multiple Access with Collision Avoidance
CV	Coefficient of Variation
CW	Contention Window
DCF	Distributed Coordination Function
DIFS	DCF Interframe Space
DisCO	Distributed Coordination
DisCO-AT	Distributed Coordination with Adaptive Target
DisCO-FT	Distributed Coordination with Fixed Target
DRA	Data Rate Adaptation
DRIVING	Delay-aware Distributed Video scheduling
DSRC	Dedicated Short-Range Communications
DTMC	Discrete-Time Markov Chain
EDCA	Enhanced Distributed Channel Access
EDF	Earliest Deadline First
ePDR	effective Packet Delivery Ratio
eTPUT	effective Throughput
Gbps	Gigabits Per Second
GHz	Gigahertz
GPS	Global Positioning System
HD	High-Definition
Hz	Hertz
IEEE	Institute of Electrical and Electronics Engineers
i.i.d.	independent and identically distributed
IP	Internet Protocol
ITS	Intelligent Transportation Systems
IVI	In-Vehicle Infotainment
JPRA	Joint Power and Rate Adaptation
LOS	Light-of-Sight

LTE	Long-Term Evolution
MAC	Media Access Control
MANET	Mobile Ad hoc Network
Mbps	Megabits per second
MHz	Megahertz
MIMO	Multiple-Input Multiple-Output
WLAN	Wireless Local Area Network
NLOS	Non-Light-of-Sight
ns-2	network simulator 2
NUM	Network Utility Maximization
OBU	On-Board Unit
OFDM	Orthogonal Frequency-Division Multiplexing
OFDMA	Orthogonal Frequency-Division Multiple Access
OnCAR	Online Control Approach of Power and Rate
PDR	Packet Delivery Ratio
PLR	Packet Loss Ratio
PHY	Physical
QAM	Quadrature Amplitude Modulation
QoS	Quality of Service
QPSK	Quadrature Phase-Shift Keying
RLS	Recursive Least Squares
RSU	Road Side Unit
RTS/CTS	Request to Send / Clear to Send
SCH	Service Channel
SIFS	Short Interframe Space
SINR	signal-to-Interference-plus-Noise Ratio
SNR	Signal-to-Noise Ratio
TCP	Transmission Control Protocol
TDMA	Time Division Multiple Access
TPA	Transmission Power Adaptation
UDP	User Datagram Protocol

U.S. DOT	United States Department of Transportation
USRP	Universal Software Radio Peripheral
V2V	Vehicle-to-Vehicle
V2I	Vehicle-to-Infrastructure
V2X	Vehicle-to-Everything
VANET	Vehicular Ad hoc Network
WAVE	Wireless Access in Vehicular Environments
WMM	Wi-Fi Multimedia
WSN	Wireless Sensor Network

A.2 Mathematical Samples

Table A.2: Mathematical Samples.

Sample	Description
$A = \{a_i\}$	The parameters of a difference equation model
A_{mi}	The stable matrix in a reference control model
$B = \{b_i\}$	The parameters of a difference equation model
$b(t)$	A backoff timer
C	The cabin path loss constant
\bar{D}	The expectation of queueing delays
$d(i, j)$	The distance between nodes i and j
d_0	The reference distance of a path loss function
d_c	The equivalent distance of a path loss function
d_{eff}	The effective range
D_{head}	The queueing delay of the head-of-the-line packet
$D^{(p)}$	The queueing delay of packet p
d_{ref}	The reference range
e	A sequence of i.i.d. random vectors with zero means
$\bar{e}(t)$	The stationary distribution of a state t in a Markov chain
E_s	The expected length of a time slot
F	The function describing the MIMO model in OnCAR

$G = \{g_i\}$	The parameters of an RLS model
$H = \{h_i\}$	The parameters of an RLS model
J	The delay jitter
\mathbb{J}	A cost function
k_i^*	A constant in a reference control model
k_i	The estimation of k_i^*
\tilde{k}_i	The estimation error of k_i^*
$L(d)$	A path loss function with respect to distance d
$l(i, j)$	The interconnection parameter between nodes i and j
$\hat{l}(i, j)$	The estimation of $l(i, j)$
$\tilde{l}(i, j)$	The estimation error of $l(i, j)$
m	The maximum number of retransmission attempts
n	The order of a regression model
N	The total number of vehicles
N_c	The total number of in-cabin Wi-Fi clients
N_d	The number of packets that miss their deadlines
N_k	The number of nodes with priority k
$N_t(i)$	The number of packets transmitted by node i
N_T	The number of packets that are transmitted from time 0 to time T
$N_r(i)$	The number of packets received by node i
$N_r(i, j)$	The number of packets transmitted by node j and successfully received by node i
$\mathbb{P}(k)$	An auxiliary vector
$P1$	The probability that the channel is busy and the head-of-line packet does not reach its re-transmission limit
$P2$	The probability that the channel is idle
$P3$	the probability that the head-of-line packet is successfully transmitted or dropped
P_a	The probability to leave the idle state
P_b	The probability that the channel is busy
\mathbb{P}_i	A symmetric positive-definite matrix

P_{real}	The real transmission power
P_s	The probability of a successful transmission
P_{tr}	The probability that at least one node is transmitting
P_v	The probability that a transmission attempt fails
P_{vir}	The virtual transmission power
\mathbf{Q}	A weighting matrix
\mathbf{R}	The control outputs
\mathbf{R}^*	The control reference
R_{avg}	The average goodput
R_{reg}	The regional goodput
\mathbf{S}	The control inputs
S_{avg}	The average throughput
S_{reg}	The regional throughput
$s(t)$	A backoff stage
t_{arr}	The time that a packet arrives at an in-cabin Wi-Fi AP
t_{cur}	The current time
t_{end}	The time that a packet is received by an in-cabin Wi-Fi client or is dropped by an AP
T_{ACK}	The time spent by an ACK packet transmission
T_c	The time spent by a failed transmission
T_p	The propagation time of the data section in a data packet
T_s	The round-trip time of a successful transmission
\mathbf{U}	The system inputs
\mathbf{U}^p	The predicted system inputs
u_1^p	The predicted selection of transmission power in OnCAR
U_1	Available power levels
u_2^p	The predicted selection of data rate in OnCAR
U_2	Available data rates
$\{u_i\}$	The transmission power of node i in DisCo
V	A Lyapunov function
\mathbf{W}	A weighting matrix

$W_{i,k}$	The contention window size at backoff stage i for a node with priority k
\mathbf{X}	The environment parameters of DSRC systems
$\{x_i\}$	The ePDR of node i in DisCo
\dot{x}_i	The derivative of x_i
x_{mi}	The target ePDR of node i
\hat{x}_{mi}	The estimation of the target ePDR
\mathbf{Y}	The system outputs
\mathbf{Y}^p	The predicted system outputs
β_i	The delay set for nodes with priority i
γ_i	A gain factor
Γ	The packet length of DSRC safety messages
$\Delta\mathbf{U}$	The system input adjustments
$\Delta\mathbf{Y}$	The residual errors in system outputs
ϵ	An arbitrarily small positive number
ε	The error vector of an RLS model
ζ	A scaling factor
θ	The parameters of an RLS model
$\hat{\theta}$	The estimated parameters of an RLS model
μ_1, μ_2	The parameters of a path loss function
ξ_i	The deadline missing ratio of node i
$\pi_{j,k}$	The stationary distribution of a state $\{j, k\}$ in a Markov chain
ρ	The probability that the queue of a node is not empty
ϕ	A combined vector of control inputs and outputs as an RLS friendly presentation
$\Omega_{eff}^{(i)}$	The neighbors within the effective range of vehicle i

]

Appendix B

Publications

Published or Accepted

1. **Xi Chen**, Chen Ma, Michel Allegue and Xue Liu, "Taming the Inconsistency of Wi-Fi Fingerprints for Device-Free Passive Indoor Localization", the 36th Annual IEEE International Conference on Computer Communications (INFOCOM 2017)(accepted for publication, to appear).
2. **Xi Chen**, Lei Rao, Qiao Xiang, Xue Liu, and Fan Bai, "DRIVING: Delay-Aware Distributed Video Scheduling Framework for In-Cabin Wi-Fi Systems", in Proceedings of the 2016 ACM on Multimedia Conference (ACM MM 2016), pp. 858-867, Amsterdam, Netherlands, 2016.
3. **Xi Chen**, Linghe Kong, Xue Liu, Lei Rao, Fan Bai and Qiao Xiang, "How Cars Talk Louder, Clearer and Fairer: Optimizing the Communication Performance of Connected Vehicles via Online Synchronous Control", in Proceedings of the 35th Annual IEEE International Conference on Computer Communications (INFOCOM 2016), pp. 1-9, San Francisco, CA, U.S.A., 2016.
4. Xue Liu, **Xi Chen** and Fanxin Kong, "Utilization Control and Optimization of Real-Time Embedded Systems", Foundations and Trends® in Electronic Design Automation: Vol. 9: No. 3, pp 211-307, 2015.
5. **Xi Chen**, Lei Rao, Yuan Yao, Xue Liu and Fan Bai, "The Answer is Rolling on Wheels: Modeling and Performance Evaluation of In-cabin Wi-Fi Communications",

- in Elsevier Journal of Vehicular Communications, vol. 2, no. 1, pp. 13-26, 2015.
6. Landu Jiang, **Xi Chen**, and Wenbo He, "SafeCam: Analyzing Intersection-Related Driver Behaviors using Multi-Sensor Smartphones", in Proc. of the 14th IEEE International Conference on Pervasive Computing and Communications (PerCom 2016), Sydney, Australia, 2016.
 7. Qiao Xiang, **Xi Chen**, Linghe Kong, Lei Rao and Xue Liu, "Data Preference Matters: A New Perspective of Safety Data Dissemination in Vehicular Ad Hoc Networks", in Proc. of the 34th Annual IEEE International Conference on Computer Communications (INFOCOM 2015) , pp. 1149 - 1157, Hong Kong, China, 2015.
 8. Linghe Kong, **Xi Chen**, Xue Liu and Lei Rao, "FINE: Frequency-divided Instantaneous Neighbors Estimation System in Vehicular Networks", in Proc. of the 13rd IEEE International Conference on Pervasive Computing and Communications (PerCom 2015) , pp. 172 - 177, St. Louis, Missouri, USA, 2015.
 9. Kai Xiong, **Xi Chen**, Lei Rao, Xue Liu and Yuan Yao, "Solving the Performance Puzzle of DSRC Multi-Channel Operations", in Proc. of IEEE International Conference on Communications 2015 (ICC 2015), London, UK, 2015.
 10. **Xi Chen**, Lei Rao, Xue Liu, Hongxing Li and Xinbing Wang, "Right Time in Right Place: Taming Workload Balancing Oscillations in Internet Data Center Cost Management", in Proc. of the 5th IEEE International Green Computing Conference (IGCC 2014), Dallas, TX, 2014.
 11. Zhonghao Sun, Fanxin Kong, Xue Liu, Xingshe Zhou and **Xi Chen**, "Intelligent Joint Spatio-temporal Management of Electric Vehicle Charging and Data Center Power Consumption", in Proc. of the 5th IEEE International Green Computing Conference (IGCC 2014), Dallas, TX, 2014.

Under Submission

1. **Xi Chen**, Linghe Kong and Xue Liu, "DisCo: Enabling Strictly Distributed Coordination of Transmission Power among Connected Vehicles", under submission to

the 18th International Symposium on Mobile Ad Hoc Networking and Computing (Mobihoc 2017).

2. **Xi Chen**, Qiao Xiang, Linghe Kong and Xue Liu, "RadioLoc: Enabling All-Terrain Vehicle Localization with FM Radio Signals", under submission to the 15th ACM International Conference on Mobile Systems, Applications, and Services (Mobisys 2017).

Bibliography

- [1] W. G. Najm, J. Koopmann, J. D. Smith, and J. Brewer, “Frequency of target crashes for intellidrive safety systems,” *DOT HS 811 381*, 2010.
- [2] L. Cheng, B. Henty, D. Stancil, F. Bai, and P. Mudalige, “Mobile vehicle-to-vehicle narrow-band channel measurement and characterization of the 5.9 GHz Dedicated Short Range Communication (DSRC) frequency band,” *IEEE Journal on Selected Areas in Communications*, vol. 25, no. 8, pp. 1501–1516, 2007.
- [3] *DSRC: The Future of Safer Driving*. [Online]. Available: http://www.its.dot.gov/factsheets/dsrc_factsheet.htm
- [4] *GM Announces Widest Deployment of 4G LTE Services in Vehicles*. [Online]. Available: http://media.gm.com/media/us/en/gm/news.detail.html/content/Pages/news/us/en/2013/Feb/0225_4g-lte.html
- [5] *Ford SYNC features*. [Online]. Available: <http://support.ford.com/sync-technology/feature-matrix>
- [6] *BMW car hotspot*. [Online]. Available: <http://www.bmw.com>
- [7] *Mercedes Connectivity*. [Online]. Available: <http://www.mercedes-benz-mobile.com>
- [8] L. Qiu, Y. Zhang, F. Wang, M. K. Han, and R. Mahajan, “A general model of wireless interference,” in *Proceedings of ACM Mobicom*, 2007, pp. 171–182.
- [9] G. Bianchi, “Performance analysis of the IEEE 802.11 distributed coordination function,” *IEEE Journal on Selected Areas in Communications*, vol. 18, no. 3, pp. 535–547, 2000.

-
- [10] *Cisco Visual Networking Index: Global Mobile Data Traffic Forecast Update, 2013 - 2018*. Cisco Systems Inc, Feb, 2014.
- [11] J. Kenney, “Dedicated Short-Range Communications (DSRC) standards in the United States,” in *Proceedings of IEEE*, vol. 99, no. 7, pp. 1162–1182, 2011.
- [12] *Qualcomm automotive*. [Online]. Available: <https://www.qualcomm.com/products/snapdragon/automotive>
- [13] *General Motors built-in Wi-Fi hotspots*. [Online]. Available: http://www.gm.com/vision/design_technology.html
- [14] *Audi enables in-car Internet connectivity*. [Online]. Available: <http://www.audiusa.com/help/audi-connect>
- [15] *Huawei mobile Wi-Fi standalone devices*. [Online]. Available: <http://www.huaweidevice.com/worldwide/productFamily.do?method=index&directoryId=5009&treeId=3619>
- [16] C. Zhang, X. Zhu, Y. Song, and Y. Fang, “C4: A new paradigm for providing incentives in multi-hop wireless networks,” in *Proceedings of IEEE INFOCOM*, Shanghai, China, 2011, pp. 918–926.
- [17] X. Wang, W. Huang, S. Wang, J. Zhang, and C. Hu, “Delay and capacity tradeoff analysis for motioncast,” *IEEE/ACM Transactions on Networking*, vol. 19, no. 5, pp. 1354–1367, 2011.
- [18] C. Han, M. Dianati, R. Tafazolli, X. Liu, and X. Shen, “A novel distributed asynchronous multichannel MAC scheme for large-scale vehicular ad hoc networks,” *IEEE Transactions on Vehicular Technology*, vol. 61, no. 7, pp. 3125–3138, 2012.
- [19] P. Li and Y. Fang, “Impacts of topology and traffic pattern on capacity of hybrid wireless networks,” *IEEE Transactions on Mobile Computing*, vol. 8, no. 12, pp. 1585–1595, 2009.
- [20] X. Chen, W. Huang, X. Wang, and X. Lin, “Multicast capacity in mobile wireless ad hoc network with infrastructure support,” in *Proceedings of IEEE INFOCOM*, Orlando, FL, 2012, pp. 271–279.

-
- [21] N. Lu and X. Shen, "Scaling laws for throughput capacity and delay in wireless networks - a survey," *IEEE Communications Surveys & Tutorials*, vol. PP, no. 99, pp. 1–16, 2013.
- [22] D. Dujovne, T. Turetli, and F. Filali, "A taxonomy of IEEE 802.11 wireless parameters and open source measurement tools," *IEEE Communications Surveys & Tutorials*, vol. 12, no. 2, pp. 249–262, 2010.
- [23] Y.-C. Cheng, J. Bellardo, P. Benkő, A. C. Snoeren, G. M. Voelker, and S. Savage, "Jigsaw: solving the puzzle of enterprise 802.11 analysis," in *Proceedings of SIGCOMM*, Pisa, Italy, 2006, pp. 39–50.
- [24] R. Mahajan, M. Rodrig, D. Wetherall, and J. Zahorjan, "Analyzing the MAC-level behavior of wireless networks in the wild," in *in Procs. of ACM SIGCOMM*, Pisa, Italy, 2006, pp. 75–86.
- [25] V. Shrivastava, S. Rayanchu, S. Banerjee, and K. Papagiannaki, "PIE in the sky: on-line passive interference estimation for enterprise WLANs," in *Proceedings of USENIX NSDI*, Berkeley, CA, 2011, pp. 25–38.
- [26] T. Sukuvaara, R. Ylitalo, and M. Katz, "IEEE 802.11p based vehicular networking operational pilot field measurement," *IEEE Journal on Selected Areas in Communications*, vol. 31, no. 9, pp. 409–417, 2013.
- [27] F. Martelli, M. E. Renda, G. Resta, and P. Santi, "A measurement-based study of beaconing performance in IEEE 802.11p vehicular networks," in *Proceedings of IEEE INFOCOM 2012*, 2012, pp. 1503–1511.
- [28] D. Malone, K. Duffy, and D. Leith, "Modeling the 802.11 distributed coordination function in nonsaturated heterogeneous conditions," *IEEE/ACM Transactions on Networking*, vol. 15, no. 1, pp. 159–172, Feb 2007.
- [29] F. Daneshgaran, M. Laddomada, F. Mesiti, and M. Mondin, "Unsaturated throughput analysis of IEEE 802.11 in presence of non ideal transmission channel and capture effects," *IEEE Transactions on Wireless Communications*, vol. 7, no. 4, pp. 1276–1286, April 2008.

-
- [30] S. Nguyen, H. Vu, and L. Andrew, "Performance analysis of IEEE 802.11 WLANs with saturated and unsaturated sources," *IEEE Transactions on Vehicular Technology*, vol. 61, no. 1, pp. 333–345, Jan 2012.
- [31] X. Ma, J. Zhang, X. Yin, and K. Trivedi, "Design and analysis of a robust broadcast scheme for VANET safety-related services," *IEEE Transactions on Vehicular Technology*, vol. 61, no. 1, pp. 46–61, 2012.
- [32] J. Misić, G. Badawy, and V. Misić, "Performance characterization for IEEE 802.11p network with single channel devices," *IEEE Transactions on Vehicular Technology*, vol. 60, no. 4, pp. 1775–1787, 2011.
- [33] C. Campolo, A. Vinel, A. Molinaro, and Y. Koucheryavy, "Modeling broadcasting in IEEE 802.11p/WAVE vehicular networks," *IEEE Communications Letters*, vol. 15, no. 2, pp. 199–201, 2011.
- [34] Y. Yao, L. Rao, X. Liu, and X. Zhou, "Delay analysis and study of IEEE 802.11p based DSRC safety communication in a highway environment," in *Proceedings of IEEE INFOCOM*, Turin, Italy, 2013.
- [35] I. Tinnirello and G. Bianchi, "Rethinking the IEEE 802.11e EDCA performance modeling methodology," *IEEE/ACM Transactions on Networking*, vol. 18, no. 2, pp. 540–553, 2010.
- [36] P. Gupta and P. Kumar, "Critical power for asymptotic connectivity," in *Proceedings of the 37th IEEE Conference on Decision and Control*, vol. 1, 1998, pp. 1106–1110.
- [37] H. Zhang, Y. Ma, D. Yuan, and H.-H. Chen, "Quality-of-service driven power and sub-carrier allocation policy for vehicular communication networks," *IEEE Journal on Selected Areas in Communications (JSAC)*, vol. 29, no. 1, pp. 197–206, 2011.
- [38] C. W. Tan, "Optimal power control in rayleigh-fading heterogeneous networks," in *Proceedings of IEEE INFOCOM 2011*, 2011, pp. 2552–2560.
- [39] A. Helmy, L. Musavian, and T. Le-Ngoc, "Energy-efficient power adaptation over a frequency-selective fading channel with delay and power constraints," *IEEE Transactions on Wireless Communications*, Sep, volume=12, number=9, pages=4529-4541, 2013.

-
- [40] X. Guan, R. Sengupta, H. Krishnan, and F. Bai, "A feedback-based power control algorithm design for VANET," in *IEEE MOVE*, 2007.
- [41] K. Xu, Q. Wang, and K. Ren, "Joint UFH and power control for effective wireless anti-jamming communication," in *Proceedings of IEEE INFOCOM 2012*, 2012, pp. 738–746.
- [42] X. Chen, Z. Zhao, and H. Zhang, "Stochastic power adaptation with multiagent reinforcement learning for cognitive wireless mesh networks," *IEEE Transactions on Mobile Computing*, vol. 12, no. 11, pp. 2155–2166, Nov 2013.
- [43] A. Mayers, P. Benavidez, G. Raju, D. Akopian, and M. Jamshidi, "A closed-loop transmission power control system using a nonlinear approximation of power-time curve," *IEEE Systems Journal*, vol. 9, no. 3, pp. 1011–1019, 2015.
- [44] P. Li, Q. Shen, Y. Fang, and H. Zhang, "Power controlled network protocols for multi-rate ad hoc networks," *IEEE Transactions on Wireless Communications*, vol. 8, no. 4, pp. 2142–2149, 2009.
- [45] H.-C. Luo, E.-K. Wu, and G.-H. Chen, "A transmission power/rate control scheme in CSMA/CA-based wireless ad hoc networks," *IEEE Transactions on Vehicular Technology*, vol. 62, no. 1, pp. 427–431, Jan 2013.
- [46] K. Ramachandran, R. Kokku, H. Zhang, and M. Gruteser, "Symphony: synchronous two-phase rate and power control in 802.11 wlans," *IEEE/ACM Transactions on Networking (ToN)*, vol. 18, no. 4, pp. 1289–1302, 2010.
- [47] M. Torrent-Moreno, J. Mittag, P. Santi, and H. Hartenstein, "Vehicle-to-vehicle communication: fair transmit power control for safety-critical information," *IEEE Transactions on Vehicular Technology (TVT)*, vol. 58, no. 7, pp. 3684–3703, 2009.
- [48] H. Lu and C. Poellabauer, "Balancing broadcast reliability and transmission range in VANETs," in *Proceedings of IEEE VNC 2010*, Dec 2010, pp. 247–254.
- [49] C.-L. Huang, Y. P. Fallah, R. Sengupta, and H. Krishnan, "Adaptive intervehicle communication control for cooperative safety systems," *IEEE Network*, vol. 24, no. 1, pp. 6–13, 2010.

-
- [50] D. B. Rawat, D. C. Popescu, G. Yan, and S. Olariu, “Enhancing VANET performance by joint adaptation of transmission power and contention window size,” *IEEE Transactions on Parallel and Distributed Systems (TPDS)*, vol. 22, no. 9, pp. 1528–1535, 2011.
- [51] A. Kamerman and L. Monteban, “WaveLAN-II: a high-performance wireless LAN for the unlicensed band,” *Bell Labs technical journal*, vol. 2, no. 3, pp. 118–133, 1997.
- [52] S. H. Wong, H. Yang, S. Lu, and V. Bharghavan, “Robust rate adaptation for 802.11 wireless networks,” in *Proceedings of ACM MobiCom*, 2006.
- [53] J. C. Bicket, “Bit-rate selection in wireless networks,” *Master’s thesis*, 2005.
- [54] G. Holland, N. Vaidya, and P. Bahl, “A rate-adaptive MAC protocol for multi-hop wireless networks,” in *Proceedings of ACM MobiCom*, 2001.
- [55] X. Chen, P. Gangwal, and D. Qiao, “RAM: Rate adaptation in mobile environments,” *IEEE Transactions on Mobile Computing*, vol. 11, no. 3, pp. 464–477, 2012.
- [56] M. Vutukuru, H. Balakrishnan, and K. Jamieson, “Cross-layer wireless bit rate adaptation,” in *Proceedings of ACM Sigcomm*, 2009.
- [57] P. Shankar, T. Nadeem, J. Rosca, and L. Iftode, “CARS: Context-aware rate selection for vehicular networks,” in *IEEE ICNP*, 2008.
- [58] K. C. Lee, J. M. Navarro, T. Y. Chong, U. Lee, and M. Gerla, “Trace-based evaluation of rate adaptation schemes in vehicular environments,” in *Vehicular Technology Conference (VTC 2010-Spring)*, 2010 *IEEE 71st*. IEEE, 2010, pp. 1–5.
- [59] T. Tielert, D. Jiang, H. Hartenstein, and L. Delgrossi, “Joint power/rate congestion control optimizing packet reception in vehicle safety communications,” in *Proceedings of ACM VANET*, Taipei, Taiwan, 2013, pp. 51–60.
- [60] P. Pahalawatta, R. Berry, T. Pappas, and A. Katsaggelos, “Content-aware resource allocation and packet scheduling for video transmission over wireless networks,” *IEEE Journal on Selected Areas in Communications*, vol. 25, no. 4, pp. 749–759, 2007.

-
- [61] A. Dua, C. Chan, N. Bambos, and J. Apostolopoulos, "Channel, deadline, and distortion (CD^2) aware scheduling for video streams over wireless," *IEEE Transactions on Wireless Communications*, vol. 9, no. 3, pp. 1001–1011, 2010.
- [62] F. Li, P. Ren, and Q. Du, "Joint packet scheduling and subcarrier assignment for video communications over downlink OFDMA systems," *IEEE Transactions on Vehicular Technology*, vol. 61, no. 6, pp. 2753–2767, 2012.
- [63] S.-P. Chuah, Z. Chen, and Y.-P. Tan, "Energy-efficient resource allocation and scheduling for multicast of scalable video over wireless networks," *IEEE Transactions on Multimedia*, vol. 14, no. 4, pp. 1324–1336, 2012.
- [64] Y. Zhang, S. Qin, and Z. He, "Fine-granularity transmission distortion modeling for video packet scheduling over mesh networks," *IEEE Transactions on Multimedia*, vol. 12, no. 1, pp. 1–12, 2010.
- [65] I.-H. Hou and P. R. Kumar, "Utility-optimal scheduling in time-varying wireless networks with delay constraints," in *Proceedings of ACM MobiHoc*, Chicago, IL, USA, 2010, pp. 31–40.
- [66] H. Wu, X. Lin, X. Liuz, and Y. Zhang, "Application-level scheduling with deadline constraints," *Proceedings of IEEE INFOCOM*, pp. 1–9, 2014.
- [67] M. Caccamo, L. Zhang, L. Sha, and G. Buttazzo, "An implicit prioritized access protocol for wireless sensor networks," in *Proceedings of IEEE RTSS*, 2002, pp. 39–48.
- [68] V. Kanodia, C. Li, A. Sabharwal, B. Sadeghi, and E. Knightly, "Distributed priority scheduling and medium access in ad hoc networks," *Springer Journal of Wireless Networks*, vol. 8, no. 5, pp. 455–466, 2002.
- [69] J. Bai, E. P. Eyisi, F. Qiu, Y. Xue, and X. D. Koutsoukos, "Optimal cross-layer design of sampling rate adaptation and network scheduling for wireless networked control systems," in *Proceedings of IEEE/ACM ICCPS*, 2012, pp. 107–116.
- [70] A. Gupta, X. Lin, and R. Srikant, "Low-complexity distributed scheduling algorithms for wireless networks," in *Proceedings of IEEE INFOCOM*, Anchorage, AK, USA, 2007, pp. 1631–1639.

-
- [71] D. Qian, D. Zheng, J. Zhang, N. Shroff, and C. Joo, “Distributed csma algorithms for link scheduling in multihop mimo networks under sinr model,” *IEEE/ACM Transactions on Networking*, vol. 21, no. 3, pp. 746–759, 2013.
- [72] L. Zhou, X. Wang, W. Tu, G. Muntean, and B. Geller, “Distributed scheduling scheme for video streaming over multi-channel multi-radio multi-hop wireless networks,” *IEEE Journal on Selected Areas in Communications*, vol. 28, no. 3, pp. 409–419, 2010.
- [73] A. Reddy, S. Banerjee, A. Gopalan, S. Shakkottai, and L. Ying, “On distributed scheduling with heterogeneously delayed network-state information,” *Springer Journal of Queueing Systems*, vol. 72, no. 3-4, pp. 193–218, 2012.
- [74] P. Si, F. Yu, H. Ji, and V. Leung, “Distributed sender scheduling for multimedia transmission in wireless mobile peer-to-peer networks,” *IEEE Transactions on Wireless Communications*, vol. 8, no. 9, pp. 4594–4603, 2009.
- [75] L. Jiang and J. Walrand, “Approaching throughput-optimality in distributed CSMA scheduling algorithms with collisions,” *IEEE/ACM Transactions on Networking*, vol. 19, no. 3, pp. 816–829, 2011.
- [76] A. Rad, J. Huang, M. Chiang, and V. Wong, “Utility-optimal random access without message passing,” *IEEE Transactions on Wireless Communications*, vol. 8, no. 3, pp. 1073–1079, 2009.
- [77] J. Ni, B. Tan, and R. Srikant, “Q-CSMA: Queue-length based CSMA/CA algorithms for achieving maximum throughput and low delay in wireless networks,” in *Proceedings of IEEE INFOCOM*, San Diego, CA, USA, 2010, pp. 1–5.
- [78] P. Ameigeiras, J. J. Ramos-Munoz, J. Navarro-Ortiz, and J. Lopez-Soler, “Analysis and modelling of YouTube traffic,” *Transactions on Emerging Telecommunications Technologies*, vol. 23, no. 4, pp. 360–377, 2012.
- [79] A. Dua, N. Kumar, and S. Bawa, “A systematic review on routing protocols for vehicular ad hoc networks,” *Vehicular Communications*, vol. 1, no. 1, pp. 33–52, 2014.

- [80] J. Toutouh, J. Garcia-Nieto, and E. Alba, "Intelligent OLSR routing protocol optimization for VANETs," *IEEE Transactions on Vehicular Technology*, vol. 61, no. 4, pp. 1884–1894, 2012.
- [81] Y. Liu, J. Niu, J. Ma, L. Shu, T. Hara, and W. Wang, "The insights of message delivery delay in VANETs with a bidirectional traffic model," *Journal of Network and Computer Applications*, vol. 36, no. 5, pp. 1287 – 1294, 2013.
- [82] M. Pan, P. Li, and Y. Fang, "Cooperative communication aware link scheduling for cognitive vehicular networks," *IEEE Journal on Selected Areas in Communications*, vol. 30, no. 4, pp. 760–768, 2012.
- [83] S.-S. Wang and Y.-S. Lin, "Passcar: A passive clustering aided routing protocol for vehicular ad hoc networks," *Computer Communications*, vol. 36, no. 2, pp. 170 – 179, 2013.
- [84] Y.-J. Kim, R. Govindan, B. Karp, and S. Shenker, "Geographic routing made practical," in *Proceedings of NSDI*, Boston, MA, USA., 2005, pp. 217–230.
- [85] K. Lee, M. Le, J. Harri, and M. Gerla, "Louvre: Landmark overlays for urban vehicular routing environments," in *Proceedings of IEEE VTC Fall*, Calgary, AB, Canada, 2008, pp. 1–5.
- [86] A. Wagh, X. Li, R. Sudhaakar, S. Addepalli, and C. Qiao, "Data fusion with flexible message composition in driver-in-the-loop vehicular {CPS}," *Ad Hoc Networks*, vol. 11, no. 7, pp. 2083–2095, 2013.
- [87] L. Zhang, D. Gao, W. Zhao, and H.-C. Chao, "A multilevel information fusion approach for road congestion detection in {VANETs}," *Mathematical and Computer Modelling*, vol. 58, no. 5–6, pp. 1206–1221, 2013.
- [88] M. Al-Rabayah and R. Malaney, "A new scalable hybrid routing protocol for vanets," *IEEE Trans on Vehicular Technology*, vol. 61, pp. 2625–2635, 2012.
- [89] L. V. Minh, Y. MingChuan, and G. Qing, "End-to-end delay assessment and hybrid routing protocol for vehicular ad hoc network," *{IERI} Procedia*, vol. 2, no. 0, pp. 727 – 733, 2012.

-
- [90] I. Rhee, A. Warriier, J. Min, and L. Xu, “DRAND: Distributed randomized TDMA scheduling for wireless ad-hoc networks,” in *Proceedings of ACM MobiHoc*, Florence, Italy, 2006, pp. 190–201.
- [91] K. Bilstrup, E. Uhlemann, E. G. Ström, and U. Bilstrup, “On the ability of the 802.11p MAC method and STDMA to support real-time vehicle-to-vehicle communication,” *EURASIP Journal of Wireless Communications and Networking*, vol. 2009, pp. 5:1–5:13, 2009.
- [92] H. Omar, W. Zhuang, and L. Li, “Vemac: A tdma-based mac protocol for reliable broadcast in VANETs,” *IEEE Transactions on Mobile Computing*, vol. 12, no. 9, pp. 1724–1736, 2013.
- [93] C. Han, M. Dianati, R. Tafazolli, X. Liu, and X. Shen, “A novel distributed asynchronous multichannel MAC scheme for large-scale vehicular ad hoc networks,” *IEEE Transactions on Vehicular Technology*, vol. 61, no. 7, pp. 3125–3138, 2012.
- [94] F. Soldo, C. Casetti, C. Chiasserini, and P. Chaparro, “Video streaming distribution in VANETs,” *IEEE Transactions on Parallel and Distributed Systems*, vol. 22, no. 7, pp. 1085–1091, 2011.
- [95] *Texas Motor Vehicle Crash Statistics*, Texas, US, 2014. [Online]. Available: <http://www.txdot.gov/government/enforcement/annual-summary.html>
- [96] *North Carolina Crash Data*, North Carolina, US, 2013. [Online]. Available: <http://nccrashdata.hsrc.unc.edu/>
- [97] *New York State Department of Motor Vehicles*, New York, US, 2013. [Online]. Available: <http://dmv.ny.gov/about-dmv/statistical-summaries>
- [98] T. Strutz, *Data Fitting and Uncertainty - A practical introduction to weighted least squares and beyond, 2011 edition*. Vieweg+Teubner Verlag, 2011.
- [99] G. C. Goodwin and K. S. Sin, *Adaptive filtering prediction and control*. Courier Dover Publications, 2013.
- [100] K. J. Åström and B. Wittenmark, *Adaptive Control*. Courier Corporation, 2013.

-
- [101] F. Bai, D. D. Stancil, and H. Krishnan, "Toward understanding characteristics of dedicated short range communications (DSRC) from a perspective of vehicular network engineers," in *ACM MOBICOM*, 2010.
- [102] F. Bai and B. Krishnamachari, "Spatio-temporal variations of vehicle traffic in VANETs: Facts and implications," in *Proceedings of ACM VANET*, Beijing, China, 2009, pp. 43–52.
- [103] *San Diego real-time traffic*. [Online]. Available: <http://www.dot.ca.gov/dist11/d11tmc/sdmap/showmap.php>
- [104] B. Bloessl, M. Segata, C. Sommer, and F. Dressler, "An IEEE 802.11a/g/p OFDM receiver for GNU radio," in *Proceedings of the Second Workshop on Software Radio Implementation Forum*, ser. SRIF '13, Hong Kong, China, 2013, pp. 9–16.
- [105] K. Narendra and S. Mukhopadhyay, "To communicate or not to communicate: A decision-theoretic approach to decentralized adaptive control," in *Proceedings of American Control Conference*, 2010, pp. 6369–6376.
- [106] K. Narendra and N. Oleng, "Exact output tracking in decentralized adaptive control systems," *IEEE Transactions on Automatic Control*, vol. 47, no. 2, pp. 390–395, 2002.
- [107] N. Balasubramanian, A. Balasubramanian, and A. Venkataramani, "Energy consumption in mobile phones: A measurement study and implications for network applications," in *Proceedings of the ACM SIGCOMM IMC*,.
- [108] F.-Y. Hung, S. Pai, and I. Marsic, "Performance modeling and analysis of the IEEE 802.11 distribution coordination function in presence of hidden stations," in *Proceedings of IEEE MILCOM*, Washington D.C., 2006, pp. 1–7.
- [109] G. Breit, H. Hachem, J. Forrester, P. Guckian, K. Kirchoff, and B. Donham, "RF propagation characteristics of in-cabin CDMA mobile phone networks," in *Proceedings of DASC*, vol. 2, Washington D.C., 2005, pp. 12–30.
- [110] K. Hurst and S. Ellingson, "Path loss from a transmitter inside an aircraft cabin to an exterior fuselage-mounted antenna," *IEEE Transactions on Electromagnetic Compatibility*, vol. 50, no. 3, pp. 504–512, 2008.

-
- [111] C. Demichelis and P. Chimento, “IP packet delay variation metric for IP performance metrics (IPPM),” 2002.
- [112] *IEEE 802.11n standard*. [Online]. Available: <http://standards.ieee.org/findstds/standard/802.11n-2009.html>
- [113] X. Zhou and X. Wang, “Channel estimation for OFDM systems using adaptive radial basis function networks,” *IEEE Transactions on Vehicular Technology*, vol. 52, no. 1, pp. 48–59, 2003.
- [114] F. Dietrich and W. Utschick, “Pilot-assisted channel estimation based on second-order statistics,” *IEEE Transactions on Signal Processing*, vol. 53, no. 3, pp. 1178–1193, 2005.
- [115] C. Pandana, Y. Sun, and K. Liu, “Channel-aware priority transmission scheme using joint channel estimation and data loading for OFDM systems,” *IEEE Transactions on Signal Processing*, vol. 53, no. 8, pp. 3297–3310, 2005.
- [116] *3GPP LTE*. [Online]. Available: <http://www.3gpp.org/LTE>
- [117] M. Zukerman, T. Neame, and R. Addie, “Internet traffic modeling and future technology implications,” in *Proceedings of IEEE INFOCOM*, vol. 1, San Francisco, CA, 2003, pp. 587–596.
- [118] A. Goldsmith, “Adaptive modulation and coding for fading channels,” in *Proceedings of IEEE Information Theory and Communications Workshop*, 1999, pp. 24–26.
- [119] D. Rawat, D. Popescu, G. Yan, and S. Olariu, “Enhancing VANET performance by joint adaptation of transmission power and contention window size,” *IEEE Transactions on Parallel and Distributed Systems*, vol. 22, no. 9, pp. 1528–1535, 2011.
- [120] X. Ma, J. Zhang, X. Yin, and K. Trivedi, “Design and analysis of a robust broadcast scheme for VANET safety-related services,” *IEEE Transactionson Vehicular Technology*, vol. 61, no. 1, pp. 46–61, 2012.
- [121] *ISO/IEC 23009-1: Information technology — Dynamic adaptive streaming over HTTP (DASH)*, 2014.